THE INFLUENCE OF SHIELDING GAS COMPOSITION ON PULSED GAS METAL ARC WELDING OF ARCTIC AND OFFSHORE STRUCTURES AND PIPELINES

Final Report By:

T.S. Thompson
A.B. Rothwell
D.V. Dorling

Work on this project was jointly funded by NOVA CORPORATION OF ALBERTA and the Metals Technology Laboratories, Canada Centre for Mineral and Energy Technology, Energy Mines and Resources Canada

DSS FILE NUMBER: 03SQ.23440-6-9113
DSS CONTRACT SERIAL NUMBER: 23440-6-9113/01-SQ
CANMET SCIENTIFIC AUTHORITY: DR. J.E.M. BRAID

November 1988

150 pp

MICROMEDIA

ABSTRACT

For the economical construction of offshore structures and pipelines, a clear need exists for welding processes which are capable of depositing weld metal of high integrity and toughness, and which offer significantly improved productivity, relative to the conventional, shielded metal arc welding process. This report examines the potential of pulsed gas metal arc welding (GMAW) for these applications. Traditionally, fixed-position gas metal arc welding has been limited to the short-circuiting mode of metal transfer, with its attendant productivity limitations and susceptibility to fusion defects. The pulsed mode, by extending controlled open-arc conditions to lower mean currents, can circumvent these difficulties and, in addition, allows for the use of shielding gases having very low oxygen potential. A previous study examined metal transfer, burn-off and fusion characteristics using a range of wire and shielding gas combinations, which led to the establishment of optimum pulse structure and synergic logic for the welding of steels for low temperature applications. This report describes a study of the influence of shielding gas composition on pulsed GMAW characteristics and weld metal mechanical properties in order to determine the optimum gas mixtures for the pulsed gas metal arc welding of structural and pipeline steels for offshore oil and gas installations. Preferred oxygen potential was determined through an investigation of the effect of variations in CO_2 content of Ar-CO_2 gas mixtures on weld metal properties; for the welding of a 19 mm thick steel with vertical down progression using a C-Mn-Ti wire, a lower bound CTOD of 0.3 mm was obtained at -5° C with a 87.5Ar-12.5CO_2 mixture, whereas, in 30 mm thick steel with vertical up progression and a C-Mn-Ti-B wire, a lower bound CTOD at -45° C of 0.7 mm was achieved with a 90Ar-10CO_2 shielding gas mixture.

Maintaining the oxygen potential constant for each welding application, the effect of additions of He and H_2 and variations in CO_2 and O_2 content on arc stability and metal transfer and on penetration and fusion characteristics were investigated. For the final stage of the program, a 82.5Ar-5He-12.5CO_2 shielding gas mixture was selected for the qualification of a welding procedure in 1067 mm O.D., 19 mm W.T., Grade 483 pipe to CSA Z187-1987 Offshore Pipeline Systems and a 82Ar-10He-6CO_2-2O_2 gas mixture was selected for the qualification of a procedure in 30 mm thick LT60 structural steel to DnV rules for the Design, Construction and Inspection of Offshore Structures.

RÉSUMÉ

Dans le domaine de la construction économique de structures et d'oléoducs maritimes, il y a un besoin manifeste pour des procédés de soudage permettant de déposer un métal d'apport d'une intégrité et d'une résistance élevées tout en améliorant la productivité de façon significative par rapport à la technique classique de soudage à l'arc avec électrode enrobée. Le rapport examine les possibilités de soudage MIG à arc pulsatoire pour ces applications. Traditionnellement le soudage MIG était limité au transfert de métal par court-circuitage, procédé qui limitait la productivité et avait tendance à produire des défauts de fusion. Avec le mode pulsatoire, qui permet d'élargir les conditions de l'arc ouvert contrôlé à des courants moyens plus faibles, ces difficultés peuvent être éliminées et on peut utiliser des gaz ayant un très faible potentiel d'oxygène. Une étude antérieure a porté sur le transfert de métal et les caractéristiques de fusion sur une gamme de combinaisons de métaux d'apport et de gaz, ce qui a permis de déterminer la structure optimale des pulsations et la logique synergique idéale pour le soudage des aciers à basses températures. Ce rapport décrit une étude de l'influence de la composition du gaz d'enrobage sur les caractéristiques du soudage MIG et les propriétés mécaniques du métal d'apport afin de déterminer les mélanges gazeux optimaux pour le soudage MIG à arc pulsatoire des structures et oléoducs marins. Le potentiel d'oxygène idéal a été déterminé à la suite d'une étude des incidences des variations de la teneur en CO_2 dans les mélanges gazeux Ar-CO_2 sur les propriétés du métal d'apport. Pour souder de l'acier de 19 mm d'épaisseur en progressant verticalement vers le bas et en utilisant un fil en C-Mn-Ti, un déplacement d'ouverture à extrémité fendue minorant de 0.3 mm a été obtenu à -5° C avec un mélange de 87.5Ar-12.5CO_2

alors qu'avec de l'acier de 30 mm d'épaisseur soudé en partant du bas, et un mélange de C-Mn-Ti-B, un déplacement d'ouverture à extrémité fendue minorant de 0.7 mm a été obtenu à -45° C avec un mélange gazeux de 90Ar-10CO_2. On a étudié les effets de l'ajout de He et de H_2 ainsi que des variations de la teneur en CO_2 et en O_2 sur la stabilité de l'arc et le transfert de métal et sur les caractéristiques de pénétration et de fusion en maintenant le potentiel d'oxygène constant pour chaque application de soudage. Pour la dernière étape du programme, on a sélectionné un mélange gazeux de 82.5Ar-5He-12.5CO_2 pour homologuer un procédé de soudage de tuyaux de 1067 mm de diam. ext., 19 mm d'épaisseur de paroi, de nuance 483 conformes à la norme CSA Z187-1987, Offshore Pipeline Systems, et on a retenu un mélange gazeux de 82Ar-10He-6CO_2-2O_2 pour l'homologation d'un procédé pour un acier de charpente LT60 de 30 mm d'épaisseur conforme aux règles de conception, de construction et d'inspection des structures marines.

TABLE OF CONTENTS

		PAGE
1.0	INTRODUCTION	1
2.0	EXPERIMENTAL APPROACH	5
3.0	EQUIPMENT AND MATERIALS	6
3.1	Pulsed GMAW Power Source	6
3.2	NOVA Pulsed GMAW Power Regulator	7
3.3	Mechanized Welding System	10
3.4	Parent Material	11
3.5	Welding Consumables	11
3.6	Instrumentation	13
4.0	EXPERIMENTAL APPROACH	14
4.1	Metallurgical Evaluation	14
4.1.1	Welding Procedures	15
4.1.2	Chemical Analysis	16
4.1.3	Mechanical Testing	17
4.1.4	Metallographic Examination	18
4.2	Fusion Characteristics	18
4.2.1	Preferred Ar-He Ratio	21
4.2.2	Effects of O_2 and H_2	23
4.2.3	Arc Stability and Metal Transfer	26
4.2.4	Welding Procedure Development	27
4.2.4.1	Mechanical Testing	28
4.2.4.2	Chemical Analysis	29
4.2.4.3	Metallographic Examination	30
5.0	RESULTS AND DISCUSSION	31
5.1	Metallurgical Evaluation	31
5.1.1	Welding Procedures	31
5.1.2	Chemical Composition	32
5.1.3	Mechanical Properties	33
5.1.3.1	Hardness Test Results	33
5.1.3.2	Tensile Test Results	33
5.1.3.3	Weld Metal Toughness Results	34
5.1.4	Metallographic Observations	35
5.2	Fusion Characteristics	37
5.2.1	Preferred Ar-He Ratio	37
5.2.2	Effects Of O_2 and H_2	39
5.3	Arc Stability And Metal Transfer	41

5.4 Procedure Development And Qualification 42
5.4.1 Chemical Composition 43
5.4.2 Mechanical Properties. 44
5.4.2.1 Hardness Test Results 45
5.4.2.2 Mechanical Test Results 45
5.4.2.3 Toughness Results 45
5.4.3 Metallographic Observations. 46

6.0 SUMMARY AND CONCLUSIONS 49

ACKNOWLEDGMENTS

REFERENCES

TABLES

FIGURES

1.0 INTRODUCTION

The idea of using a gas to provide a controlled protective shield for both the welding arc and weld metal, to prevent contamination by the surrounding air, can be traced back to the first decade of the 20th century. However, it was not until 1940 that experiments were begun with the deliberate intention of developing a gas shielded welding method (1). In the 1960s, successful use of carbon-dioxide made gas shielded arc welding competitive with other established welding processes for many practical welding applications. Since then, the technical and economic advantages of the gas metal arc welding (GMAW) process over the more conventional manual welding techniques such as shielded metal arc welding (SMAW) have been widely discussed and recognized (2,4).

Presently, mechanized GMAW is being used by NOVA and its affiliates as the standard technique for the construction of major, large diameter cross-country pipelines in Canada (2,3). It has also been widely used in the construction of offshore pipelines, where its productivity advantages and the compact nature of the welding equipment make its use highly desirable. The all-positional capability of mechanized GMAW is currently achieved by the short circuiting mode of metal transfer using CO_2 or high percentages of CO_2 in Ar as the gas shielding. Adequate fusion is dependent upon the accurate positioning of the arc in relation to the joint preparation.

Along with the attendant limitations of the process in terms of heat input and, consequently, tendency towards inter-run and side-wall fusion defects, minimum oxygen levels in weld deposits are restricted to the range of 400-500 ppm because of the high oxygen potential shielding gas which is used to enhance fusion characteristics. Consequently, there is an inherent limitation in the toughness levels of the deposited weld metal which can be achieved.

The development of more-advanced power sources provided the opportunity to solve these problems (4). The control of metal transfer through current pulsation enables the GMAW process to be used in a controlled, spray transfer mode over a wide range of mean currents. An early feasibility study on the application of GMAW techniques to the mechanized welding of cross-country pipelines showed that pulsed GMAW offered the potential for reduced incidence of lack-of-fusion defects through improved metal transfer characteristics. In addition, better CTOD toughness properties were achieved as a direct result of the use of lower oxygen potential shielding gas mixtures (5). A research program recently completed at NOVA, which investigated the application of pulsed GMAW to the welding of thick-section steels for low-temperature applications (6), demonstrated the feasibility of economically applying it to fabrication of offshore structures and Arctic vessels. Excellent arc stability and fusion characteristics were obtained in the vertical uphill progression with a low oxygen potential argon-5% carbon dioxide gas mixture. However, Charpy, CTOD and metallographic results from the research project clearly identified the need to establish a better balance between wire consumable and shielding gas compositions. The selection of appropriate wire/shielding gas combinations should allow the range of toughness levels attainable with the pulse GMAW process to be significantly extended.

There have been numerous papers published covering the subject of gases and gas mixtures for the GMAW and GTAW processes; however, there is a limited amount of published information available regarding the role of gas composition in pulsed GMAW in terms of arc characteristics and weld metal properties. Some preliminary work performed at NOVA indicated that a systematic investigation was required in order to establish optimum gas compositions in combination with appropriate wire compositions.

The majority of investigations on the application of pulsed GMAW have been carried out using uphill progression, together with relatively high heat inputs to maximize productivity. Offshore pipelines present an application which requires a similar optimization effort but with downhill progression in a narrow gap joint preparation, which is presently used for circumferential butt welding of line pipe. Since the rate of progress of a lay barge is determined by the rate at which welds can be completed and inspected, the use of downhill progression, with its higher travel speed, is mandatory. In essence, it is the time to complete one pass which must be minimized; obviously, the individual passes must be sufficiently large to complete the weld, consistent with the number of stations which can be accommodated. A consideration of the axial strains which may be experienced during pipe installation indicates that further improvements in toughness, particularly crack tip opening displacement, will be necessary. Calculations using the methods of Appendix K to CSA Z184 (as revised) (7) suggest that even the existing workmanship standards for weld acceptance may be marginal, with the levels of CTOD currently achievable. Presently, using the short-circuiting process, economical lay-rates can often only be achieved by a relaxation of the workmanship standards for imperfections such as lack-of-fusion (8). As installation conditions become more extreme, the potential role of pulsed GMAW, which is less susceptible to fusion defects and potentially allows higher toughness to be achieved, becomes apparent. Clearly then it is appropriate to extend the research program to include welding in the downhill progression. Deposition characteristics will not be the same as with uphill progression, and because of the large difference in heat input, the optimum balance between weld metal composition and shielding gas, in particular in terms of oxygen potential, will change.

The establishment of appropriate gas compositions for both vertical up and vertical down welding should allow further improvements in toughness properties to be achieved, while

maintaining desirable metal transfer and arc stability characteristics. With the maintenance of the high productivity and quality potential already established, the benefits in terms of the cost of fabrication of offshore structures and Arctic vessels, as well as the installation of offshore pipelines, could be very significant.

2.0 EXPERIMENTAL APPROACH

The principal objective of this investigation was to determine optimum shielding gas mixtures for the mechanized and automated welding of structural and pipeline steels of Arctic and offshore oil/gas installations. To pursue this objective required the experimental program to be divided into five individual tasks.

The first task involved optimization of shielding gas oxygen potential for the pulsed gas metal arc welding of thick-sectioned structural and submarine pipeline steels through a systematic investigation of the effect of variations in CO_2 content of Ar-CO_2 mixtures on weld metal mechanical properties.

The second task of the program involved optimization of an Ar-He ratio to obtain optimum fusion geometry in Ar-He-CO_2 gas mixtures, while maintaining desirable metal transfer and arc stability.

Using the preferred Ar-He ratio as the base gas mixture, task three required the evaluation of the effect of variations in CO_2-O_2 and H_2 contents in the base gas mixture on arc stability, metal transfer and fusion characteristics.

Operating envelopes of pulse parameters suitable for satisfactory metal transfer and arc stability were developed in task four for the optimum shielding gas mixtures determined from the previous tasks given above.

In the fifth and final task, using the optimum gas mixtures, welding procedures were developed and qualified in thick-sectioned structural steel to DnV Rules for the Design, Construction and Inspection of Offshore Structures, and in a pipeline steel, to CSA-Z187-M87 Offshore Pipelines.

3.0 EQUIPMENT AND MATERIALS

3.1 Pulsed GMAW Power Source

Welding for the first task of this program was carried out using the M450PS pulsed GMAW power source manufactured by GEC Industrial Controls Limited of the United Kingdom. The M450PS had already been successfully used by Dorling et al (6) (after modifications described in the reference) and again was selected because of its high degree of flexibility and repeatability. This is best illustrated by the following brief description of its operation. The M450PS can be divided into two main sections, power control section, and pulse logic section as shown in the block diagram in Figure 1. The pulse logic section can be considered as the outer control loop which sets the mean current, wire feed rate and any automatic stability compensation required. The power control section, which is the inner control loop, is a high-performance, feedback control system that maintains the correct arc current as well as controlling special conditions such as arc starting and short circuiting. It also has safety shutdown features to prevent destruction of expensive, high-current control devices.

The M450PS has two modes of operation; programmable and synergic. These are selected by a front-panel, pushbutton switch. In the programmable mode, the pulse parameters, (peak current, Ip, peak time, Tp, background current, Ib, and background time, Tb), are selected by thumbwheel switches and the wire feed rate is set by the main, front-panel potentiometer control. In this mode, the average current is determined solely by the programmed pulse parameters and the power supply operates as a current control. Changes in wire-feed rate result only in changes in arc voltage.

In the synergic mode, the power source can be programmed with one set of pulse parameters through four internal potentiometers, one each for Ip, Tp, Ib and Tb. However, it is important to note that,

for the present work, the pulse logic section of the MP450PS power source has been modified from that of its factory program. As outlined in detail by Dorling et al (6), the pulse logic was modified to be able to operate the unit synergically while maintaining the optimum pulse parameters, Ip and Tp constant, for a one drop-per-pulse transfer over a wide range of average current values. The modified pulse logic is shown in Figure 2. In this way, wire-feed speed can be varied by the main, front panel control and the pulse parameters will track according to the modified synergic logic to give the required average current to match burn-off with the selected wire-feed speed. The modified wave form programmed into the M450PS is as illustrated in Figure 3; Ip and Tp remain constant and only Ib and Tb vary with changes in average current.

In the programmable mode the pulse parameters can be independently varied in small increments over a wide range:

Ip: 0-450 A in 1 A steps
Ib: 0-450 A in 1 A steps
Tp: 0.1-99.9 ms in 0.1 ms steps
Tb: 0.1-99.9 ms in 0.1 ms steps

In this mode, optimum pulse parameters can be precisely determined for specific applications. With the power source in the synergic mode, these optimum pulse parameters can be programmed into the unit and further procedure development and production applications carried out with one-knob, synergic control.

3.2 NOVA Pulsed GMAW Power Regulator

General Description

As the name implies the NOVA pulsed GMAW power regulator is not a power source, but a power regulator. Input power is from a standard

motor generator set with a rating of at least 55 V D.C. at 300 A. The main control sections are shown in Fig. 4-6 and they are:

Fig. 4. Instantaneous arc current control
Fig. 5. Synergic pulse logic control
Fig. 6. Average arc voltage control

The arc current control is a PWM 20 kHz switching regulator with a 500 A/ms current feedback control loop that precisely maintains the current at the value set by the synergic pulse logic section. It also has overcurrent sensing and shutdown logic in case of a control and/or device failure.

The synergic pulse logic control maintains the correct pulse structure in response to changes in mean current demands, which depends mainly on wire-feed speed.

The average arc voltage control is a proportional and integral controller that changes the mean current setpoint in order to obtain a constant average arc voltage, which is directly proportional to arc length. In open arc pulse welding, it is impossible to avoid occasional short circuiting of the arc. This is caused by larger than normal droplet detachment and lasts at the most 10 ms. The controller must not respond to these short duration short circuits and therefore it has a speed of response limit built in that greatly reduces its response to events shorter than 23 ms.

Operational Description

The NOVA regulator was designed to operate in the constant voltage mode and at the same time maintain the synergic pulse logic established at Cranfield. It has a 3-digit LED panel display with a selector switch that can be used to set and/or monitor 6 different operation parameters.

$\bar{I}$	-	mean current	50-300 A
Vm	-	average voltage setpoint	18.0-30.0 V
Ip	-	peak pulse current	100-500 A
Tp	-	time at peak current	1.00-5.00 ms
$F/\bar{I}$	-	pulse frequency	.40-.70 Hz/A
Ib	-	background current	30-150 A (typical)

Ip, Tp, and $F/\bar{I}$ are constant parameters that are set by means of internal potentiometers, accessible through small screwdriver holes in the front panel. In operating mode, the mean current setpoint is controlled by the average voltage control loop. This mode can be disabled by a front panel switch and the mean current set by a front panel potentiometer. By setting the mean current to 100 A, $F/\bar{I}$ can then be set by adjusting the internal potentiometer until the reading is equal to the desired frequency per 100 A. The background current is the result of setting the previous parameters, through the relationship: $\bar{I} = (Ip\ Tp + Ib\ Tb)F$.

The mean voltage is set directly by a front-panel potentiometer and the difference between this setpoint and the measured arc voltage is the error that controls the mean current. To obtain the desired welding mean current, the operator sets the wire-feed speed. The regulator will control the average voltage (which keeps the arc length constant) by changing the mean current to track changes in wire-feed speed. It will also change the mean current momentarily to compensate for changes in stickout, e.g. on encountering the side-walls when welding in a groove. This results in very stable operating conditions for a wide range of mean current (100 A to 250 A). A remote voltage control is provided for the operator to trim the arc length. Built in instrumentation is also provided for recording and observing the instantaneous values of arc voltage and current. Two 3-digit LED meters display the average arc voltage and current to assist the operator in the trimming of the wire-feed and arc length.

3.3 Mechanized Welding System

The mechanized systems selected for the investigation were the CRC-Evans Model M-200 and the CRC-Evans Model P-100. The M-200 system has already been successfully used in production by NOVA for the site welding of large-diameter, heavy-wall pipe and piping components (9) while the P-100 has been used for the welding of many thousands of miles of large-diameter, cross-country and offshore pipelines. The M-200 and the P-100, Figure 7, are orbital welding machines which travel on a 120 mm wide, spring-steel band. Each unit has three sections; a carriage section, control-box section and welding section. The carriage section consists of a hinged base that can be adjusted for diameters from 254 mm to flat plate, a 24 V drive motor and gear box, and a cam mechanism used to latch the machine onto the band. There are also three grooved guide wheels and a knurled drive wheel that ride on the edges of the band. The control box of the M-200 contains three printed circuit boards that control travel speed, wire-feed speed, oscillation frequency and dwell time, and wire and gas shutoff delay. The control box of the P-100, unlike the M-200, contains four printed circuit boards that control travel speed, wire-feed speed, oscillation frequency and wire and gas shut off delay. There are check buttons for each function of the units and on and off control buttons to energize and de-energize all control circuits. A power switch applies 24 V DC to the circuits. A thumb-wheel control on the M-200 sets the oscillation width and single-turn potentiometers set the left and right dwells, as well as oscillation speed. Oscillation speed on the P-100 is set by an internal potentiometer on the oscillation printed circuit board, and width is controlled by a mechanical-cam mechanism. On both units, ten-turn potentiometers control travel and wire speeds. The welding section consists of a welding tip, wire-drive motor, oscillation motor, gas nozzle and capacity for a 4.5 kg spool of wire on the M-200 and 2.7 kg spool on the P-100.

3.4 Parent Material

For the vertical up welding of thick-section structural steel, test panels for metallurgical evaluation (Task 1) and procedure development (Task 5) were prepared from 30 mm thick Lloyds LT60 steel plate supplied by Algoma Steel, the composition of which is given in Table 1. For the vertical down welding of submarine pipelines, test panels for metallurgical evaluation (Task 1) and procedure development (Task 5) were prepared from 19 mm thick CSA Z245.1 Grade 483 steel line pipe, the composition of which is also given in Table 1. Fusion geometry evaluation (Tasks 2 and 3) was carried out using 20 mm and 25 mm thick, mild steel plate. Process parameter evaluation (Task 4) was carried out on 25 mm thick, mild steel plate.

3.5 Welding Consumables

Two commercial gas metal arc welding wires with varying microalloying additions were used throughout the program.

A 1.2 mm diameter C-Mn-Ti-B wire was used for vertical up welding of thick-section structural steels for low temperature applications. A C-Mn-Si-Ti wire, 0.9 mm in diameter, was used for vertical down welding of submarine pipelines. The chemical compositions of the wires are given in Table 2.

The selection of the C-Mn-Ti-B wire for welding of thick-section structural steel was arrived at from considering the results of an investigation evaluating the potential of the pulsed process for the mechanized and automated welding of offshore oil and gas installations and Arctic vessels by Dorling et al (6). Their results indicated that wires of the C-Mn-Ti-B type produce weld deposits consisting entirely of fine, acicular ferrite, with concomitant good toughness.

Similarly, the choice of the C-Mn-Si-Ti wire for the welding of submarine pipelines was arrived at from a consideration of the conclusions of an investigation evaluating the factors influencing weld metal toughness in mechanized GMAW by Hart and Hutt (10). They concluded that wires of the C-Mn-Si-Ti type produced predominantly acicular ferrite weld deposits exhibiting good toughness at -10° C over a considerable range of welding parameter variables, e.g. shielding gas CO_2 content.

The gases chosen for the various experimental shielding mediums used in the program were mixtures of two or more of argon, carbon dioxide, oxygen, helium and hydrogen. The objective of each task of the experimental program dictated the compositions of shielding gas mixtures used.

It is well documented that most GMAW welding of pipeline steels is carried out using argon-based shielding gas mixtures containing carbon dioxide (or oxygen) although for some all positional applications use is made of CO_2 alone to enhance fusion characteristics under short-arc metal transfer conditions. However, the use of oxygen, helium and hydrogen is less obvious.

Oxygen, used as a shielding gas in small additions, is more easily ionized than carbon dioxide and consequently the arc is more effectively stabilized and metal transfer is improved. Oxygen additions are primarily used in the spray transfer mode, due to its beneficial effects at the anode (electrode tip). Helium, although not beneficial in terms of arc stability, has the characteristic of improving fusion geometry of weldments, as was concluded by Urmston (25). Hydrogen has been reported to improve lateral stability of the arc and reduce the amount of uneven or preferential weld penetration to one side commonly observed with Ar-CO_2 mixtures (6, 23).

The experimental gas mixtures were produced in the laboratory using a Matheson 7400 Series four tube Rotameter flowmeter. Each flowmeter tube is accurate to within 1% of its 150 mm graduated scale length. The concentrations of experimental shielding gases were periodically checked for accuracy and reproducibility by gas chromatography. A flowrate of 16.5 l/min was used throughout.

3.6 Instrumentation

Pulse parameters were continuously monitored and, in the case of synergic operation of the GEC M450PS power source, were programmed using a 20 MHz Gould OS4000 digital storage oscilloscope. Average current and arc voltage were monitored on digital meters built into the front panel of the M450PS.

When using the custom-built pulse power regulator, pulse parameters were programmed with use of a selector switch and internal potentiometers accessible through the front of the regulator. As with the M450PS, average current and average arc voltage were monitored on digital panel meters on the front of the regulator.

For the work on arc stability and metal transfer (Task 4), average current and arc voltage were filtered through a Wavetek Rockland Model 752A Brickwall filter, and then recorded on a THORN EMI SE7000 portable tape recorder. In some preliminary work, as is discussed below, some signals were played back and examined using a Hewlett Packard HP 5423A digital signal analyzer.

4.0 EXPERIMENTAL PROCEDURE

4.1 Metallurgical Evaluation

It is generally accepted that the choice of shielding gas is an important factor in GMAW welding, as the gas not only prevents atmospheric contamination, but also has significant influence on weldment geometry, metal transfer characteristics and weld metal mechanical properties. The role of shielding gas composition and its affect on weld metal toughness can be related to the chemical interaction which takes place between the liquid metal and the surrounding arc atmosphere when welding is performed under Ar-CO_2 and/or O_2. The influence of the resulting weld metal oxygen content on both the as-deposited microstructure and toughness of weld metals has been widely discussed and published (11-18). In the most recent work by Ahlblom (18), the results and conclusions of a selection of studies on the general effects of oxygen on weld metal toughness have been summarized and the following are believed to be general effects for wide variations in oxygen content:

a) Low toughness at high oxygen levels can partially be explained by the presence of many and/or coarse inclusions, at least when fracture occurs in a ductile mode.

b) Microstructure development is affected by oxide inclusions controlling the austenite grain structure and the nucleation of ferrite.

c) Moderate oxygen contents favour the formation of fine acicular ferrite with good impact toughness.

d) High oxygen contents favour the formation of coarse polygonal ferrite structure of inferior toughness.

e) Extremely low oxygen contents promote the formation of large packets of ferrite side plates with aligned second phase showing poor impact toughness.

In practice, for any given welding system, there will be an optimum oxygen content which will vary with wire composition and cooling rate; in GMAW, this will primarily be controlled by the oxygen potential of the shielding gas and can be determined by systematically changing the CO_2 content in Ar-CO_2 mixtures. Using a C-Mn-Ti-B wire with vertical up welding and a C-Mn-Si-Ti wire for vertical down welding, the object of the first stage of this investigation was to identify the optimum oxygen content which favoured the formation of fine acicular ferrite with concomitant optimum toughness properties.

4.1.1 Welding Procedures

Eight test panels, 0.61 m long by 0.34 m wide, were prepared in 30 mm thick Lloyds LT60 steel plate. The edge preparation, a 60° included angle with a 3 mm land, was produced by first flame cutting followed by machining and then the plates were assembled as shown in Figure 8-a. Restraint bars 750 mm by 340 mm, of the same LT60 material, were welded at either end of the test panels to minimize rotation about the weld. These test panels were welded in the vertical up progression using the CRC-Evans M-200 mechanized welding system, with power supplied by the modified-logic GEC M450PS power source. No preheat was applied and the interpass temperature was 200° C maximum, as measured 25 mm from the weld preparation. The test panels were welded using the 1.2 mm diameter C-Mn-Ti-B wire with gas compositions varying from Ar-2.5CO_2 to Ar-20CO_2 in 2.5CO_2 increments, using welding procedures developed in a previous investigation (6) for thick-section structural steels for low temperature applications.

Using pipeline welding procedures developed at NOVA for the application of the pulsed gas metal arc welding process to cross country pipeline construction, a second series of eight test panels was prepared from 19 mm thick steel line pipe. The test panels, 0.46 m long by 0.305 m wide, were flame cut from NPS 42 Z245.1 Gr.483 pipe and flattened in a 75-ton press. The edge preparation, the standard CRC-Evans reduced gap preparation used in pipeline construction, was produced by machining and the plates were then assembled as shown in Figure 8-b. Again, restraint bars 70 mm by 305 mm, made from 19 mm mild steel plate, were welded at either end to minimize rotation about the weld. These test panels were welded in the vertical down welding direction using the CRC-Evans M-200 mechanized welding system, with power being supplied by the modified GEC M450PS power source. As with the vertical up welding, no preheat was applied and the interpass temperature was 200° C maximum, as measured 25 mm from the weld preparation. Using the same shielding gas mixtures as above, these eight test panels were welded using the 0.9 mm diameter C-Mn-Si-Ti wire.

4.1.2 Chemical Analysis

Broken tensile pieces were used to supply weld metal for chemical analysis; wire samples were taken directly as were parent material samples. Non-gaseous elements were analyzed spectrographically while gaseous elements were analyzed by the high temperature, inert-gas fusion technique.

The analysis of the gaseous elements oxygen and nitrogen, in a multirun weldment, requires correct sampling procedures to ensure representative, through thickness concentrations are obtained. A considerable amount of work to identify suitable sampling procedures for analysis of oxygen and nitrogen has been carried out by Stevens and Moreton (19), and their work provides an appropriate background for this investigation. For shielded gas metal arc welds, they concluded that, for representative concentrations in a multirun

weld, samples should be taken at regular intervals along the length of the weld as well as sampling at different depths through the thickness of the weld. They also pointed out that sampling in the cap region and root region should be avoided, where an overall average weld oxygen concentration is sought.

Thus, sampling of the multirun weld deposits for oxygen and nitrogen analysis was carried out as follows. Broken tensile pieces, broken charpy pieces and an additional third sample were used, each representing one third of the length of the weld and depth of the weld, excluding the cap and root regions. Deposit boundaries from these pieces were identified after sectioning by polishing to 6 micron and etching with 10% nital. The deposits were separated with a fine cut-off wheel and a total of three samples were obtained, each weighing 0.5-1.0 grams.

4.1.3 Mechanical Testing

Each of the sixteen welded test panels was sectioned for mechanical testing as shown in Figure 9. One all-weld metal tensile testpiece of 12 mm diameter for the 30 mm thick steel and one 4 mm diameter for the 19 mm thick steel, to ASTM A370, was extracted from 2 mm below the plate surface and tested at room temperature. Yield strength, ultimate tensile strength, percent elongation and percent reduction of area were measured. Three weld metal Charpy V-notch specimens obtained from each test panel in accordance to ASTM E23 were also obtained from 2 mm below the plate surface. The subsurface Cv specimens were broken at two temperatures to reflect typical minimum service conditions; -45° C for the specimens obtained from the 30 mm thick sectioned steel, and -5° C for those obtained from the 19 mm thick steel. Three B x 2B CTOD specimens were prepared from each test panel, with the notch at the weld centerline and in the through-thickness direction. These were tested in accordance with BS 5762 at the same test temperatures as the Cv specimens. Local compression was performed on each CTOD

specimen prior to fatigue cracking; a platen of suitable diameter was used to cause an indent depth equivalent to 0.5% of the specimen thickness on each side, and thereby provide a sufficient amount of mechanical stress relief to ensure uniform fatigue crack growth. Macrosections were prepared for examination of bead profiles, potential for defects and weld run sequence, and a hardness survey was conducted at a load of 0.5 kgf.

4.1.4 Metallographic Examination

Charpy specimens broken at -45° C and -5° C that exhibited an impact value similar to the average value of each set of specimens were selected for metallographic examination. The notched surfaces were ground flush to the notch root, mounted in bakelite, polished, etched in 2% nital and examined for identification of microstructural features adjacent the fracture surface.

4.2 Fusion Characteristics

The influence of shielding gas composition on fusion characteristics in pulsed GMAW has been covered in some detail by Bicknell and Patchett (23), Mistry (24) and Urmston (25). However, each of these studies investigated the fusion characteristics of bead-on-plate deposits. Although this type of analysis is useful in determining parameters such as wetting angle and penetration on flat plate, it is not appropriate to extend bead-on-plate studies to joint preparations of groove geometry. It was decided, therefore, to investigate the influence of shielding gas composition on fusion geometry of bead-in-groove deposits in joint preparations reflective of field applications.

Fusion characteristics obtained when welding represent a critical element in determining weld quality. The requirements for fusion characteristics vary for specific applications but optimization of fusion geometry is of primary importance, particularly with GMAW,

which is commonly associated with fusion defects. It was the object of this stage of the program to optimize the depth that fusion extends into the base metal (side wall fusion) and into adjacent beads (interpass fusion) in joint configurations commonly used in the welding of offshore structure and pipelines.

For the above reasons, the investigation into fusion characteristics was divided in two sequential exercises as follows:

a) Determine the preferred Ar-He ratio through an investigation of the effect of variations in He content of Ar-He-CO_2 mixtures on fusion characteristics while maintaining desirable metal transfer and arc stability.

b) Using the preferred Ar-He ratio as the base gas mixture, evaluate the effect of O_2 and H_2 additions on fusion geometry while maintaining desirable metal transfer and arc stability.

For both exercises the oxygen potential was maintained constant as determined in Task 1. However, before this phase of the investigation could begin, it was necessary to commission the custom-built NOVA pulsed GMAW power regulator, as unidentifiable operating problems were detected with the M450PS power source after completion of Task 1. This preliminary work was confined to bead-on-plate deposits in the flat position on 12.7 mm thick mild steel plate over the required range of mean current values for both wire diameters. Arc length was maintained at 4 mm and contact-tip-to-work distance remained constant at 13 mm. Arc stability and metal transfer were monitored by current/voltage traces recorded on the portable tape recorder.

It was quickly established that desirable arc stability and metal transfer could be achieved with peak conditions from the first task of this investigation and background conditions using a 50 Hz/100 A frequency/mean current relationship, as suggested by Quintino and

Allum for 1.2 mm diameter wire (20). However, process instability and consequently, unacceptable metal transfer was encountered when using peak conditions from the first task and background conditions given by the 60 Hz/100 A frequency/mean current relationship for the 0.9 mm diameter wire, again as was suggested by Quintino and Allum (20). Thus, it was important to identify suitable peak parameters and a frequency/mean current relationship to achieve acceptable arc stability and metal transfer for the 0.9 mm wire.

The influence of background conditions on droplet characteristics has been identified by Allum (4) and Smati (21) as an important variable for satisfactory arcing conditions in pulsed GMAW. Furthermore, as indicated above, Quintino and Allum proposed a "rule of thumb", whereby a pulse frequency of 60 Hz/100 A for 0.9 mm wire should result in a droplet of approximately the same diameter as the electrode wire. Although the restriction of droplet size in this way has been suggested as providing ideal, controlled metal transfer, it also clearly poses an ultimate restriction on average melting rate, wire feed speed and mean current. In order to preserve the high productivity of the CRC mechanized welding process, a mean current of around 230 A is necessary for the hot pass. This compensates for the extremely high travel speed required to allow the hot pass, with two bugs per station, to keep up with the four or six-head root bead welder. This mean current corresponds to a wire-feed speed of 218 mm/s (Table 4). Since the length of wire corresponding to a spherical droplet of diameter 0.9 mm is given by

$$\frac{4}{3} (.45)^3 / (.45)^2 = 0.6,$$

the required frequency to match this WFS is 218/0.6, or 363 Hz. This clearly cannot be maintained, for practical levels of Ip and Tp to maintain stable, one drop/pulse transfer; a larger droplet size must thus be adopted. A droplet diameter of 1.2 mm, as used in the

uphill welding, was found to result in a suitable pulse structure for the present application. The length of wire corresponding to one droplet is then

$$\frac{4}{3} (.6)^3 / (.45)^2 = 1.42 \text{ mm}$$

The corresponding frequency, for a WFS of 218 mm/s, is thus 154 Hz, corresponding to an $F/\bar{I}$ ratio of 0.67. Bead-on-plate tests were repeated, using background conditions defined by a 70 Hz/100 A relationship, and confirmed that stable arcing could be maintained up to the required mean current levels.

Using the same relationship to define background conditions, peak parameters were re-determined, to ensure that droplet detachment was occurring at the trailing edge of the high-current pulse, a criterion which has been identified by many workers as ideal for controlled metal transfer in pulsed GMAW (4, 6, 21, 22). Analysis of current and voltage traces recorded during bead-on-plate welds, combined with the observations of the welding operator, revealed that a peak time of 1.6 ms at a peak current of 350 A, as used in Task 1, was insufficient to give consistent droplet detachment at the trailing edge of the pulse. Through systematic evaluation of peak duration values from 1.5 to 3.5 ms, the critical value, at a peak current of 350 A, was found to be 2.5 ms. The following two tasks, for the 0.9 mm wire (downhill welding of line pipe), were thus performed using peak parameters of 350 A and 2.5 ms, together with background conditions defined by a 70 Hz/100 A rule.

4.2.1 Preferred Ar-He Ratio

As stated above, a considerable amount of work has been performed evaluating the influence of shielding gas composition on fusion geometry. Although the work was performed on flat plate, the general conclusion on the effect of He was that it improved bead

profile and increased penetration when compared with conventional mixtures of Ar-CO_2. Urmston (25) concluded that a proprietary gas mixture containing 38% He gave superior performance in providing adequate fusion area and dilution. Bicknell and Patchett (23), however, concluded that there were no obvious benefits in increasing the helium content above 10% of the volumetric gas composition. It was thus felt that a clear need existed to systematically evaluate the effect of He content from 5 to 40% on fusion geometry in a groove.

The influence of He was assessed through bead-in-groove weld deposits made in 25 mm thick, mild steel plate machined to simulate the first fill pass of a 60° V-groove, as typically used for the vertical up welding of thick section steels. Conversely, for the vertical down welding of pipeline steels, bead-in-groove weld deposits were made in 19 mm thick, mild steel plate machined to simulate the first fill pass of a CRC-Evans reduced gap preparation, as typically used for pipeline construction. Details of the test plates and machined grooves for both applications are illustrated in Figures 10 and 11. To determine the preferred Ar-He ratio, the following shielding gas mixtures were evaluated:

Ar- 5He-CO_2
Ar-10He-CO_2
Ar-20He-CO_2
Ar-40He-CO_2

The CO_2 content, or "oxygen potential", was maintained constant at the optimum value in each case as previously determined in the first task.

Originally, it had been intended to vary the He content in 5% increments, but some initial work showed negligible difference in fusion characteristics and process stability with such small changes.

In an attempt to eliminate any competing or compounding effect other than He on fusion geometry, all bead-in-groove deposits were completed in the flat position. For the deposits made in the 25 mm thick plate with the 1.2 mm diameter C-Mn-Ti-B wire, travel speeds were adjusted to 68 mm/min. Ip and Tp remained constant as previously used in task one and background conditions were derived from the 50 Hz/100 A rule. Similarly, travel speed was adjusted to 330 mm/min for weld deposits made in the 19 mm thick plate with the 0.9 mm diameter C-Mn-Si-Ti wire. Peak parameters, Ip and Tp, remained constant as determined above and background conditions were derived from the 70 Hz/100 A rule. The travel speeds duplicated those used in the fill-pass region of test panels completed in the initial task. Contact tip-to-work distance was maintained at 13 mm and arc length was maintained at 4 mm for all weld deposits. Arc stability and metal transfer were monitored through the subjective assessment of the welding operator and from the current and voltage traces. Duplicate weld deposits were made in each experimental shielding gas; each deposit was sectioned in two predetermined places within the groove. These were prepared for metallographic examination by wet grinding on graded silicon carbide papers and polishing on a rotating cloth pad using 6 micron diamond paste. After etching in a 10% Nital solution, the bead shape was evaluated qualitatively for uniformity and fusion characteristics were quantitatively measured on a Zeiss stereomicroscope, as illustrated in Figure 12.

4.2.2 Effects of O_2 and H_2

Although a number of investigations have studied the influence of shielding gas composition on fusion geometry of pulsed GMAW deposits, most of the work has concentrated on effects in traditional mixtures of argon, carbon-dioxide and helium. With regard to the effects of hydrogen, and combinations of carbon-dioxide and oxygen, there is little to no published data available.

Oxygen, having the lowest ionization potential of all the traditional shielding gases, exhibits electron emission characteristics which theoretically should greatly improve arc stability and ease of arc starting. Oxygen is also traditionally added in amounts of 1 to 5 percent to Ar gas mixtures to promote stable, axially directed spray transfer. The amount added depends on a number of variables; joint geometry, welding position, welding technique and consumable composition.

The need to study the effect of hydrogen on fusion geometry and process characteristics is less obvious. In an investigation on the effects of shielding gas composition on fusion characteristics in pulsed gas metal arc welds by Bicknell and Patchett (23), they concluded that a gas mixture containing 0.5% H_2 improved lateral stability of the arc and reduced the amount of uneven or preferential penetration to one side observed with Ar-CO_2 mixtures. This was also confirmed by Dorling et al (6), who found that lateral displacement of finger penetration observed in weld deposits made in Ar-CO_2 gas mixtures was absent in the same mixtures containing 0.5% H_2. They also observed that the addition of 0.5% H_2 improved sidewall wetting, while little difference in process stability was detected. The improvement in sidewall wetting can be attributed, in theory, to the fact that hydrogen is a dissociable gas with substantial thermal conductivity at welding temperatures, and this can promote fusion.

One of the major concerns in the welding of steels is hydrogen-induced cold cracking in the HAZ and/or weld metal. In the study conducted by Dorling et al (6), there was no indication of any tendency towards cracking of weldments made with a 0.5% hydrogen containing gas. Although no hydrogen determinations were performed in this work, Bicknell and Patchett (23) found hydrogen contents between 3 and 7 ppm in GMA welds made under short-circuiting conditions with a shielding gas containing 1% H_2. This is well within the range normally considered "low hydrogen".

Evaluation of the influence of O_2 and H_2 on fusion geometry and process stability was performed in an identical manner to that used in identifying the preferred Ar-He ratio. Bead-in-groove weld deposits were made in machined weld preparations for thick sectioned steels and pipeline steels, followed by detailed metallography to evaluate fusion characteristics. Arc stability and metal transfer were monitored from current and voltage traces and through the subjective assessment of the welding operator.

The preferred Ar-He ratio, once determined above, was used as the base gas mixture for the shielding gas mixtures required to investigate the influence of CO_2, O_2 and H_2 additions on pulsed GMAW fusion and process characteristics:

$Ar\text{-}He\text{-}CO_2$
$Ar\text{-}He\text{-}CO_2\text{-}H_2$
$Ar\text{-}He\text{-}O_2$
$Ar\text{-}He\text{-}O_2\text{-}H_2$
$Ar\text{-}He\text{-}CO_2\text{-}O_2$
$Ar\text{-}He\text{-}CO_2\text{-}O_2\text{-}H_2$
$Ar\text{-}He\text{-}CO_2\text{-}O_2$
$Ar\text{-}He\text{-}CO_2\text{-}O_2\text{-}H_2$
Etc.

The preferred oxygen potential of the gas mixtures, as was determined in the first task, was maintained constant by using the following formula which approximately expresses the oxidation potential of $Ar\text{-}CO_2$ mixtures with up to 25% CO_2, in terms of $Ar\text{-}O_2$ mixtures:

$$\frac{\%CO_2}{2} = \%O_2 \text{ in } Ar\text{-}O_2 \text{ mixtures}$$

This formula is based on the interpretive work of Shackleton and Ruckdeschel which correlates weld deposit oxygen content with shielding gas composition; this work is summarized by Smith (26).

4.2.3 Arc Stability and Metal Transfer

A considerable amount of work to determine the influence of pulse structure on arc stability and metal transfer has been carried out by Allum (4,20), and his work provides an appropriate background for this investigation. For steel wires, Allum found that, with a constant peak condition, background conditions and hence mean current had little influence on droplet detachment. Further experiments conducted to investigate the influence of peak parameters on metal transfer showed that, for a given peak current, there was a critical peak duration Tpc, which had to be reached before a droplet was detached consistently in the peak. When this duration was reached, droplet detachment occurred at the trailing edge of the pulse peak. The detachment remained at the trailing edge even when the pulse duration was increased by 1 to 2 ms; however, with further increases in pulse duration, detachment occurred earlier within the peak. This behavior is shown in Figure 13. When peak current was varied, it was observed that one droplet per pulse was detached if,

$$Ip^{n}Tp = \text{constant, where n is not far from 2.}$$

Similar results had previously been reported by Amin (22) and more recently by Smati (27). All three present results for "mild steel" wire in Ar-5CO_2; however, there is no reason to believe that the Ip-Tp relationship or "zone" for one drop per pulse transfer will be unaffected by changes in either wire or shielding gas composition (see previous work Dorling et al).

The object of this fourth stage of the investigation was to determine the zones or "operating envelopes" for satisfactory metal

transfer and arc stability for the combinations of the two wires and two selected optimum shielding gas mixtures. Bead-on-plate runs were deposited in the flat position on 25 mm thick, surface-ground, mild steel plate. Peak current was varied in 50 A increments from 300 A to 400 A. At each peak current value, peak duration was varied from 2 ms up to 5 ms in 0.2 to 0.5 ms increments for the large diameter C-Mn-Ti-B wire. For the small diameter C-Mn-Si-Ti wire, peak duration was varied 0.5 ms up to 4.5 ms in 0.2 to 0.5 ms increments. Contact-tip-to-work distance remained constant at 13 mm and arc length was maintained at approximately 4 mm. Droplet detachment was detected by a voltage spike from voltage traces recorded as detailed earlier. Arc stability was evaluated through the subjective assessment of the welding operator and from the current and voltage traces; the observations were correlated with detachment phenomena.

4.2.4 Welding Procedure Development

Based on the results of the previous tasks, two shielding gas mixtures, one for the welding of structural steels for low temperature applications and one for the welding of pipeline steels, were selected for procedure development and qualification to DnV Rules and CSA-Z187 respectively.

A single test panel was used for the procedure qualification of thick-section steels. The test panel, 0.61 m long by 0.34 m wide, was prepared in 30 mm thick Lloyds LT60 steel plate. The edge preparation, illustrated in Figure 14, was produced by first flame cutting followed by machining. Restraint bars, 75 mm by 340 mm of the same LT60 material, were welded at either end of the test panel to minimize rotation about the weld, as is illustrated in Figure 15. The test panel was welded in the vertical position, uphill progression, using the CRC-Evans M-200 mechanized welding system, with power being supplied by the NOVA pulsed GMAW power regulator. Travel speeds were based on maintaining the arc at the leading edge

of the weld pool, and oscillation rate and dwell times were selected to optimize fusion characteristics and overall bead appearance. The welding procedure adopted was essentially the same as that used in the first task of this investigation, with the exception that a backweld technique was used for the root region (Figure 14); the 60° included angle weld preparation was filled and capped, the test panel turned, the root region ground to sound metal, checked by magnetic particle examination, and the backweld completed in one pass with the M-200. No preheat was applied and the interpass temperature was 200° C maximum. The test panel was subjected to radiography according to the requirements of DnV Rules for the Design, Construction and Inspection of Offshore Structures, Section 6.5.

A complete girth weld was made in the fixed, 5G position (pipe axis horizontal) with vertical down progression in NPS 42, 19 mm W.T., Gr. 483 steel line pipe for the pipeline welding procedure qualification. The CRC-Evans narrow gap bevel, as shown in Figure 16, was prepared by machining and the weld completed using the CRC-Evans mechanized welding system. Welding parameters were chosen to parallel the high-productivity, mechanized technique already applied to advantage on offshore pipeline construction. Other variables such as head angle, oscillation rates and dwell times were selected to optimize fusion characteristics and overall bead appearance. No preheat was applied and the interpass temperature was 200° C maximum, as measured 25 mm from the weld preparation. The completed girth weld was subjected to radiography in accordance with the requirements of CSA-Z187-M87 Offshore Pipelines, Clause 6.2.3.2 .

4.2.4.1 Mechanical Testing

Mechanical testing of the 30 mm Lloyds structural steel test panel was performed in accordance with DnV rules, Appendix C. Sectioning of the test plate for mechanical testing, as shown in Figure 17, was

to DnV rules, Appendix C, with the exception of the addition of 3 B x 2B CTOD specimens. Testing of the girth weld was performed in accordance to CSA-Z184-M87, as referenced by CSA-Z187-M87, Section 6.2, test specimens were cut from the joint at the locations shown in Figure 6.6 of CSA-Z184. Three B x 2B CTOD specimens were also obtained from approximately the 12 o'clock position of the pipe, as is outlined in Appendix K of Z184. Full thickness transverse tensile testpieces were tested at room temperature and yield strength, tensile strength, elongation and location of fracture were recorded. Four sets of Charpy V-notch specimens were obtained from 2 mm below the top surface of the 30 mm thick test panel. Each set, representing the weld metal, the fusion line HAZ, 2 mm from the fusion line and 5 mm from the fusion line, was tested at -45° C. Two sets of Charpy V-notch specimens were obtained from the girth weld 90° from the CTOD specimen location, each of these representing weld metal and heat affected zone; these were tested at -5° C. The CTOD specimens were prepared with the notch at the weld centerline and in the through-thickness direction. These were tested in accordance with BS 5762 at test temperatures of -45° C and -5° C, for the 30 mm thick test panel and the girth weld, respectively. Local compression was carried out on each specimen prior to fatigue cracking; a platen of suitable diameter was used to cause an indent depth equivalent to 0.5% of the specimen thickness of each side, and thereby provide a sufficient amount of mechanical stress relief to ensure uniform fatigue crack growth. Macrosections were prepared for examination of bead profiles, potential for defects and weld run sequence, and a hardness survey was conducted at a load of 0.5 kgf.

4.2.4.2 Chemical Analysis

Broken tensile testpieces were used to supply weld metal for chemical analysis. Non-gaseous elements were analyzed spectrographically and gaseous elements by the high temperature, inert-gas fusion technique.

4.2.4.3 Metallographic Examination

Weld metal Charpy specimens broken at the two test temperatures, -45° C and -5° C, that exhibited impact values similar to the average value of each set of specimens, were selected for metallographic examination. The notched surfaces were machined flush to the notch root, mounted in bakelite, polished, etched in 2% nital and examined for identification of microstructural features adjacent the fracture surface.

5.0 RESULTS AND DISCUSSION

5.1 Metallurgical Evaluation

5.1.1 Welding Procedures

The welding procedures used to complete test panels in the 30 mm thick Lloyds LT60 plate and in the flattened 19 mm Gr. 483 MPa steel line pipe, in Task 1, are given in Tables 3 and 4. In general, as the CO_2 content in the shielding gas increased, welding characteristics in the vertical uphill progression became less favourable, particularly at levels exceeding $12.5CO_2$. At these high levels of CO_2 content, the mode of metal transfer approached the globular type, which resulted in a noticeable increase in weld spatter, coincident with intermittent short circuiting and arc instability. At the lower levels of CO_2 content, i.e. $2.5\text{-}12.5CO_2$, axially directed spray transfer was achieved, characterized by an audible "hiss" sound coupled with the absence of spatter. Similarly, with the vertical down progression, welding characteristics deteriorated as the CO_2 content in the shielding gas increased from 2.5 to 20 percent. At the low voltage used throughout this initial task, the metal transfer mode lay at the border between short circuit and spray, characterized by an audible "sizzling" sound, in low CO_2 content shielding gases, and a short arc mode of metal transfer, characterized by an accompanying "crackle", in the high CO_2 content shielding gases. Spatter was always evident due to the low voltages, but its severity, in quantity, size and distribution, increased with increasing CO_2 content. It is worthy of note that pulse structure for vertical down welding was not optimized at this stage.

The quantity of silicate slag formed increased with increasing active gas content for both welding positions. At low levels of CO_2 content, the slag was thin and intermittent, and could easily be removed by slight brushing. At CO_2 levels of 15 percent and

greater, the slag formed was continuous and heavy, and its adherence to the weld was such that the process of deslagging was difficult and time consuming.

With vertical uphill progression, only fill passes were deposited in the 60° included angle butt joint; no backweld was deposited. This was a result of considering the conclusions of Dorling et al (6) in which they observed overall CTOD values were compromised as a result of a backweld root bead procedure used in welding the 30 mm thick steel. Therefore, for the purpose of direct correlation between weld metal toughness properties and oxygen potential of the shielding gas, only the fill pass region of the butt joint was evaluated in the vertical up welding of the 30 mm thick Lloyds LT60 steel.

5.1.2 Chemical Composition

The results of the all-weld metal chemical analyses are shown in Table 5 for the eight test welds deposited with the C-Mn-Ti-B wire in the vertical up position, and for the eight test welds deposited with the C-Mn-Si-Ti wire in the vertical down position. Analyses of the gaseous elements, oxygen and nitrogen, are graphically illustrated in Figures 18 and 19 for the vertical up position and vertical down position, respectively. As expected, these graphs illustrate clearly that, as the "oxygen potential" (CO_2 in Ar) of the shielding gases increased, final oxygen content in the welds correspondingly increased; this trend has been observed by other workers (16-18). It is interesting to note that overall weld metal oxygen contents are within the 200-400 ppm range considered by Ito et al (16) to be optimum for preferred microstructural development of C-Mn-Ti-B and C-Mn-Si-Ti GMA welds.

The nitrogen content of the welds remained relatively constant, primarily reflecting the corresponding low nitrogen levels in the wires.

A general comparison with the wire chemical compositions in Table 2 shows that, in all sixteen welds, dilution levels from the base material are uniformly low; the low carbon content of the wire is reflected in the weld as are most of the residual and impurity elements. Recovery of deoxidants/alloying elements manganese, silicon and titanium decreases with increasing oxygen potential of the shielding gas.

5.1.3 Mechanical Properties

5.1.3.1 Hardness Test Results

Detailed results of the hardness tests for each weldment are given in Tables 6-21, and are summarized in Tables 22a and 22b.

In the vertical up welds, there was a gradual reduction in hardness in the fill pass region with increasing oxygen potential, reflecting the expected effect of oxygen on transformation behaviour in these deposits. Hardness in the vertical down welds, on the other hand, was dominated by the high cooling rate associated with the low heat input, and no trend of hardness with oxygen potential is discernible.

5.1.3.2 Tensile Test Results

The results of the all-weld-metal tensile tests are shown in Tables 23a and 23b. Yield strengths in general are higher than would be considered optimum for welding structural steel with yield strengths up to 355 MPa and pipeline steels with yield strengths up to 483 MPa. Generally speaking, this results from the alloying systems used to obtain acceptable low-temperature toughness properties.

As can be seen from Table 23a, there were significant changes in yield strength and ultimate tensile strength of the vertical up

deposits with changing oxygen content, whereas there were no detectable trends observed in elongation and/or reduction in area. The yield strength and the ultimate tensile strength decreased with increasing oxygen potential of the shielding gas. No trends could be detected in yield strength, ultimate tensile strength, elongation or reduction in area with increasing CO_2 content with the vertical down welds, as illustrated in Table 23b, and as might have been anticipated from the hardness results.

5.1.3.3 Weld Metal Toughness Results

The toughness results of the eight test panels welded in the vertical up progression, with the C-Mn-Ti-B wire, are shown in Tables 24 and 25, and appear graphically in Figure 20. Similarly, the toughness results of the eight test panels welded in the vertical down direction, with the C-Mn-Si-Ti wire, are illustrated in Tables 26 and 27, and appear graphically in Figure 21. The graphic illustrations, which provide for direct comparison of crack tip opening displacement (CTOD) toughness and Charpy V-notch (Cv) impact toughness, represent lower bounds for each toughness test technique at each CO_2 level.

Viewed overall, the Charpy and CTOD toughness data indicate the existence of a broad optimum in the variation of toughness with oxygen potential. In particular, the CTOD values at -45° C in the C-Mn-Ti-B welds increased progressively, from 2.5 to 7.5% CO_2, remained essentially constant, at around 0.8 mm, up to 12.5% CO_2, before again deteriorating with further increases in CO_2 content. Perhaps surprisingly, excellent CTOD results were also obtained at 20% CO_2. Charpy toughness was excellent across the optimum CO_2 range, at more than 200 J. In the C-Mn-Si-Ti welds, both Charpy energy and CTOD values at -5° C showed a steady rise as the CO_2 content was increased to 12.5%. Below 10% CO_2, CTOD tests were dominated by unstable, cleavage fracture, while above 12.5% CO_2, all

testpieces failed by stable, ductile tearing. There was some evidence of a slight decline in toughness beyond 17.5% CO_2.

5.1.4 Metallographic Observations

Representative macrographs of the sixteen test panels, two for the vertical up welding direction, and two for the vertical down welding direction, are shown in Figures 22 and 23 respectively. These indicate general geometry, bead placement and weld run sequence.

The proportions of refined microstructure of each vertical up weld, in the regions corresponding to those sampled by the Charpy specimens, are shown in Table 28. The proportions ranged from 50 to 62% and no trend could be detected as the CO_2 content increased. By contrast, there was no discernible refined microstructure in the vertical down welds.

Representative micrographs exhibiting typical as-deposited microstructural features are shown in Figures 24 and 25. The Figures are useful in understanding the trends observed in the CTOD/Cv results previously discussed. The nomenclature adopted in qualitatively describing the weld-metal microstructures generally follows that proposed by Subcommission IXJ of the IIW.

The 5% CO_2 C-Mn-Ti-B deposit shows a relatively coarse microstructure consisting of ferrite outlining prior austenitic grain boundaries, occasional regions of intragranular ferrite and acicular ferrite. The coarse and non-uniform intragranular structure of this deposit may be largely attributable to its low oxygen content, approximately 200 ppm, suggesting overall inclusion population was not adequate for the consistent nucleation of acicular ferrite. According to Ito et al (16), the critical oxygen level below which acicular ferrite may fail to form is about 200 ppm, and in fact, the 5% CO_2 deposit exhibited an as-deposited microstructure with the lowest proportion of acicular ferrite of any

of the deposits. Similarly, the 5% CO_2 C-Mn-Si-Ti deposit consists of ferrite and intragranular regions containing a mixture of acicular ferrite and ferrite with aligned second phase. These types of as-deposited structures, in both welds, would be expected to have a detrimental effect on cleavage resistance and is this in fact reflected in the poor toughness exhibited by these welds, Figures 20 and 21.

The 10% CO_2 C-Mn-Ti-B deposit, which exhibited the optimum CTOD/Cv toughness property relationship (as was discussed in the previous section), is entirely composed of fine acicular ferrite, reflecting an ideal balance between hardenability, cooling rate and inclusion content. Similarly, the 12.5% CO_2 C-Mn-Si-Ti deposit exhibited a microstructure consisting mainly of extremely fine intragranular acicular ferrite with a limited amount of ferrite outlining prior austenite grain boundaries. Although the microstructure contained some grain boundary transformation products, the beneficial influence of the high proportion of acicular ferrite was undoubtedly the dominant factor contributing to the high toughness of this weld.

The as-deposited microstructure of the 17.5% CO_2 C-Mn-Ti-B deposit, which exhibited low resistance to cleavage fracture, is coarse and nonuniform, consisting of grain boundary ferrite, large amounts of polygonal ferrite and some ferrite with aligned second phase. This deposit had the second lowest proportion of acicular ferrite of C-Mn-Ti-B deposits; as a result, the adverse effect of large amounts of polygonal ferrite and ferrite with aligned second phase can be expected to dominate over any potentially beneficial influence of a low oxygen content, ie. low inclusion content.

The 20% CO_2 C-Mn-Si-Ti deposit, in which there was a slight decrease from the optimum toughness properties beyond the 12.5% CO_2 deposit, is composed of intragranular acicular ferrite, ferrite outlining prior austenitic grain boundaries and ferrite with aligned second phase. The high acicular ferrite content, being uniform and

fine-grained, is the beneficial factor leading to the high toughness properties of the weld. However, the presence of the ferrite with aligned second phase, which is known to have poor cleavage resistance properties, is probably the cause for the slight decrease in toughness.

As a whole, the metallographic observations, taken together with the CTOD/Cv results, suggest as-deposited microstructures consisting predominantly of fine-grained acicular ferrite, with concomitant optimum toughness properties, can be obtained with an oxygen potential of approximately 10% CO_2 (range 7.5%-12.5%) with a C-Mn-Ti-B consumable, and of approximately (range 12.5%-17.5%) 12.5% CO_2 with a C-Mn-Si-Ti consumable.

5.2 Fusion Characteristics

5.2.1 Preferred Ar-He Ratio

The influence of helium on fusion characteristics, as assessed through the bead-in-groove weld deposits, is illustrated graphically in Figures 26 and 27 for the vertical up welding of thick section steels, and in Figures 28 and 29 for the vertical down welding of pipeline steels. The vertical line extending from the average value represents the sample standard deviation. The weld bead shape characteristics for the Ar-He-CO_2 gas mixtures investigated are shown in Figures 30 and 31.

With regard to the influence of helium on fusion of welds made with the C-Mn-Ti-B wire, helium had little effect on sidewall fusion of the V-groove deposits. Figure 26 provides graphic illustration of this result and clearly shows sidewall fusion remains relatively constant at 1.7 mm from the base gas mixture of Ar-10CO_2 up to 40% helium.

From Figure 27 however, there was a definite improvement in interpass fusion with the gas mixture containing 10% helium. When compared with the base gas mixture of Ar-10CO_2, interpass fusion was increased 112% with the addition of 10% helium. Note the small standard deviation bars at the 10% level, in all probability a direct result of the stable, axially-directed spray transfer achieved. With helium contents greater than 10%, metal transfer became progressively irregular and globular transfer dominated. At high contents of helium, in some instances, large droplets formed at the tip of the electrode and were deflected to the side and forced away from the workpiece. This type of "repelled transfer" caused process instabilities and spatter, and the results shown in Figure 27 at 20% and 40% helium levels with the large standard deviation bars, clearly support these observations.

From Figure 30, "a" through "e", bead shape characteristics remain relatively unchanged from the base gas composition deposit in "a" to the high helium deposit in "e". Bead shape in all cases could be described as being lenticular or parabolic exhibiting uniform and consistent fusion symmetry.

With regard to the influence of helium on welds made with the C-Mn-Si-Ti wire in the narrow gap preparations, unlike the V-groove deposits, there was a distinct improvement in sidewall fusion in deposits made with 5% and 10% helium additions to the base composition of Ar-12.5CO_2. From Figure 28, at the 5% level, sidewall fusion was increased 60% when compared with the base gas mixture. From the observations of the welding operator, metal transfer and arc stability appeared to be unaffected at the 5% and 10% helium levels, however, there was a tendency to fine spatter with the gas mixture containing 10% helium, when metal detachment at the trailing edge was indicated. At helium contents greater than 10%, the arc appeared to the operator as "soft", this characteristic coinciding with the rapid decrease in sidewall fusion at contents in excess of 10% helium.

There was little variation in depth of interpass fusion for all five shielding gases investigated with the C-Mn-Si-Ti wire. Figure 29 shows the effect of helium on interpass fusion, which remains unchanged and relatively constant at an average value of 3.1 mm.

Bead shape was relatively unaffected with increasing helium content. From Figure 31, "a" through "e", the basic bead shape can be described as being conical with uniform and consistently symmetrical fusion. All macros exhibited a "finger" type of interpass fusion profile, the result of the formation of a strong plasma jet during welding. Lateral stability of the arc was good as indicated by the consistently central location of the finger at the base of the plasma jet. While the addition of 5% helium to the Ar-12.5CO_2 mixture produced a more-rounded finger profile, and thereby enhanced the secondary fusion area, helium additions in excess of 5% resulted in no apparent benefit or change.

The above results for both V-groove deposits and narrow gap deposits confirm the findings of a previous investigation (23) which concluded that there are no benefits, with respect to fusion characteristics or bead shape, associated with increasing the helium content above 10 percent of the volumetric gas composition.

5.2.2 Effects of O_2 and H_2

The weld bead shape characteristics for selected shielding gas combinations are shown in Figures 32 and 33 in the V-groove preparation and narrow gap preparation, respectively. The representative macrographs summarize the trend observed for all the shielding gases investigated.

The 0.5 percent hydrogen addition, whether it was added to the gas combinations for deposits in the V-groove preparation or the narrow gap preparation, had little influence on overall fusion characteristics. Although previous investigations (6,23) observed

improved lateral stability in welds deposited in Ar-CO_2 gas mixtures containing the 0.5% H_2 addition, in the present investigation, lateral instability of the arc was not encountered. The macrographs in Figures 32 and 33 further illustrate this point. However, the conclusions of the previous investigations (6,23) were based on the results from bead-on-plate welds, and consequently, direct comparison of those results to those of this investigation may not be appropriate.

Figure 34 summarizes the effect of oxygen on fusion characteristics for both wires and groove types.

There was a distinct improvement in interpass fusion of deposits made in the V-groove preparation with increasing oxygen content, when compared with the base composition of Ar-10CO_2-10He (Fig. 34a). However, at oxygen levels in excess of 2% incomplete fusion defects were found. The arrows in the micrographs of Figure 32 provide illustration of these defects. Shielding gas oxygen content had no effect on sidewall fusion characteristics. Arc stability with 2% oxygen was significantly enhanced and although this is not a factor which is easily quantifiable, the arc was characterized by the operator as being "stiff" and more obviously penetrating than the "soft" arc associated with the base composition. Metal transfer was consistent and regular even though there was evidence of a tendency to fine spatter. However, in consideration of all the results, optimum mechanical properties and fusion characteristics while maintaining desirable arc characteristics were achieved with a wire/shielding gas combination of C-Mn-Ti-B/Ar-10He-6CO_2-2O_2 for the vertical up welding of thick section steels.

For welds made in the narrow gap preparation, the addition of oxygen to the base composition Ar-5He-12.5CO_2 had a negative effect on interpass fusion (Figure 34b). In addition, oxygen contents in excess of 1% resulted in undercutting the sidewall of the groove. The macrophotographs in Figure 33 clearly illustrate this

observation. The depth of the interpass fusion was maintained at a 1% oxygen level; however, there were no obvious benefits in terms of arc characteristics or fusion characteristics when compared to the base composition. The macrographs provide further illustration of this point. Clearly then, in consideration of all the results, a wire/shielding gas combination of C-Mn-Si-Ti/Ar-5He-12.5CO_2 appears to be optimum for the vertical down welding of pipeline steels using a narrow gap joint preparation.

5.3 Arc Stability and Metal Transfer

The zones or "operating envelopes" for satisfactory metal transfer and arc stability for the selected wire/shielding gas combinations are shown in Figures 35 and 36. Voltage and current traces recorded as detailed earlier were used to determine the relationship between Ip and Tp for the regular "one drop" per pulse metal transfer. Droplet detachment phenomenon was assessed from the occurrence of spikes on the voltage traces, whilst arc stability was monitored from the regularity and uniformity of both voltage and current traces.

From analysis of current and voltage traces and from the observations of the welding operator, the occurrence of voltage spikes in the background period coincided with process instabilities, short circuiting, severe spatter, and irregular metal transfer. This type of condition was observed when the time at peak was less than the critical peak duration, Tpc, for a given constant peak current. The arc instability, other than the qualitative indicators of severe spatter and short circuiting, was indicated by inconsistencies in the level of background current attained after each pulse. At peak duration values when the arc was very stable and the voltage traces showed consistent and regular spikes at the trailing edge of the pulse peak, this defined the onset of the critical peak duration value, Tpc. Peak duration values to the right of the operating envelope were identified by the onset of

"within the peak" detachments as indicated by voltage spikes back from the trailing edge. Although the arc remained stable, primarily the result of consistent and regular droplet transfer, there was a tendency to fine spatter.

In a previous report by Dorling et al (6), it was observed that while current and voltage traces were useful for determining the critical peak duration, Tpc, for the beginning of stable, one drop per pulse metal transfer, they gave no indication of the initial breakdown of this condition, i.e., one drop per pulse to multiple drops per pulse. From high-speed video, it was observed that at long peak duration values, even though voltage spikes were regularly observed at the trailing edge of the pulse peak, droplet detachment was immediately followed by a stream of fine droplets. However, in their work, favourable correlation was established between high speed video and voltage traces of one drop per pulse metal transfer at shorter peak duration within the operating envelopes. Consequently, the underlying basis of parameter selection for the remainder of this investigation has been the adoption of conditions relating to one drop per pulse between the minimum and midpoint of the developed operating envelopes.

A pulse peak of 350 A for 3.5 ms was selected for final procedure development and qualification with the wire/shielding gas combination of C-Mn-Ti-B/Ar-10He-6CO_2-2O_2 for the vertical up welding of thick section steels. Similarly, a pulse peak of 350 A for 3.0 ms was selected for final procedure development and qualification with the wire/shielding gas combination of C-Mn-Si-Ti/Ar-5He-12.5CO_2 for the vertical down welding of pipeline steels.

5.4 Procedure Development and Qualification

The welding procedure developed for welding the 30 mm thick Lloyds LT60 steel plate in the 3G vertical up direction is shown in

Table 29. As mentioned above, the peak parameters were 350 A for 3.5 ms, with background conditions selected based on the 50 Hz/100 A rule. Other parameters were chosen to maximize productivity, while maintaining optimum fusion characteristics. Oscillation rate of the welding head was matched with travel speed to ensure optimum interpass fusion; oscillation width and balanced sidewall dwell times were set to achieve optimum sidewall fusion. Smooth and stable arcing conditions were maintained throughout, with a total absence of spatter. The test panel was subjected to radiography and met the requirements of DnV.

The procedure developed for completing the girth weld in the CSA Z245.1 1067 mm O.D. x 19 mm W.T. GR 483 pipe, is given in Table 30. The peak parameters were, as previously mentioned, 350 A for 3.0 ms, with background conditions being determined by the 70 Hz/100 A rule. Welding parameters selected for the internal root bead, external hot pass, fill and cap passes were selected for suitability for completing the whole circumference in the 5G position.

In the fill pass region of the narrow gap preparation, from the 45° overhead to the direct overhead position, progressive crowning of the weld deposit occurred, leaving a less than ideal bead profile for application of subsequent passes. Crowning of the deposits were minimized although not totally eliminated through incorporating a 5° dragging head angle and by manipulating oscillation width and travel speed. Consequently, capping in this region was accomplished with some difficulty resulting in marginally acceptable undercut along the edges of the cap. The completed weld was subject to radiography and met the requirement of CSA Z184-86.

5.4.1 Chemical Composition

The results of the all-weld-metal chemical analyses are shown in Table 31 for both wire/shielding gas combinations.

The essential features of the deposit compositions can be summarized as follows. A general comparison of the chemical composition of the wires in Table 2 with the weld metal composition suggests minimal dilution from the base materials. The carbon content of the C-Mn-Ti-B deposit, as well as most of the residual and impurity elements for both deposits, are essentially carried over directly from the wires. The carbon content of the C-Mn-Si-Ti deposit is higher than the nominal C content of either the consumable or the base material; this is highly unlikely to be the result of carbon pickup and is probably accounted for by limitations in the precision and accuracy of the analytical sampling technique. As would be expected, levels of primary deoxidants, Mn and Si, and of easily oxidized alloying elements, Ti and B, decreased in the weld deposits relative to the wire.

For the C-Mn-Ti-B deposit, the weld metal oxygen content is marginally higher than that associated with the optimum CO_2 content range in Task 1, which may indicate the need for some fine-tuning of the O_2-CO_2 equivalence which was used to design the oxygen-containing gases. Clearly, this small change could simply reflect sampling and analysis difficulties, but the metallographic and toughness results described below are consistent with the measured oxygen content.

For the C-Mn-Si-Ti deposit, the weld metal oxygen content is lower than any of those recorded in Task 1. Nevertheless, as mentioned in following sections, the microstructure and toughness properties remain similar to those determined, in the previous task, in conjunction with the optimum CO_2 range. This observation, also, may simply indicate the difficulty of representative sampling and analysis for gaseous elements, but, in any event, provides confirmation that oxygen potential in the shielding gas may be used as a reliable guide to anticipated weld performance.

5.4.2 Mechanical Properties

5.4.2.1 Hardness Test Results

The hardness values obtained for each procedure qualification weldment appear in tabular form in Tables 32 and 33. Weld metal hardnesses are summarized in Table 34. In general, the hardness values were as expected; the root region of both weldments exhibited consistently higher hardness than the subsurface region and, in the case of the C-Mn-Si-Ti deposit, than the center portion.

5.4.2.2 Mechanical Test Results

The results of the transverse tensile tests are shown in Table 35. On the vertical up procedure weld made with the C-Mn-Ti-B/Ar-10He-6CO_2-2O_2 wire/shielding gas combination, the most stringent tensile requirements of the Lloyd's LT60 specification (490 MPa minimum tensile strength (28)) were achieved in both transverse weld tensiles. The side bend tests, as required by DnV rules for procedure qualification, met all requirements.

The tensile properties of the pipeline weld, deposited with the C-Mn-Si-Ti/Ar-5He-12.5CO_2 wire/shielding gas combination, met the minimum tensile requirements of CSA Z184-M86. The other mechanical tests of eight side bends and four nick breaks as per Figure 6.6 of Z184, also met the requirements of the standard.

5.4.2.3 Toughness Results

The results from the impact tests and from the CTOD tests of the procedure welds are tabulated in Tables 36 and 37 respectively. In considering the weld metal Charpy V-notch toughness properties, both wire/shielding gas combinations exhibited toughness similar to that determined as being optimum in the initial task of this investigation. Certainly these results were not unexpected; however, in the case of the vertical up weld where CO_2 in the shielding gas was in part replaced by O_2 for stability and improved

fusion, the small difference in average weld metal toughness is in all probability entirely related to differences in oxygen potential between the two shielding gases.

The concern of the low heat affected zone toughness of the LT60 steel used for procedure qualification with the wire/shielding gas combination of C-Mn-Ti-B/Ar-10He-6CO_2-2O_2, is far from unique. This problem has been observed and documented, for example, by Ackert et al (28) in their study of LT60 plate for Arctic applications.

The CTOD toughness levels achieved in the C-Mn-Si-Ti weld were slightly lower than those observed in Task 1, for the same CO_2 content, but still quite comparable with the previous results. In the case of the C-Mn-Ti-B weld, the CTOD values were significantly lower than had been observed, at the optimum oxygen potential, in the previous phase, though initiation was still by ductile tearing and the specific values quite acceptable. In this case, the toughness observed was consistent with an oxygen content slightly beyond the optimum range observed in Task 1, as was indicated by the chemical analysis. An additional, potential source of the difference in CTOD performance, for this weld, relates to dynamic strain-aging effects in the root region as a result of the joint completion procedure. Though no additional CTOD testing was carried out, in the present case, to confirm this possibility, Dorling et al (6) had previously found evidence that such effects could arise, in similar weld configurations.

5.4.3 Metallographic Observations

Macrographs representative of the two procedure test welds are shown in Figure 37, and indicate the general geometry and the bead placement adopted. Note the excellent fusion characteristics, in particular for the vertical down weld in the narrow gap preparation, (Fig. 37b) which have been referred to previously.

Representative micrographs of the procedure welds, illustrating typical microstructural constituents in the as-deposited region, are shown in Figure 38.

The as-deposited structure of the vertical up weld made with the C-Mn-Ti-B/Ar-10He-6CO_2-2O_2 combination is entirely composed of uniform, acicular ferrite (Figure 38a). The grain-size is noticeably coarser than in the corresponding weld (Ar-10CO_2) from Task 1 (Figure 24b), and the microstructure also appears to contain significantly greater quantities of non-ferritic micro-phases. This is consistent with the suggestion that the inferior CTOD toughness of this weld, relative to the corresponding weld from Task 1, is primarily accounted for by an oxygen content slightly beyond the optimum, corresponding to the down-slope in the curve of Figure 20, beyond 12.5% CO_2. This implies that the CO_2-O_2 equivalence, in these complex gases, may need to be adjusted, but also that relatively simple fine-tuning of the gas composition could restore excellent CTOD performance, while maintaining desirable deposition characteristics.

The as-deposited microstructure of the vertical down weld made with the C-Mn-Si-Ti/Ar-5He-12.5CO_2 combination is virtually indistinguishable from that of the corresponding weld from Task 1, consisting predominantly of very fine acicular ferrite, together with a small amount of grain-boundary-nucleated transformation products. Again, this suggests that the oxygen potential of the shielding gas remained close to the optimum, as expected, rather than being reduced, as indicated by the oxygen analysis referred to previously.

Overall, comparing the microstructures of these welds with those observed in Task 1, it can be concluded that the substitution of part of the argon by helium has no significant effect. The effect of oxygen, on the other hand, may need a little further attention, since the 2:1 equivalence with CO_2 which was used as an initial

rule-of-thumb may not be accurate for the design of these complex gases.

6.0 SUMMARY AND CONCLUSIONS

From the results of this investigation, it has been shown that shielding gas composition significantly influences weld metal chemistry, weld metal as-deposited microstructures, weld metal toughness properties, arc stability and metal transfer and fusion characteristics of welds deposited by the pulsed gas metal arc welding process. The main implication of these observations is that, to fully exploit the potential benefits offered by pulse GMAW, extensive experimentation may initially be required to identify appropriate wire/shielding gas combinations for optimum mechanical properties, quality, and welding characteristics for a specific production application. It was not the intention of this project to investigate in detail the mechanisms responsible for the development of optimum mechanical properties and fusion characteristics as influenced by shielding gas composition, as these factors have been widely discussed and previously documented. For the present investigation, two wire/shielding gas combinations have been identified which offer the potential to consistently achieve optimum weld metal mechanical properties and fusion characteristics for the pulsed gas metal arc welding of structural and pipeline steels for offshore oil and gas installations. Welding procedures were developed for each application with the applicable wire/gas combination, and then qualified to appropriate code requirements. The following are the principle conclusions of the program:

(1) "Oxidation potential", CO_2 in Argon, of the shielding gas significantly influenced toughness properties of deposited weld metal. The preferred oxygen potential was determined for the welding of a 30 mm thick steel with vertical up welding progression using a C-Mn-Ti-B wire; a lower bound CTOD at -45° C of 0.7 mm was achieved with a 90Ar-10CO_2 shielding gas. Similarly, in a 19 mm thick steel with vertical down welding progression using a C-Mn-Si-Ti wire; a lower bound CTOD of

0.3 mm was obtained at -5° C with a 87.5Ar-12.5CO_2 gas mixture.

(2) Fusion characteristics were significantly affected by the addition of helium. Interpass fusion was improved by 112% when welding under 80Ar-10He-10CO_2 for the vertical up welding of thick section steels, while sidewall fusion was improved by 60% when welding under 82.5Ar-12.5CO_2-5He for the vertical down welding of pipeline steels,

(3) Fusion characteristics, as well as process stability, were unaffected by the addition of 0.5% hydrogen.

(4) Oxygen additions of greater than 2% to the base composition of 80Ar-10He-10CO_2 resulted in a high incidence of weld metal lack-of-fusion defects. Process stability and metal transfer were significantly enhanced when welding with the addition of 2% oxygen. Additionally, interpass fusion was further increased by 80% with the same addition.

(5) Oxygen additions of greater than 1% to the base composition of 82.5Ar-12.5CO_2-5He resulted in sidewall undercutting in the narrow gap preparation commonly used in pipeline welding. No obvious benefits were obtained at a 1% O_2 level in terms of fusion characteristics or process stability when compared to the base composition.

6) A C-Mn-Ti-B/82Ar-10He-6CO_2-2O_2 wire/shielding gas combination was selected for the qualification of a procedure in 30 mm thick LT60 structural steel to DnV rules for the Design, Construction and Inspection of Offshore Structures. Similarly, a C-Mn-Si-Ti/82.5Ar-5He-12.5CO_2 wire/shielding gas combination was selected for the procedure development and qualification in 1067 mm O.D. 19 mm W.T., Grade 483 pipe to CSAZ187-1984 Offshore Pipeline Systems. All qualification requirements were

met, and encouraging levels of CTOD, at the appropriate temperature, were achieved. In the case of the LT60 qualification test, the results obtained were consistent with the hypothesis that weld metal oxygen contents were somewhat above the optimum. It should be possible, by a relatively simple fine-tuning of O_2 and CO_2 contents, to give a weld metal oxygen content from 200-250 ppm, to reproduce with the more complex gas mixture the extremely high CTOD values obtained in Task 1, while maintaining excellent welding performance.

ACKNOWLEDGEMENTS

This work was partially funded by the Metals Technology Laboratories, CANMET, Energy Mines and Resources Canada, under Supply and Services Canada Contract 23440-6-9113/01-SQ. Lloyds LT60 material, also produced under a CANMET program, was supplied by the Algoma Steel Corporation. Thanks are due to CRC-Evans Automatic Welding for the loan of the P-100 and M-200 welding systems.

Any data presented, opinions, findings, conclusions or recommendations expressed in this report are those of the authors, and do not necessarily reflect the views of CANMET.

Crown copyright of this report is reserved.

REFERENCES

1. P.T. Houldcroft: Welding Process Technology, Cambridge University Press, 1977.

2. A.B. Rothwell and D.V. Dorling: The Toughness Properties of Girth Welds in Modern Pipeline Steels, In "HSLA Steels, Technology And Applications", p. 943. American Society for Metals, Metals Park, OH., 1984.

3. D.V. Dorling and A.B. Rothwell: The Toughness of Mechanized Gas Metal Arc Welds. Proc. Conf. "Welding in Energy Related Projects", p. 379. Pergamon, Toronto, 1984.

4. C.S. Allum: MIG Welding, Time for Reassessment. Metal Construction, 1983, 15 No 6, 347.

5. A. Ditschun, B. Zajaczowski and D.V. Dorling: Pulsed FM-GMA Welding. Proc. WIC/ASM Conf. "Welding for Challenging Environments", p. 21 Pergamon, Toronto, 1986.

6. D.V. Dorling, R.M. Huntley, J. Geerligs and A.B. Rothwell: Pulsed Gas Metal Arc Welding of Thick-Section Steels for Low Temperature Applications. NOVA Corporation of Alberta/CANMET. Unpublished Report, 1986.

7. Canadian Standard Z184-M1986: Gas pipeline Systems, Appendix K. CSA, Rexdale, Ontario

8. J.D. Harrison: The Economics of a Fitness-For-Purpose Approach to Weld Defect Acceptance. Proc. TWI Seminar "Toughness of Pipeline Welds - Engineering and Materials Aspects", Houston, Dec. 1984.

9. R.M. Huntley, D.V. Dorling and A.B. Rothwell: Pipeline Girth Welding Using the Flux-Cored Arc Welding Process. Proc. Conf. "Welding in Energy-Related Projects", p. 85. Pergamon, Toronto, 1984.

10. P.H.M. Hart and G.A. Hutt: An Investigation into the Factors Influencing Mechanized MIG Weld Metal Toughness. Proc. Conf. "Welding and Performance Of Pipelines", Paper 71, The Welding Institute, London, Nov. 1986.

11. J.E. Indacochea and D.L. Olson: Relationship of Weld-Metal Microstructure and Penetration to Weld-Metal Oxygen Content. J. Materials for Energy Systems, Vol. 5, No. 3, Dec. 1983.

12. D.J. Abson and R.J. Pargeter: Factors Influencing As-Deposited Strength, Microstructure and Toughness of Manual Metal Arc Welds Suitable for C-Mn Steel Fabrications. International Metals Reviews, Vol. 31, No. 4, 1986.

13. S. Lui and D.L. Olson: The Role of Inclusions in Controlling HSLA Steel Weld Microstructures Welding Journal 65 (6): 139-s to 149-s.

14. M. Ferrante and R.A. Farrar: The Role of Oxygen Rich Inclusions in Determining The Microstructure Of Weld Metal Deposits. Journal of Materials Science 17 (1982) p. 3293-3298.

15. P.R. Kirkwood: Microstructural and Toughness Control in Low Carbon Weld Metals. Metal Construction, May 1978 p. 260-264.

16. Y. Ito, M. Nakanishi and Y. Komizo: Effects of Oxygen on Low Carbon Steel Weld Metal. Metal Construction, Sept. 1982 p. 472-478.

17. S. Ohkita, H. Homma, S. Tsushima and N. Mori: The Effect of Oxide Inclusions on Micro-Structure of Ti-B Containing Weld Metal. Australian Welding Journal, Spring 1984.

18. B. Ahlblom: Oxygen and its Role in Determining Weld Metal Microstructure and Toughness - A State-Of-The-Art Review. IIW Doc IX - 1322 - 84.

19. S.M. Stevens and J. Moreton: Sampling and Analysis for Oxygen and Nitrogen. Welding Institute Research Bulletin V. 20 #5, 1979.

20. L. Quintino and C.J. Allum: Pulsed GMAW of Mild Steel: Interactions Between Process Parameters, Parts 1 and 2. Welding and Metal Fabrication, 1984, 52 Nos. 2 and 3, 85 and 126.

21. Z. Smati: Automatic Pulsed MIG Welding. Metal Construction, 1986, 18 No 1, 38 R.

22. M. Amin: Pulsed Current Parameters for Arc Stability and Controlled Metal Transfer. Metal Construction, 1983, 15 No 5, 272.

23. A.C. Bicknell and B.M. Patchett: Pulsed GMA Welding: Shielding Gas Effects on Fusion Characteristics. University of Alberta, Department of Mineral Engineering. Unpublished Report, 1984.

24. H.R. Mistry: Effect of Wire and Shielding Gas Composition on Toughness of Pulsed MIG Welds in HSLA Steel. Cranfield Institute of Technology, Master of Science Thesis, 1986.

25. S.A. Urmston: Effect of Shielding Gas Composition on Transfer and Fusion Characteristics in Pulsed GMAW of Carbon Steels. Cranfield Institute of Technology, Master of Science Thesis, 1985.

26. A.A. Smith: Classification of Shielding Gases used in the Gas Shielded Arc Welding of Ferrous Metals - on the Basis of their Oxygen Potential. International Institute of Welding, Doc. X11-669-77,(Ex. Doc. X11 - 631-76).

27. R.J. Ackert, M.K. McLean and J.D. Ray: LT60 Plate for Arctic Application. Steels for Offshore and Arctic Applications. PMRL/CANMET, Ottawa, July 1985.

TABLE 1

TEST PANEL CHEMICAL COMPOSITION

a) LT60 Plate

C	Mn	P	S	Si	Ni	Cr	Mo	Cu	Al	V	Nb	O	N
.07	1.32	<.005	<.005	.27	.23	.26	.01	.01	.032	.063	.015	.0134	.0049

b) Grade 483 Steel Line Pipe

C	Mn	P	S	Si	Ni	Cr	Mo	Cu	Al	V	Nb	O	N
.06	1.72	.01	<.005	.31	.01	.22	.22	.03	.013	.046	.039	.0072	.0097

TABLE 2

CHEMICAL COMPOSITION OF ELECTRODE WIRES

Electrode	C	Mn	P	S	Si	Ni	Cr	Mo	Cu	Al	V	Nb	B	Ti	O	N
C-Mn-Si-Ti	.06	1.40	.011	<.005	.70	<.01	.03	.01	.08	.008	<.005	<.005	<.0005	.033	.0139	.0093
C-Mn-Ti-B	.06	1.76	.009	<.005	.35	.02	.11	.01	.30	<.005	<.005	.005	.0055	.053	.0142	.0020

TABLE 3

TYPICAL TEST PANEL WELDING PROCEDURE WITH C-Mn-Ti-B CONSUMABLE

Wire Diameter and Type: 1.2 mm Kobe MGS - 50LT
Shielding Gas: Ar-CO_2; 2.5CO_2 Increments up to 20CO_2
Power Source: GEC M450PS
Plate Thickness and Type: 30 mm Lloyds LT-60

Joint/Preparation Details

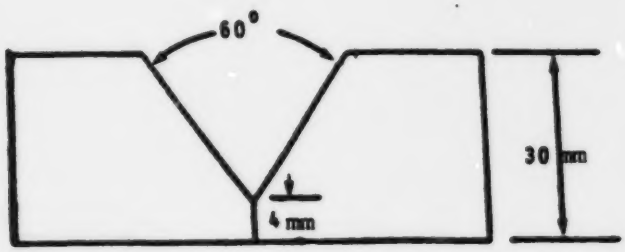

Bead Placement

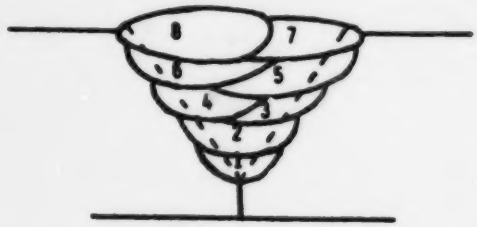

Welding Parameters

Pass	Wire Feed Speed (mm/min)	Travel (mm/min)	Oscillation Width (mm)	Oscillation Velocity (mm/s)	Stickout (mm)	Dwell L (s)	Dwell R (s)	Arc Voltage (V)	Mean Current (A)
1	4050	111	5	112	12.7	0.2	0.2	19	160
2	3750	68	12	81	12.7	1.2	1.2	20	150
3	3750	68	9	81	12.7	0	1.0	21	150
4	3750	68	8	81	12.7	1.2	0.8	21	150
5	3750	68	11	71	12.7	1.2	1.8	21	150
6	3750	68	11	71	12.7	1.8	1.2	21	150
7	3750	68	16	71	12.7	1.4	1.4	21	150
8	3750	62	17	61	12.7	1.8	1.8	21	150

Pulse Parameters

Mean Current A	Peak Current A	Time at Peak ms	Background Current A	Frequency Hz
160	350	3	100	80
150	350	3	92	75

TABLE 4

TYPICAL TEST PANEL WELDING PROCEDURE WITH C-Mn-Si-Ti CONSUMABLE

Wire Diameter and Type: 0.9 mm Thyssen K-NOVA
Shielding Gas: Ar-CO_2; 2.5CO_2 Increments up to 20CO_2
Power Source: GEC M450PS
Plate Thickness and Type: 19 mm CSA Z245.1 CAT II Grade 483 Steel

Joint/Preparation Details

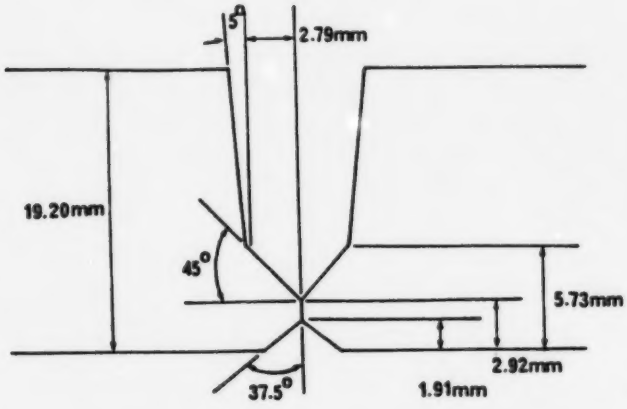

Bead Placement

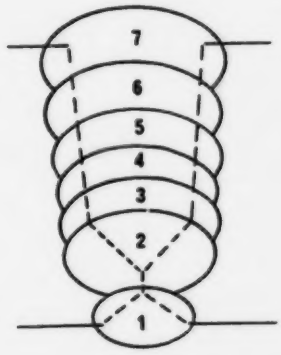

Welding Parameters

Pass	Wire Feed Speed (mm/min)	Travel (mm/min)	Oscillation Width (mm)	Oscillation Velocity (mm/s)	Stickout (mm)	Dwell L (s)	Dwell R (s)	Arc Voltage (V)	Mean Current (A)
1	10500	825	-	-	9.5	-	-	20	200
2	13100	1270	-	-	12.7	-	-	20	230
3	12370	330	2.5	112	12.7	-	-	21	215
4	12370	330	3.0	112	12.7	-	-	21	215
5	12370	330	3.0	112	12.7	-	-	21	215
6	12370	330	3.5	112	12.7	-	-	21	215
7	7550	312	3.5	112	12.7	0.3	0.3	21	150

Pulse Parameters

Mean Current A	Peak Current A	Time at Peak ms	Background Current A	Frequency Hz
200	350	1.6	165	120
230	350	1.6	198	138
215	350	1.6	178	129
150	350	1.6	116	90

TABLE 5

WELD METAL CHEMICAL COMPOSITION

a) Electrode: C-Mn-Ti-B

Shielding Gas	C	Mn	P	S	Si	Ni	Cr	Mo	Cu	Al	V	Nb	Ti	B
97.5Ar-2.5CO_2	.06	1.76	.009	<.005	.35	.04	.12	.01	.17	.015	.010	<.005	.024	.0046
95Ar-5CO_2	.06	1.72	.010	<.005	.34	.03	.12	.01	.17	<.005	.008	<.005	.023	.0048
92.5Ar-7.5CO_2	.06	1.61	.008	<.005	.30	.06	.13	.01	.15	<.005	.015	<.005	.020	.0039
90Ar-10CO_2	.06	1.68	.009	<.005	.32	.04	.12	.01	.16	<.005	.009	<.005	.018	.0045
87.5Ar-12.5CO_2	.06	1.60	.009	<.005	.30	.05	.13	.01	.15	<.005	.012	.005	.018	.0040
85Ar-15CO_2	.06	1.56	.009	<.005	.29	.06	.13	.01	.14	<.005	.014	.005	.016	.0038
82.5Ar-17.5CO_2	.06	1.57	.009	<.005	.29	.06	.14	.01	.14	<.005	.015	.005	.019	.0038
80Ar-20CO_2	.06	1.61	.009	<.005	.29	.06	.14	.01	.14	<.005	.015	.005	.017	.0038

TABLE 5 (cont)

WELD METAL CHEMICAL COMPOSITION

b) Electrode: C-Mn-Si-Ti

Shielding Gas	C	Mn	P	S	Si	Ni	Cr	Mo	Cu	Al	V	Nb	Ti	B
97.5Ar-2.5CO_2	.06	1.60	.014	<.005	.69	.01	.04	.02	.08	.015	.010	<.005	.024	<.005
95Ar-5CO_2	.06	1.58	.014	<.005	.69	.01	.04	.02	.08	<.005	.009	<.005	.021	<.005
92.5Ar-7.5CO_2	.06	1.59	.014	<.005	.67	.01	.04	.03	.08	<.005	.010	.005	.020	<.005
90Ar-10CO_2	.06	1.69	.011	<.005	.62	.01	.04	.03	.07	.024	.011	<.005	.034	<.005
87.5Ar-12.5CO_2	.06	1.59	.013	<.005	.73	<.01	.03	.02	.08	.011	.009	<.005	.024	<.005
85Ar-15CO_2	.06	1.55	.014	<.005	.68	<.01	.03	.02	.08	<.005	.008	<.005	.019	<.005
82.5Ar-17.5CO_2	.07	1.56	.014	<.005	.66	.01	.04	.03	.08	.018	.009	<.005	.019	<.005
80Ar-20CO_2	.06	1.56	.014	<.005	.65	.01	.05	.03	.08	<.005	.011	.006	.018	<.005

TABLE 6

HARDNESS TEST RESULTS FOR C-Mn-Ti-B/97.5Ar-2.5CO_2

Type of Test: Vickers Microhardness (500 gram load, 15 sec. time)

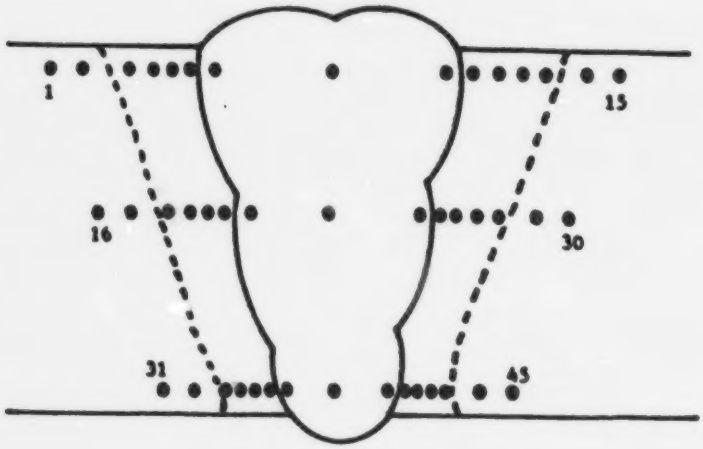

FG - Fine Grain
CG - Coarse Grain

LOCATION	HVN	LOCATION	HVN
1. Parent Metal	161	24. Weld Metal	236
2. Parent Metal	172	25. HAZ (CG)	237
3. HAZ (FG)	196	26. HAZ (CG)	228
4. HAZ (FG)	180	27. HAZ (FG)	188
5. HAZ (CG)	232	28. HAZ (FG)	199
6. HAZ (CG)	226	29. Parent Metal	173
7. Weld Metal	247	30. Parent Metal	166
8. Weld Metal	230	31. Parent Metal	168
9. Weld Metal	240	32. Parent Metal	193
10. HAZ (CG)	240	33. HAZ (FG)	196
11. HAZ (CG)	224	34. HAZ (FG)	217
12. HAZ (FG)	215	35. HAZ (CG)	222
13. HAZ (FG)	214	36. HAZ (CG)	234
14. Parent Metal	178	37. Weld Metal	247
15. Parent Metal	180	38. Weld Metal	253
16. Parent Metal	176	39. Weld Metal	258
17. Parent Metal	183	40. HAZ (CG)	246
18. HAZ (FG)	214	41. HAZ (CG)	233
19. HAZ (FG)	194	42. HAZ (FG)	203
20. HAZ (CG)	234	43. HAZ (FG)	207
21. HAZ (CG)	243	44. Parent Metal	177
22. Weld Metal	222	45. Parent Metal	182
23. Weld Metal	199		

TABLE 7

HARDNESS TEST RESULTS FOR C-Mn-Ti-B/95Ar-5CO_2

Type of Test: Vickers Microhardness (500 gram load, 15 sec. time)

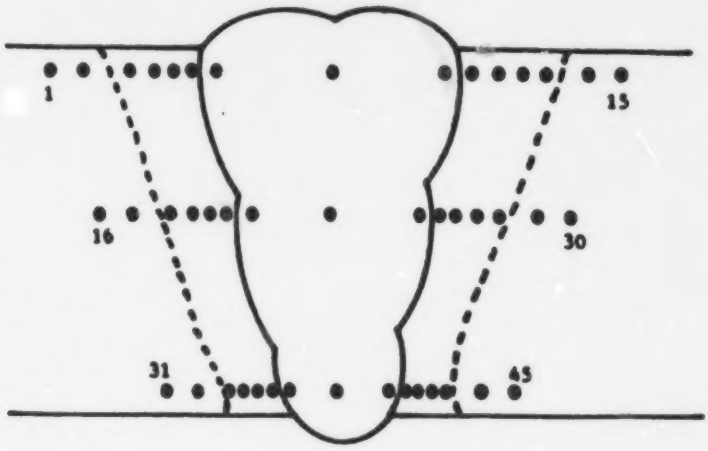

FG - Fine Grain
CG - Coarse Grain

LOCATION	HVN	LOCATION	HVN
1. Parent Metal	187	24. Weld Metal	214
2. Parent Metal	182	25. HAZ (CG)	214
3. HAZ (FG)	192	26. HAZ (CG)	200
4. HAZ (FG)	205	27. HAZ (FG)	197
5. HAZ (CG)	203	28. HAZ (FG)	190
6. HAZ (CG)	228	29. Parent Metal	170
7. Weld Metal	210	30. Parent Metal	162
8. Weld Metal	200	31. Parent Metal	175
9. Weld Metal	210	32. Parent Metal	181
10. HAZ (CG)	253	33. HAZ (FG)	195
11. HAZ (CG)	238	34. HAZ (FG)	202
12. HAZ (FG)	224	35. HAZ (CG)	234
13. HAZ (FG)	212	36. HAZ (CG)	268
14. Parent Metal	175	37. Weld Metal	238
15. Parent Metal	188	38. Weld Metal	258
16. Parent Metal	173	39. Weld Metal	248
17. Parent Metal	183	40. HAZ (CG)	248
18. HAZ (FG)	187	41. HAZ (CG)	227
19. HAZ (FG)	190	42. HAZ (FG)	204
20. HAZ (CG)	250	43. HAZ (FG)	208
21. HAZ (CG)	264	44. Parent Metal	177
22. Weld Metal	201	45. Parent Metal	174
23. Weld Metal	199		

TABLE 8

HARDNESS TEST RESULTS FOR C-Mn-Ti-B/92.5Ar-7.5CO_2

Type of Test: Vickers Microhardness (500 gram load, 15 sec. time)

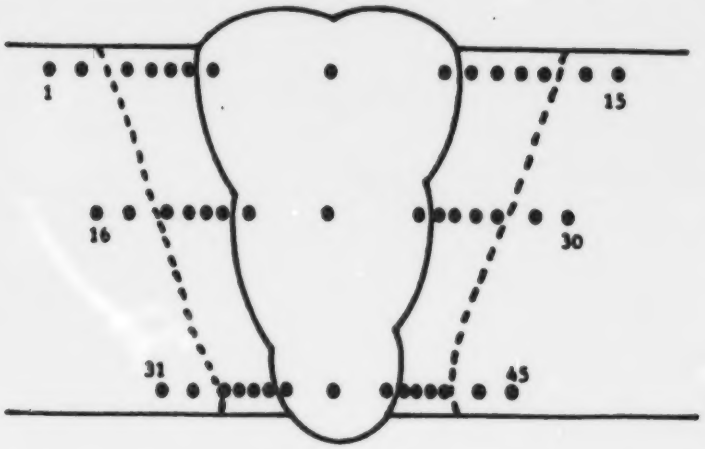

FG - Fine Grain
CG - Coarse Grain

LOCATION	HVN	LOCATION	HVN
1. Parent Metal	166	24. Weld Metal	216
2. Parent Metal	170	25. HAZ (CG)	237
3. HAZ (FG)	193	26. HAZ (CG)	203
4. HAZ (FG)	198	27. HAZ (FG)	186
5. HAZ (CG)	236	28. HAZ (FG)	186
6. HAZ (CG)	231	29. Parent Metal	177
7. Weld Metal	229	30. Parent Metal	193
8. Weld Metal	244	31. Parent Metal	168
9. Weld Metal	235	32. Parent Metal	182
10. HAZ (CG)	247	33. HAZ (FG)	184
11. HAZ (CG)	243	34. HAZ (FG)	196
12. HAZ (FG)	203	35. HAZ (CG)	234
13. HAZ (FG)	195	36. HAZ (CG)	243
14. Parent Metal	177	37. Weld Metal	240
15. Parent Metal	175	38. Weld Metal	235
16. Parent Metal	168	39. Weld Metal	229
17. Parent Metal	164	40. HAZ (CG)	238
18. HAZ (FG)	186	41. HAZ (CG)	214
19. HAZ (FG)	188	42. HAZ (FG)	191
20. HAZ (CG)	213	43. HAZ (FG)	197
21. HAZ (CG)	225	44. Parent Metal	185
22. Weld Metal	208	45. Parent Metal	175
23. Weld Metal	194		

TABLE 9

HARDNESS TEST RESULTS FOR C-Mn-Ti-B/90Ar-10CO_2

Type of Test: Vickers Microhardness (500 gram load, 15 sec. time)

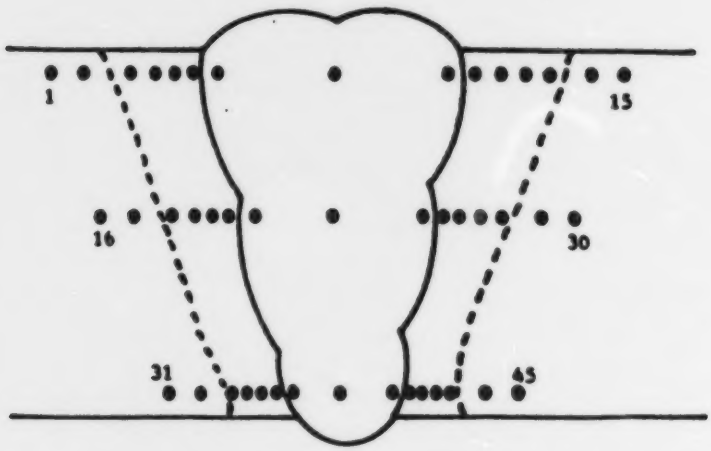

FG - Fine Grain
CG - Coarse Grain

LOCATION	HVN	LOCATION	HVN
1. Parent Metal	177	24. Weld Metal	202
2. Parent Metal	173	25. HAZ (CG)	227
3. HAZ (FG)	197	26. HAZ (CG)	214
4. HAZ (FG)	201	27. HAZ (FG)	189
5. HAZ (CG)	220	28. HAZ (FG)	186
6. HAZ (CG)	222	29. Parent Metal	185
7. Weld Metal	234	30. Parent Metal	163
8. Weld Metal	239	31. Parent Metal	175
9. Weld Metal	168	32. Parent Metal	174
10. HAZ (CG)	234	33. HAZ (FG)	185
11. HAZ (CG)	217	34. HAZ (FG)	191
12. HAZ (FG)	215	35. HAZ (CG)	238
13. HAZ (FG)	193	36. HAZ (CG)	258
14. Parent Metal	169	37. Weld Metal	238
15. Parent Metal	172	38. Weld Metal	232
16. Parent Metal	168	39. Weld Metal	250
17. Parent Metal	174	40. HAZ (CG)	258
18. HAZ (FG)	180	41. HAZ (CG)	248
19. HAZ (FG)	179	42. HAZ (FG)	205
20. HAZ (CG)	224	43. HAZ (FG)	202
21. HAZ (CG)	239	44. Parent Metal	184
22. Weld Metal	208	45. Parent Metal	173
23. Weld Metal	208		

TABLE 10

HARDNESS TEST RESULTS FOR C-Mn-Ti-B/87.5Ar-12.5CO_2

Type of Test: Vickers Microhardness (500 gram load, 15 sec. time)

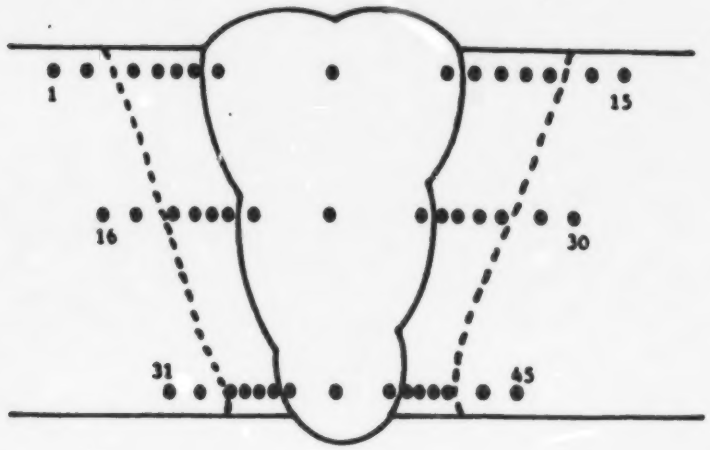

FG - Fine Grain
CG - Coarse Grain

LOCATION	HVN	LOCATION	HVN
1. Parent Metal	177	24. Weld Metal	193
2. Parent Metal	173	25. HAZ (CG)	231
3. HAZ (FG)	173	26. HAZ (CG)	221
4. HAZ (FG)	198	27. HAZ (FG)	181
5. HAZ (CG)	215	28. HAZ (FG)	175
6. HAZ (CG)	216	29. Parent Metal	171
7. Weld Metal	218	30. Parent Metal	178
8. Weld Metal	207	31. Parent Metal	179
9. Weld Metal	226	32. Parent Metal	182
10. HAZ (CG)	228	33. HAZ (FG)	193
11. HAZ (CG)	220	34. HAZ (FG)	202
12. HAZ (FG)	188	35. HAZ (CG)	252
13. HAZ (FG)	190	36. HAZ (CG)	258
14. Parent Metal	183	37. Weld Metal	245
15. Parent Metal	178	38. Weld Metal	235
16. Parent Metal	180	39. Weld Metal	251
17. Parent Metal	189	40. HAZ (CG)	263
18. HAZ (FG)	197	41. HAZ (CG)	236
19. HAZ (FG)	191	42. HAZ (FG)	191
20. HAZ (CG)	216	43. HAZ (FG)	196
21. HAZ (CG)	228	44. Parent Metal	179
22. Weld Metal	209	45. Parent Metal	170
23. Weld Metal	221		

TABLE 11

HARDNESS TEST RESULTS FOR C-Mn-Ti-B/85Ar-15CO_2

Type of Test: Vickers Microhardness (500 gram load, 15 sec. time)

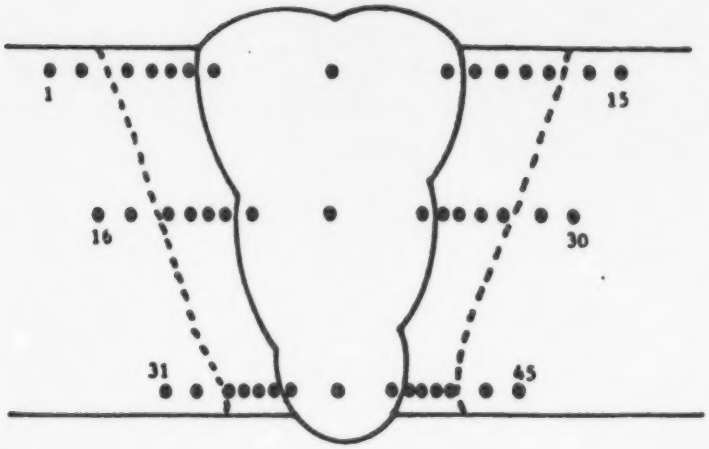

FG - Fine Grain
CG - Coarse Grain

LOCATION	HVN	LOCATION	HVN
1. Parent Metal	186	24. Weld Metal	180
2. Parent Metal	178	25. HAZ (CG)	258
3. HAZ (FG)	177	26. HAZ (CG)	231
4. HAZ (FG)	210	27. HAZ (FG)	201
5. HAZ (CG)	205	28. HAZ (FG)	191
6. HAZ (CG)	219	29. Parent Metal	166
7. Weld Metal	229	30. Parent Metal	178
8. Weld Metal	218	31. Parent Metal	175
9. Weld Metal	235	32. Parent Metal	182
10. HAZ (CG)	221	33. HAZ (FG)	188
11. HAZ (CG)	214	34. HAZ (FG)	202
12. HAZ (FG)	188	35. HAZ (CG)	242
13. HAZ (FG)	180	36. HAZ (CG)	258
14. Parent Metal	177	37. Weld Metal	239
15. Parent Metal	182	38. Weld Metal	234
16. Parent Metal	178	39. Weld Metal	224
17. Parent Metal	177	40. HAZ (CG)	258
18. HAZ (FG)	184	41. HAZ (CG)	245
19. HAZ (FG)	189	42. HAZ (FG)	188
20. HAZ (CG)	204	43. HAZ (FG)	190
21. HAZ (CG)	228	44. Parent Metal	168
22. Weld Metal	183	45. Parent Metal	167
23. Weld Metal	172		

TABLE 12

HARDNESS TEST RESULTS FOR C-Mn-Ti-P/82.5Ar-17.5CO_2

Type of Test: Vickers Microhardness (500 gram load, 15 sec. time)

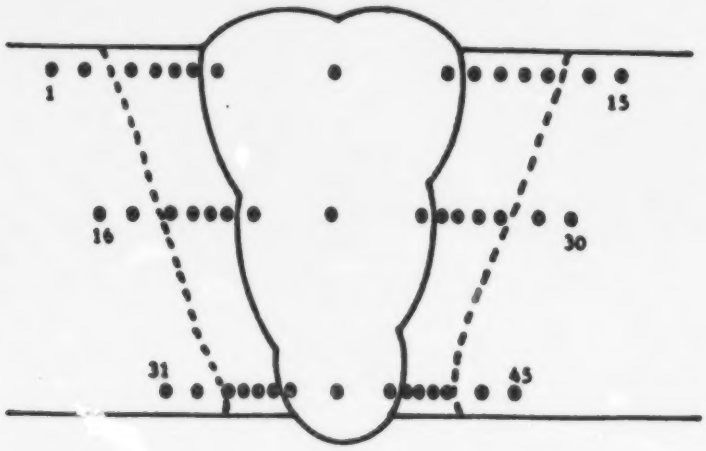

FG - Fine Grain
CG - Coarse Grain

LOCATION	HVN	LOCATION	HVN
1. Parent Metal	187	24. Weld Metal	174
2. Parent Metal	183	25. HAZ (CG)	236
3. HAZ (FG)	186	26. HAZ (CG)	236
4. HAZ (FG)	203	27. HAZ (FG)	193
5. HAZ (CG)	229	28. HAZ (FG)	193
6. HAZ (CG)	239	29. Parent Metal	168
7. Weld Metal	217	30. Parent Metal	182
8. Weld Metal	205	31. Parent Metal	171
9. Weld Metal	236	32. Parent Metal	180
10. HAZ (CG)	228	33. HAZ (FG)	216
11. HAZ (CG)	223	34. HAZ (FG)	205
12. HAZ (FG)	188	35. HAZ (CG)	235
13. HAZ (FG)	198	36. HAZ (CG)	258
14. Parent Metal	179	37. Weld Metal	229
15. Parent Metal	181	38. Weld Metal	224
16. Parent Metal	183	39. Weld Metal	229
17. Parent Metal	173	40. HAZ (CG)	258
18. HAZ (FG)	188	41. HAZ (CG)	215
19. HAZ (FG)	199	42. HAZ (FG)	184
20. HAZ (CG)	210	43. HAZ (FG)	196
21. HAZ (CG)	230	44. Parent Metal	163
22. Weld Metal	195	45. Parent Metal	171
23. Weld Metal	208		

TABLE 13

HARDNESS TEST RESULTS FOR C-Mn-Ti-B/80Ar-20CO_2

Type of Test: Vickers Microhardness (500 gram load, 15 sec. time)

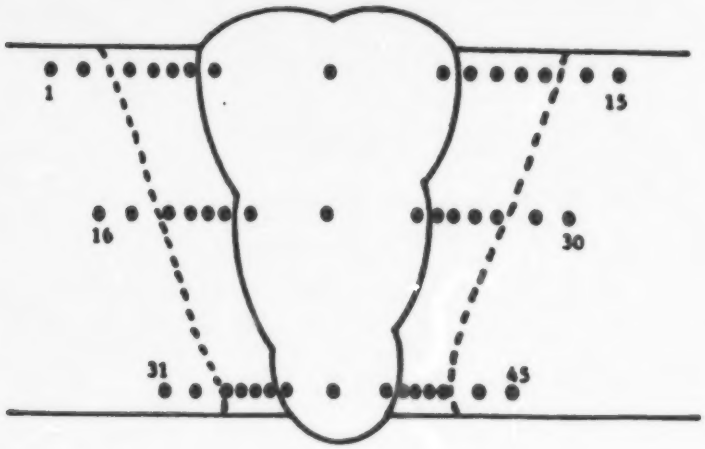

FG - Fine Grain
CG - Coarse Grain

LOCATION	HVN	LOCATION	HVN
1. Parent Metal	171	24. Weld Metal	195
2. Parent Metal	185	25. HAZ (CG)	238
3. HAZ (FG)	196	26. HAZ (CG)	224
4. HAZ (FG)	186	27. HAZ (FG)	197
5. HAZ (CG)	224	28. HAZ (FG)	190
6. HAZ (CG)	213	29. Parent Metal	158
7. Weld Metal	220	30. Parent Metal	169
8. Weld Metal	210	31. Parent Metal	171
9. Weld Metal	214	32. Parent Metal	184
10. HAZ (CG)	226	33. HAZ (FG)	190
11. HAZ (CG)	221	34. HAZ (FG)	205
12. HAZ (FG)	189	35. HAZ (CG)	203
13. HAZ (FG)	193	36. HAZ (CG)	232
14. Parent Metal	176	37. Weld Metal	208
15. Parent Metal	182	38. Weld Metal	227
16. Parent Metal	174	39. Weld Metal	203
17. Parent Metal	162	40. HAZ (CG)	240
18. HAZ (FG)	172	41. HAZ (CG)	230
19. HAZ (FG)	184	42. HAZ (FG)	193
20. HAZ (CG)	217	43. HAZ (FG)	180
21. HAZ (CG)	227	44. Parent Metal	182
22. Weld Metal	168	45. Parent Metal	178
23. Weld Metal	173		

TABLE 14

HARDNESS TEST RESULTS FOR C-Mn-Si-Ti/97.5Ar-2.5CO_2

Type of Test: Vickers Microhardness (500 gram load, 15 sec. time)

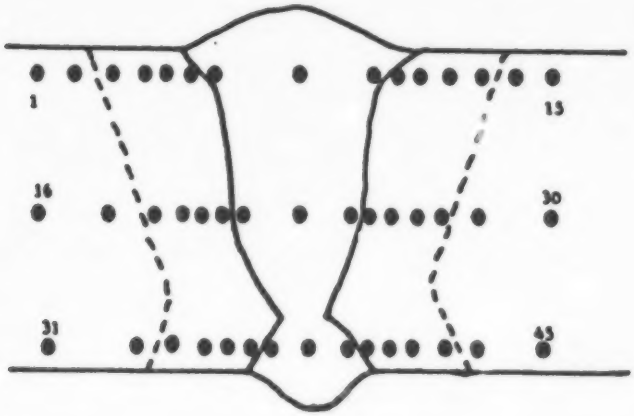

FG - Fine Grain
CG - Coarse Grain

LOCATION	HVN	LOCATION	HVN
1. Parent Metal	216	24. Weld Metal	251
2. Parent Metal	217	25. HAZ (CG)	343
3. HAZ (FG)	245	26. HAZ (CG)	318
4. HAZ (FG)	258	27. HAZ (FG)	269
5. HAZ (CG)	316	28. HAZ (FG)	275
6. HAZ (CG)	338	29. Parent Metal	216
7. Weld Metal	228	30. Parent Metal	234
8. Weld Metal	258	31. Parent Metal	210
9. Weld Metal	254	32. Parent Metal	214
10. HAZ (CG)	340	33. HAZ (FG)	258
11. HAZ (CG)	326	34. HAZ (FG)	271
12. HAZ (FG)	258	35. HAZ (CG)	322
13. HAZ (FG)	246	36. HAZ (CG)	340
14. Parent Metal	222	37. Weld Metal	278
15. Parent Metal	229	38. Weld Metal	289
16. Parent Metal	219	39. Weld Metal	283
17. Parent Metal	220	40. HAZ (CG)	317
18. HAZ (FG)	264	41. HAZ (CG)	335
19. HAZ (FG)	293	42. HAZ (FG)	293
20. HAZ (CG)	339	43. HAZ (FG)	287
21. HAZ (CG)	350	44. Parent Metal	239
22. Weld Metal	245	45. Parent Metal	243
23. Weld Metal	246		

TABLE 15

HARDNESS TEST RESULTS FOR C-Mn-Si-Ti/95Ar-5CO_2

Type of Test: Vickers Microhardness (500 gram load, 15 sec. time)

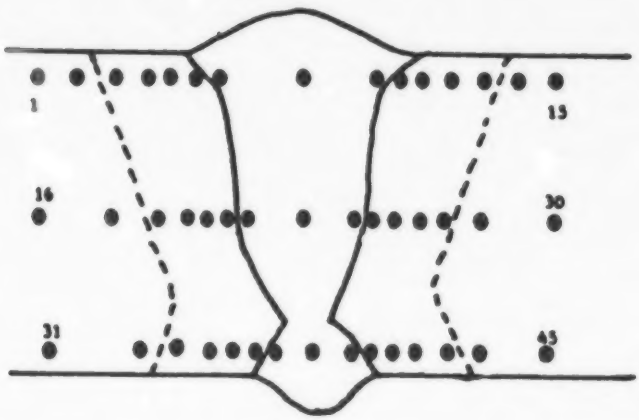

FG - Fine Grain
CG - Coarse Grain

LOCATION	HVN	LOCATION	HVN
1. Parent Metal	225	24. Weld Metal	267
2. Parent Metal	220	25. HAZ (CG)	282
3. HAZ (FG)	238	26. HAZ (CG)	289
4. HAZ (FG)	253	27. HAZ (FG)	279
5. HAZ (CG)	336	28. HAZ (FG)	258
6. HAZ (CG)	343	29. Parent Metal	247
7. Weld Metal	265	30. Parent Metal	218
8. Weld Metal	282	31. Parent Metal	207
9. Weld Metal	258	32. Parent Metal	222
10. HAZ (CG)	359	33. HAZ (FG)	247
11. HAZ (CG)	347	34. HAZ (FG)	248
12. HAZ (FG)	280	35. HAZ (CG)	322
13. HAZ (FG)	263	36. HAZ (CG)	320
14. Parent Metal	224	37. Weld Metal	308
15. Parent Metal	229	38. Weld Metal	293
16. Parent Metal	224	39. Weld Metal	291
17. Parent Metal	224	40. HAZ (CG)	335
18. HAZ (FG)	273	41. HAZ (CG)	336
19. HAZ (FG)	298	42. HAZ (FG)	282
20. HAZ (CG)	309	43. HAZ (FG)	253
21. HAZ (CG)	303	44. Parent Metal	225
22. Weld Metal	252	45. Parent Metal	258
23. Weld Metal	263		

TABLE 16

HARDNESS TEST RESULTS FOR C-Mn-Si-Ti/92.5Ar-7.5CO_2

Type of Test: Vickers Microhardness (500 gram load, 15 sec. time)

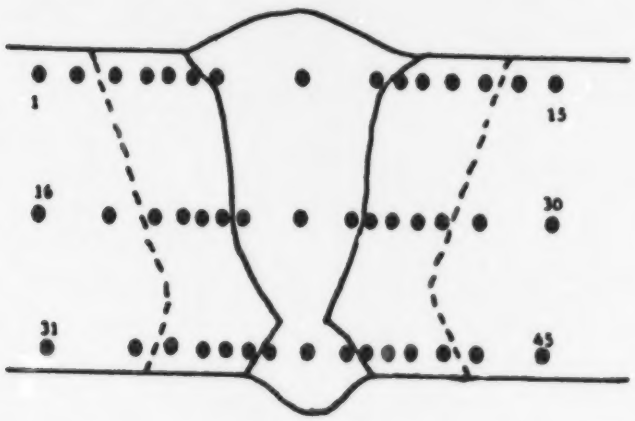

FG - Fine Grain
CG - Coarse Grain

LOCATION	HVN	LOCATION	HVN
1. Parent Metal	224	24. Weld Metal	248
2. Parent Metal	232	25. HAZ (CG)	330
3. HAZ (FG)	236	26. HAZ (CG)	331
4. HAZ (FG)	258	27. HAZ (FG)	246
5. HAZ (CG)	324	28. HAZ (FG)	258
6. HAZ (CG)	340	29. Parent Metal	244
7. Weld Metal	258	30. Parent Metal	240
8. Weld Metal	274	31. Parent Metal	211
9. Weld Metal	258	32. Parent Metal	220
10. HAZ (CG)	338	33. HAZ (FG)	258
11. HAZ (CG)	336	34. HAZ (FG)	262
12. HAZ (FG)	258	35. HAZ (CG)	316
13. HAZ (FG)	239	36. HAZ (CG)	330
14. Parent Metal	220	37. Weld Metal	291
15. Parent Metal	233	38. Weld Metal	297
16. Parent Metal	211	39. Weld Metal	282
17. Parent Metal	220	40. HAZ (CG)	313
18. HAZ (FG)	264	41. HAZ (CG)	303
19. HAZ (FG)	258	42. HAZ (FG)	258
20. HAZ (CG)	304	43. HAZ (FG)	242
21. HAZ (CG)	333	44. Parent Metal	224
22. Weld Metal	258	45. Parent Metal	231
23. Weld Metal	258		

TABLE 17

HARDNESS TEST RESULTS FOR C-Mn-Si-Ti/90Ar-10CO_2

Type of Test: Vickers Microhardness (500 gram load, 15 sec. time)

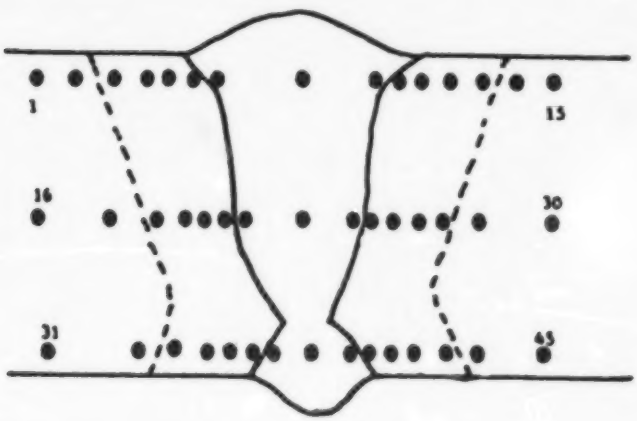

FG - Fine Grain
CG - Coarse Grain

LOCATION	HVN	LOCATION	HVN
1. Parent Metal	226	24. Weld Metal	258
2. Parent Metal	223	25. HAZ (CG)	328
3. HAZ (FG)	232	26. HAZ (CG)	316
4. HAZ (FG)	248	27. HAZ (FG)	281
5. HAZ (CG)	320	28. HAZ (FG)	258
6. HAZ (CG)	336	29. Parent Metal	226
7. Weld Metal	258	30. Parent Metal	230
8. Weld Metal	243	31. Parent Metal	220
9. Weld Metal	242	32. Parent Metal	224
10. HAZ (CG)	365	33. HAZ (FG)	258
11. HAZ (CG)	334	34. HAZ (FG)	268
12. HAZ (FG)	258	35. HAZ (CG)	322
13. HAZ (FG)	246	36. HAZ (CG)	315
14. Parent Metal	220	37. Weld Metal	298
15. Parent Metal	224	38. Weld Metal	291
16. Parent Metal	224	39. Weld Metal	296
17. Parent Metal	220	40. HAZ (CG)	326
18. HAZ (FG)	265	41. HAZ (CG)	316
19. HAZ (FG)	281	42. HAZ (FG)	279
20. HAZ (CG)	280	43. HAZ (FG)	249
21. HAZ (CG)	271	44. Parent Metal	231
22. Weld Metal	247	45. Parent Metal	218
23. Weld Metal	246		

TABLE 18

HARDNESS TEST RESULTS FOR C-Mn-Si-Ti/87.5Ar-12.5CO_2

Type of Test: Vickers Microhardness (500 gram load, 15 sec. time)

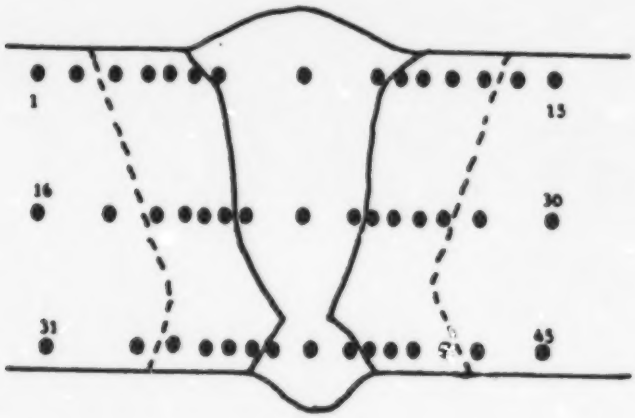

FG - Fine Grain
CG - Coarse Grain

LOCATION	HVN	LOCATION	HVN
1. Parent Metal	224	24. Weld Metal	258
2. Parent Metal	234	25. HAZ (CG)	320
3. HAZ (FG)	236	26. HAZ (CG)	310
4. HAZ (FG)	243	27. HAZ (FG)	258
5. HAZ (CG)	339	28. HAZ (FG)	258
6. HAZ (CG)	326	29. Parent Metal	220
7. Weld Metal	268	30. Parent Metal	220
8. Weld Metal	258	31. Parent Metal	258
9. Weld Metal	258	32. Parent Metal	229
10. HAZ (CG)	333	33. HAZ (FG)	245
11. HAZ (CG)	334	34. HAZ (FG)	253
12. HAZ (FG)	285	35. HAZ (CG)	317
13. HAZ (FG)	244	36. HAZ (CG)	318
14. Parent Metal	221	37. Weld Metal	309
15. Parent Metal	234	38. Weld Metal	301
16. Parent Metal	231	39. Weld Metal	304
17. Parent Metal	228	40. HAZ (CG)	312
18. HAZ (FG)	273	41. HAZ (CG)	315
19. HAZ (FG)	258	42. HAZ (FG)	282
20. HAZ (CG)	309	43. HAZ (FG)	258
21. HAZ (CG)	316	44. Parent Metal	226
22. Weld Metal	240	45. Parent Metal	229
23. Weld Metal	258		

TABLE 19

HARDNESS TEST RESULTS FOR C-Mn-Si-Ti/85Ar-15CO_2

Type of Test: Vickers Microhardness (500 gram load, 15 sec. time)

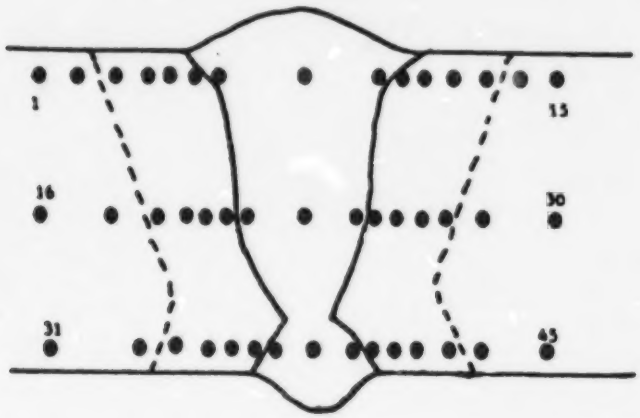

FG - Fine Grain
CG - Coarse Grain

LOCATION	HVN	LOCATION	HVN
1. Parent Metal	244	24. Weld Metal	244
2. Parent Metal	235	25. HAZ (CG)	317
3. HAZ (FG)	258	26. HAZ (CG)	307
4. HAZ (FG)	307	27. HAZ (FG)	272
5. HAZ (CG)	340	28. HAZ (FG)	258
6. HAZ (CG)	338	29. Parent Metal	242
7. Weld Metal	278	30. Parent Metal	225
8. Weld Metal	268	31. Parent Metal	251
9. Weld Metal	274	32. Parent Metal	243
10. HAZ (CG)	319	33. HAZ (FG)	278
11. HAZ (CG)	333	34. HAZ (FG)	268
12. HAZ (FG)	269	35. HAZ (CG)	338
13. HAZ (FG)	258	36. HAZ (CG)	328
14. Parent Metal	220	37. Weld Metal	310
15. Parent Metal	220	38. Weld Metal	309
16. Parent Metal	236	39. Weld Metal	302
17. Parent Metal	239	40. HAZ (CG)	329
18. HAZ (FG)	266	41. HAZ (CG)	320
19. HAZ (FG)	289	42. HAZ (FG)	274
20. HAZ (CG)	298	43. HAZ (FG)	251
21. HAZ (CG)	335	44. Parent Metal	228
22. Weld Metal	269	45. Parent Metal	221
23. Weld Metal	264		

TABLE 20

HARDNESS TEST RESULTS FOR C-Mn-Si-Ti/82.5Ar-17.5CO_2

Type of Test: Vickers Microhardness (500 gram load, 15 sec. time)

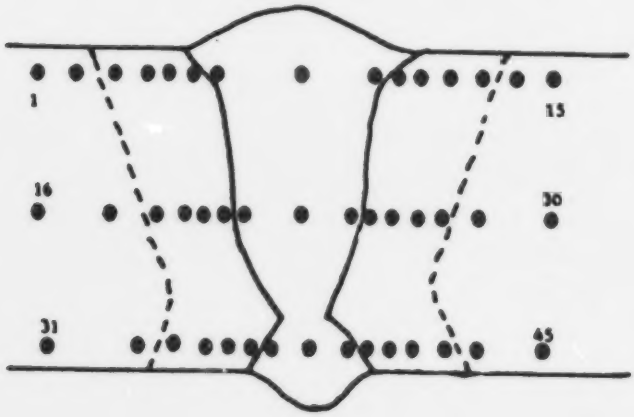

FG - Fine Grain
CG - Coarse Grain

LOCATION	HVN	LOCATION	HVN
1. Parent Metal	222	24. Weld Metal	235
2. Parent Metal	225	25. HAZ (CG)	294
3. HAZ (FG)	246	26. HAZ (CG)	316
4. HAZ (FG)	220	27. HAZ (FG)	258
5. HAZ (CG)	289	28. HAZ (FG)	258
6. HAZ (CG)	300	29. Parent Metal	218
7. Weld Metal	252	30. Parent Metal	220
8. Weld Metal	252	31. Parent Metal	228
9. Weld Metal	239	32. Parent Metal	238
10. HAZ (CG)	298	33. HAZ (FG)	240
11. HAZ (CG)	278	34. HAZ (FG)	258
12. HAZ (FG)	248	35. HAZ (CG)	331
13. HAZ (FG)	241	36. HAZ (CG)	346
14. Parent Metal	228	37. Weld Metal	299
15. Parent Metal	214	38. Weld Metal	309
16. Parent Metal	241	39. Weld Metal	318
17. Parent Metal	248	40. HAZ (CG)	333
18. HAZ (FG)	253	41. HAZ (CG)	318
19. HAZ (FG)	258	42. HAZ (FG)	265
20. HAZ (CG)	302	43. HAZ (FG)	268
21. HAZ (CG)	310	44. Parent Metal	205
22. Weld Metal	238	45. Parent Metal	226
23. Weld Metal	232		

TABLE 21

HARDNESS TEST RESULTS FOR C-mn-Si-Ti/80Ar-20CO_2

Type of Test: Vickers Microhardness (500 gram load, 15 sec. time)

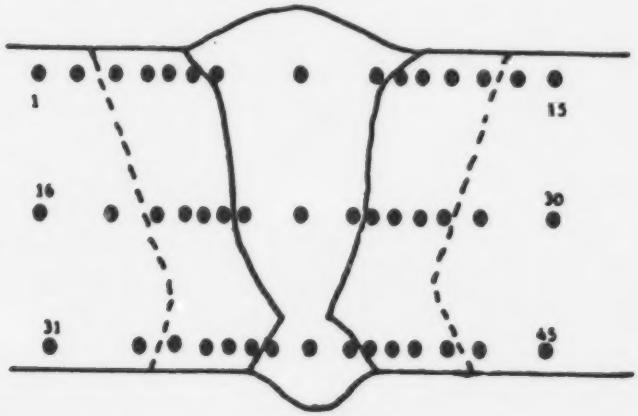

FG - Fine Grain
CG - Coarse Grain

LOCATION	HVN	LOCATION	HVN
1. Parent Metal	220	24. Weld Metal	238
2. Parent Metal	239	25. HAZ (CG)	287
3. HAZ (FG)	263	26. HAZ (CG)	279
4. HAZ (FG)	251	27. HAZ (FG)	258
5. HAZ (CG)	313	28. HAZ (FG)	251
6. HAZ (CG)	309	29. Parent Metal	240
7. Weld Metal	247	30. Parent Metal	237
8. Weld Metal	248	31. Parent Metal	210
9. Weld Metal	253	32. Parent Metal	225
10. HAZ (CG)	311	33. HAZ (FG)	258
11. HAZ (CG)	303	34. HAZ (FG)	278
12. HAZ (FG)	258	35. HAZ (CG)	326
13. HAZ (FG)	258	36. HAZ (CG)	320
14. Parent Metal	225	37. Weld Metal	285
15. Parent Metal	215	38. Weld Metal	294
16. Parent Metal	236	39. Weld Metal	289
17. Parent Metal	235	40. HAZ (CG)	325
18. HAZ (FG)	258	41. HAZ (CG)	320
19. HAZ (FG)	264	42. HAZ (FG)	299
20. HAZ (CG)	278	43. HAZ (FG)	275
21. HAZ (CG)	310	44. Parent Metal	258
22. Weld Metal	239	45. Parent Metal	268
23. Weld Metal	253		

TABLE 22

SUMMARY OF WELD-METAL HARDNESS TEST RESULTS

a) Electrode: C-Mn-Ti-B

Shielding Gas	Weld Metal Hardness, Hv 0.5 kg		
	Subsurface	Centre	Bottom
97.5Ar-2.5CO_2	230 - 247 / 239	199 - 236 / 219	247 - 258 / 253
95Ar-5CO_2	200 - 210 / 207	199 - 214 / 205	238 - 258 / 248
92.5Ar-7.5CO_2	229 - 244 / 236	194 - 216 / 206	229 - 240 / 235
90Ar-10CO_2	168 - 239 / 214	202 - 208 / 206	232 - 250 / 240
87.5Ar-12.5CO_2	207 - 226 / 217	193 - 221 / 208	235 - 251 / 244
85Ar-15CO_2	218 - 235 / 227	172 - 183 / 178	224 - 239 / 232
82.5Ar-17.5CO_2	205 - 236 / 219	174 - 208 / 192	224 - 229 / 227
80Ar-20CO_2	210 - 220 / 215	168 - 195 / 179	203 - 227 / 213

TABLE 22 (cont)

SUMMARY OF WELD METAL HARDNESS TEST RESULTS

b) Electrode: C-Mn-Si-Ti

Shielding Gas	Weld Metal Hardness, Hv 0.5 kg		
	Subsurface	Centre	Bottom
97.5Ar-2.5CO_2	228 - 258 / 247	245 - 251 / 247	278 - 289 / 283
95Ar-5CO_2	258 - 282 / 268	252 - 267 / 261	291 - 308 / 297
92.5Ar-7.5CO_2	258 - 274 / 263	248 - 258 / 255	282 - 297 / 290
90Ar-10CO_2	242 - 258 / 248	246 - 258 / 250	291 - 298 / 295
87.5Ar-12.5CO_2	258 - 268 / 261	240 - 258 / 252	301 - 309 / 305
85Ar-15CO_2	268 - 278 / 273	244 - 269 / 259	302 - 310 / 307
82.5Ar-17.5CO_2	239 - 252 / 248	232 - 238 / 235	299 - 318 / 309
80Ar-20.0CO_2	247 - 253 / 249	238 - 253 / 243	285 - 294 / 289

TABLE 23

VERTICAL UP ALL-WELD-METAL TENSILE PROPERTIES

a) Electrode: C-Mn-Ti-B

Shielding Gas	YS MPa	UTS MPa	Elong. %	RA %
97.5Ar-2.5CO_2	616	691	26	78
95Ar-5CO_2	549	635	31	73
92.5Ar-7.5CO_2	548	631	29	77
90Ar-10CO_2	542	637	29	76
87.5Ar-12.5CO_2	524	615	28	76
85Ar-15CO_2	508	602	31	79
82.5Ar-17.5CO_2	498	601	29	72
80Ar-20CO_2	491	589	32	79

TABLE 23 (cont)

VERTICAL DOWN ALL-WELD-METAL TENSILE PROPERTIES

b) Electrode: C-Mn-Si-Ti

Shielding Gas	YS MPa	UTS MPa	Elong. %	RA %
97.5Ar-2.5CO_2	638	719	13	60
95Ar-5CO_2	650	742	18	67
92.5Ar-7.5CO_2	665	743	16	62
90Ar-10CO_2	653	724	17	66
87.5Ar-12.5CO_2	636	712	19	67
85Ar-15CO_2	657	731	19	66
82.5Ar-17.5CO_2	640	720	16	64
80Ar-20CO_2	674	735	16	67

TABLE 24

VERTICAL UP CHARPY IMPACT TEST RESULTS

Electrode: C-Mn-Ti-B
Temperature: -45°C

Shielding Gas	Location	Cv Energy J	Shear Area %
97.5Ar-2.5CO_2	Subsurface	220	77
	"	192	72
	"	216	81
95Ar-5CO_2	"	109	26
	"	109	45
	"	101	35
92.5Ar-7.5CO_2	"	205	66
	"	205	75
	"	225	75
90Ar-10CO_2	"	222	88
	"	256	90
	"	235	90
87.5Ar-12.5CO_2	"	239	85
	"	207	80
	"	239	85
85Ar-15CO_2	"	203	72
	"	206	77
	"	206	82
82.5Ar-17.5CO_2	"	181	62
	"	184	75
	"	207	85
80Ar-20CO_2	"	245	86
	"	206	79
	"	232	90

TABLE 25

VERTICAL UP CTOD TEST RESULTS

Electrode: C-Mn-Ti-B
Temperature: -45°C

Shielding Gas	CTOD mm
97.5Ar-2.5CO_2	0.035
	0.083
	0.334*
95Ar-5CO_2	0.209*
	0.390*
	0.732*
92.5Ar-7.5CO_2	0.799**
	0.810**
	0.781**
90Ar-10CO_2	0.809**
	0.789**
	0.772**
87.5Ar-12.5CO_2	0.792**
	0.792**
	0.802**
85Ar-15CO_2	0.785**
	0.261*
	0.796**
82.5Ar-17.5CO_2	0.132*
	0.138*
	0.267*
80Ar-20CO_2	0.810**
	0.812**
	0.817**

* Indicates δ_u
** Indicates δ_m
All other values δ_c

TABLE 26

VERTICAL DOWN CHARPY IMPACT TEST RESULTS

Electrode: C-Mn-Si-Ti
Temperature: -5°C

Shielding Gas	Location	Cv Energy Joules	Shear Area %
97.5Ar-2.5CO_2	Subsurface	37	35
	"	72	40
	"	53	35
95Ar-5CO_2	"	37	30
	"	37	43
	"	49	30
92.5Ar-7.5CO_2	"	104	2
	"	92	59
	"	102	66
90Ar-10CO_2	"	115	62
	"	110	60
	"	121	59
87.5Ar-12.5CO_2	"	132	75
	"	128	77
	"	129	70
85Ar-15CO_2	"	123	69
	"	126	72
	"	129	70
82.5Ar-17.5CO_2	"	143	80
	"	133	85
	"	134	80
80Ar-20CO_2	"	118	81
	"	125	80
	"	131	77

TABLE 27

VERTICAL DOWN CTOD TEST RESULTS

Electrode: C-Mn-Si-Ti
Temperature: -5°C

Shielding Gas	CTOD mm
97.5Ar-2.5CO_2	0.067
	0.031
	0.039
95Ar-5CO_2	0.053
	0.042
	0.037
92.5Ar-7.5CO_2	0.151*
	0.075*
	0.082
90Ar-10CO_2	0.243*
	0.445**
	0.149*
87.5Ar-12.5CO_2	0.342**
	0.329**
	0.329*
85Ar-15CO_2	0.421**
	0.358**
	0.324**
87.5Ar-17.5CO_2	0.353**
	0.312**
	0.323**
80Ar-20CO_2	0.253**
	0.255**
	0.333**

* Indicates δ_u
** Indicates δ_m
All other values δ_c

TABLE 28

PROPORTION OF REFINED MICROSTRUCTURE IN NOTCH PLANE
OF IMPACT TESTPIECES

Electrode: C-Mn-Ti-B

Shielding Gas	% Refined Microstructure
97.5Ar-2.5CO_2	62
95Ar-5CO_2	60
92.5Ar-7.5CO_2	50
90Ar-10CO_2	50
87.5Ar-12.5CO_2	52
85Ar-15CO_2	50
82.5Ar-17.5CO_2	59
80Ar-20CO_2	56

TABLE 29

FINAL WELDING PROCEDURE WITH C-Mn-Ti-B CONSUMABLE

Wire Diameter and Type: 1.2 mm Kobe MGS-50LT
Shielding Gas: 82Ar-10He-6CO_2-2O_2
Power Source: NOVA/NHRC GMA Pulse Power Regulator
Plate Thickness and Type: 30 mm Lloyds LT-60

Joint/Preparation Details

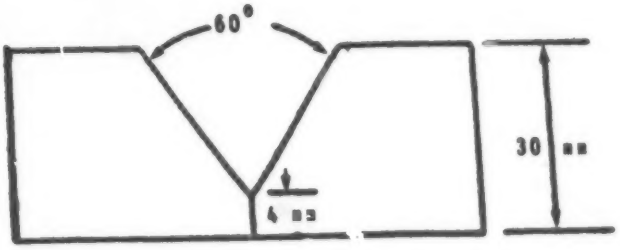

Bead Placement

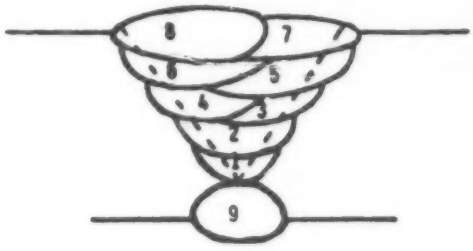

Welding Parameters

Pass	Wire Feed Speed (mm/min)	Travel (mm/min)	Oscillation Width (mm)	Oscillation Velocity (mm/s)	Stickout (mm)	Dwell L (s)	Dwell R (s)	Arc Voltage (V)	Mean Current (A)
1	4050	111	5	112	12.7	1.0	1.0	20.0	160
2	3750	68	12	81	12.7	1.2	1.2	20.0	150
3	3750	68	8	81	12.7	0	1.2	20.5	150
4	3750	68	8	81	12.7	1.2	0.8	20.5	150
5	3750	68	11	71	12.7	1.2	1.8	20.5	150
6	3750	68	11	71	12.7	1.8	1.8	20.5	150
7	3750	62	16	71	12.7	1.4	1.8	22.0	150
8	3750	62	17	61	12.7	1.8	1.8	22.0	150
9	3750	77	13	71	12.7	1.4	1.4	21.5	150

Pulse Parameters

Mean Current A	Peak Current A	Time at Peak ms	Background Current A	Frequency Hz
160	350	3.5	86	80
150	350	3.5	78	75

TABLE 30

FINAL WELDING PROCEDURE WITH C-Mn-Si-Ti CONSUMABLE

Wire Diameter and Type: 0.9 mm Thyssen K-NOVA
Shielding Gas: 82.5Ar-5He-12.5CO_2
Power Source: NOVA/NHRC GMA Pulse Power Regulator
Plate Thickness and Type: CSA Z245.1 19 mm W.T. X 1067 mm O.D. X Gr. 483

Joint/Preparation Details

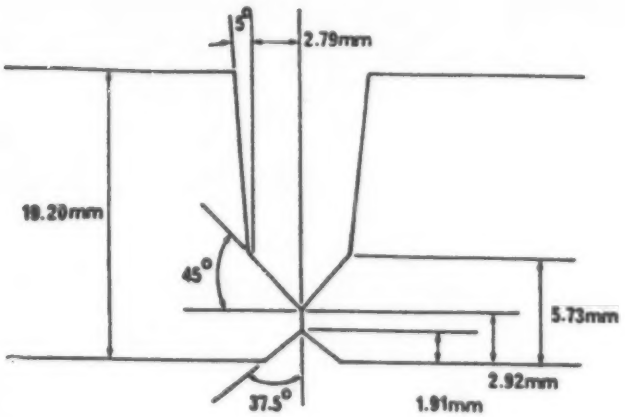

Bead Placement

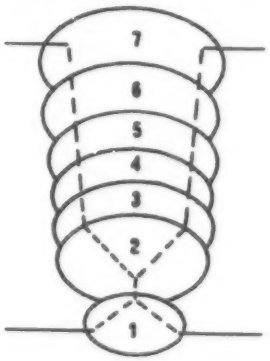

Welding Parameters

Pass	Wire Feed Speed (mm/min)	Travel (mm/min)	Oscillation Width (mm)	Oscillation Speed (beads/min)	Stickout (mm)	Dwell L (s)	Dwell R (s)	Arc Voltage (V)	Mean Current (A)
1	11900	710	-	-	9.0	-	-	24	200
2	12950	1270	-	-	9.0	-	-	24	220
3	11900	360	2.5-3.0	146-134	9.0	.25	.25	23	200
4	11900	360	2.5-3.3	146-132	9.0	.25	.25	23	200
5	11900	360	2.8-3.7	136-130	9.0	.25	.25	23	200
6	11900	360	2.8-4.7	136-124	9.0	.25	.25	23	200
7	8380	330	7.5-11	160-112	12.7	-	-	23.5	150

Pulse Parameters

Mean Current A	Peak Current A	Time at Peak ms	Background Current A	Frequency Hz
200	350	3.0	91	140
220	350	3.0	109	154
150	350	3.0	58	105

TABLE 31

WELD METAL CHEMICAL COMPOSITION OF PROCEDURE QUALIFICATION WELDS

a) Electrode: C-Mn-Ti-B

Shielding Gas	C	Mn	P	S	Si	Ni	Cr	Mo	Cu	Al	V	Nb	Ti	B	O	N
Ar-10He-6CO_2-2O_2	.06	1.37	.008	<.005	.24	.02	.13	.03	.14	<.005	.009	.007	.017	.0043	.027	.0068

b) Electrode: C-Mn-Si-Ti

Shielding Gas	C	Mn	P	S	Si	Ni	Cr	Mo	Cu	Al	V	Nb	Ti	B	O	N
Ar-5He-12.5CO_2	.08	1.35	.009	.008	.52	.02	.09	.05	.12	<.005	.012	.011	.012	<.0005	.028	.0085

TABLE 32

HARDNESS TEST RESULTS FOR C-Mn-Ti-B/Ar-10He-6CO_2-2O_2

Type of test: Vickers Microhardness (500 gram load, 15 sec. time)

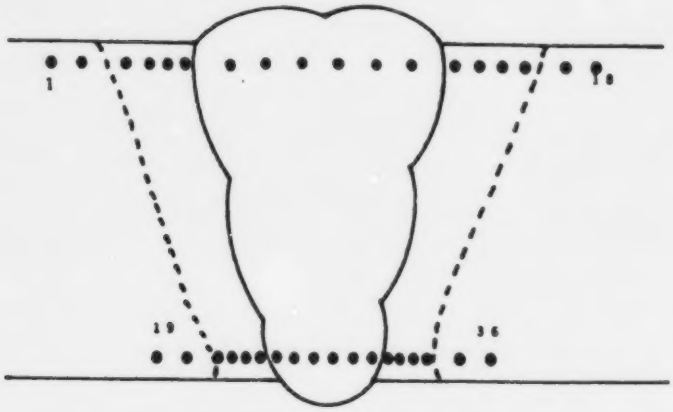

FG - Fine Grain
CG - Coarse Grain

LOCATION	HVN	LOCATION	HVN
1. Parent Metal	163	19. Parent Metal	154
2. Parent Metal	186	20. Parent Metal	182
3. HAZ (FG)	190	21. HAZ (FG)	240
4. HAZ (FG)	199	22. HAZ (FG)	242
5. HAZ (CG)	207	23. HAZ (CG)	236
6. HAZ (CG)	220	24. HAZ (CG)	244
7. Weld Metal	202	25. Weld Metal	240
8. Weld Metal	201	26. Weld Metal	235
9. Weld Metal	205	27. Weld Metal	230
10. Weld Metal	210	28. Weld Metal	234
11. Weld Metal	208	29. Weld Metal	234
12. Weld Metal	214	30. Weld Metal	234
13. HAZ (CG)	200	31. HAZ (CG)	258
14. HAZ (CG)	190	32. HAZ (CG)	255
15. HAZ (FG)	194	33. HAZ (FG)	225
16. HAZ (FG)	182	34. HAZ (FG)	217
17. Parent Metal	166	35. Parent Metal	185
18. Parent Metal	154	36. Parent Metal	168

TABLE 33

HARDNESS TEST RESULTS FOR C-Mn-Si-Ti/Ar-5He-12.5CO_2

Type of Test: Vickers Microhardness (500 gram load, 15 sec. time)

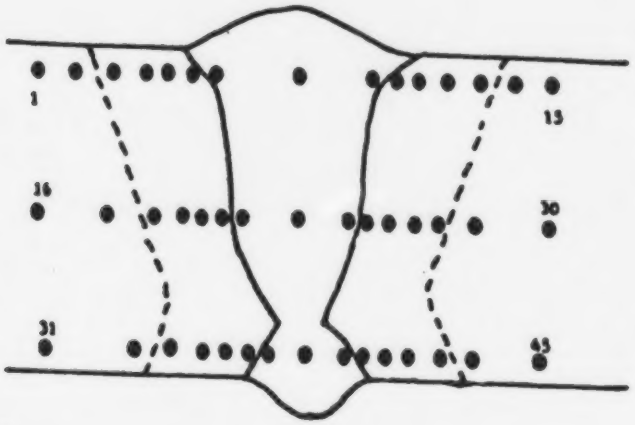

FG - Fine Grain
CG - Coarse Grain

LOCATION	HVN	LOCATION	HVN
1. Parent Metal	217	24. Weld Metal	261
2. Parent Metal	221	25. HAZ (CG)	339
3. HAZ (FG)	225	26. HAZ (CG)	356
4. HAZ (FG)	231	27. HAZ (FG)	304
5. HAZ (CG)	275	28. HAZ (FG)	267
6. HAZ (CG)	291	29. Parent Metal	183
7. Weld Metal	248	30. Parent Metal	230
8. Weld Metal	240	31. Parent Metal	248
9. Weld Metal	271	32. Parent Metal	208
10. HAZ (CG)	350	33. HAZ (FG)	264
11. HAZ (CG)	324	34. HAZ (FG)	280
12. HAZ (FG)	278	35. HAZ (CG)	329
13. HAZ (FG)	261	36. HAZ (CG)	294
14. Parent Metal	231	37. Weld Metal	259
15. Parent Metal	226	38. Weld Metal	258
16. Parent Metal	214	39. Weld Metal	261
17. Parent Metal	213	40. HAZ (CG)	275
18. HAZ (FG)	265	41. HAZ (CG)	291
19. HAZ (FG)	253	42. HAZ (FG)	312
20. HAZ (CG)	285	43. HAZ (FG)	280
21. HAZ (CG)	320	44. Parent Metal	220
22. Weld Metal	215	45. Parent Metal	234
23. Weld Metal	262		

TABLE 34

SUMMARY OF WELD METAL HARDNESS TEST
RESULTS FOR PROCEDURE QUALIFICATION WELDS

a) Electrode: C-Mn-Ti-B

Shielding Gas	Weld Metal Hardness, Hv 0.5 kg	
	Subsurface	Root
Ar-10He-6CO_2-2O_2	201 - 214 / 207	230 - 240 / 236

b) Electrode: C-Mn-Si-Ti

Shielding Gas	Weld Metal Hardness, Hv 0.5 kg		
	Subsurface	Centre	Root
Ar-5He-12.5CO_2	240 - 271 / 253	215 - 262 / 246	258 - 261 / 259

TABLE 35

TRANSVERSE TENSILE PROPERTIES
OF PROCEDURE QUALIFICATION TEST WELDS

a) Wire/Shielding Gas: C-Mn-Ti-B/Ar-10He-6CO_2-2O_2

Test Specimen	YS MPa	UTS MPa	Elong. %	Fracture Location
T1	419	549	46	Parent Metal
T2	418	547	45	Parent Metal

b) Wire/Shielding Gas: C-Mn-Si-Ti/Ar-5He-12.5CO_2

Test Specimen	YS MPa	UTS MPa	Elong. %	Fracture Location
T1	587	718	31	Parent Metal
T2	607	727	32	Parent Metal
T3	602	725	30	Parent Metal
T4	598	706	30	Parent Metal

TABLE 36

CHARPY IMPACT TEST RESULTS OF
PROCEDURE QUALIFICATION TEST WELDS

a) Wire/Shielding Gas: C-Mn-Ti-B/Ar-10He-6CO_2-2O_2
Temperature: -45°C

Location	Cv Energy J	Shear Area %
WELD	193	75
"	204	72
"	239	83
FUSION LINE	10	6
"	12	6
"	7	6
2mm from F.L.	18	5
"	11	5
"	10	5
5mm from F.L.	127	50
"	136	45
"	137	50

b) Wire/Shielding Gas: C-Mn-Si-Ti/Ar-5He-12.5CO_2
Temperature: -5°C

Location	Cv Energy J	Shear Area %
WELD	114	75
"	120	85
"	124	100
HAZ	220	100
"	289	100
"	187	74

TABLE 37

CTOD TEST RESULTS OF PROCEDURE
QUALIFICATION TEST WELDS

a) Electrode: C-Mn-Ti-B
Temperature: -45°C

Shielding Gas	CTOD mm
Ar-10He-6CO_2-2O_2	0.278
	0.232
	0.315

b) Electrode: C-Mn-Si-Ti
Temperature: -5°C

Shielding Gas	CTOD mm
Ar-5He-12.5CO_2	* 0.274
	* 0.290
	* 0.305

* Indicates δ_m; All other values δ_u.

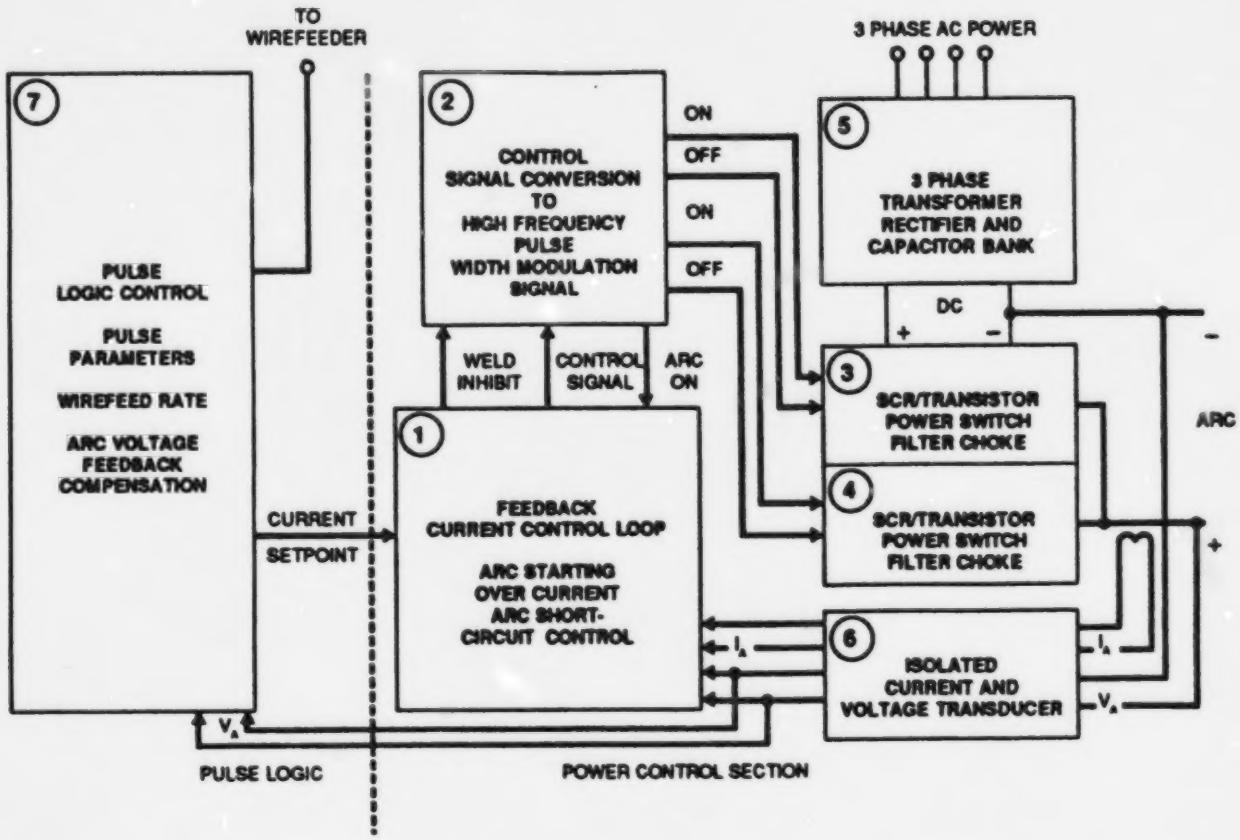

Figure 1: GEC M450PS Programmable/Synergic Pulsed GMAW Power Source.

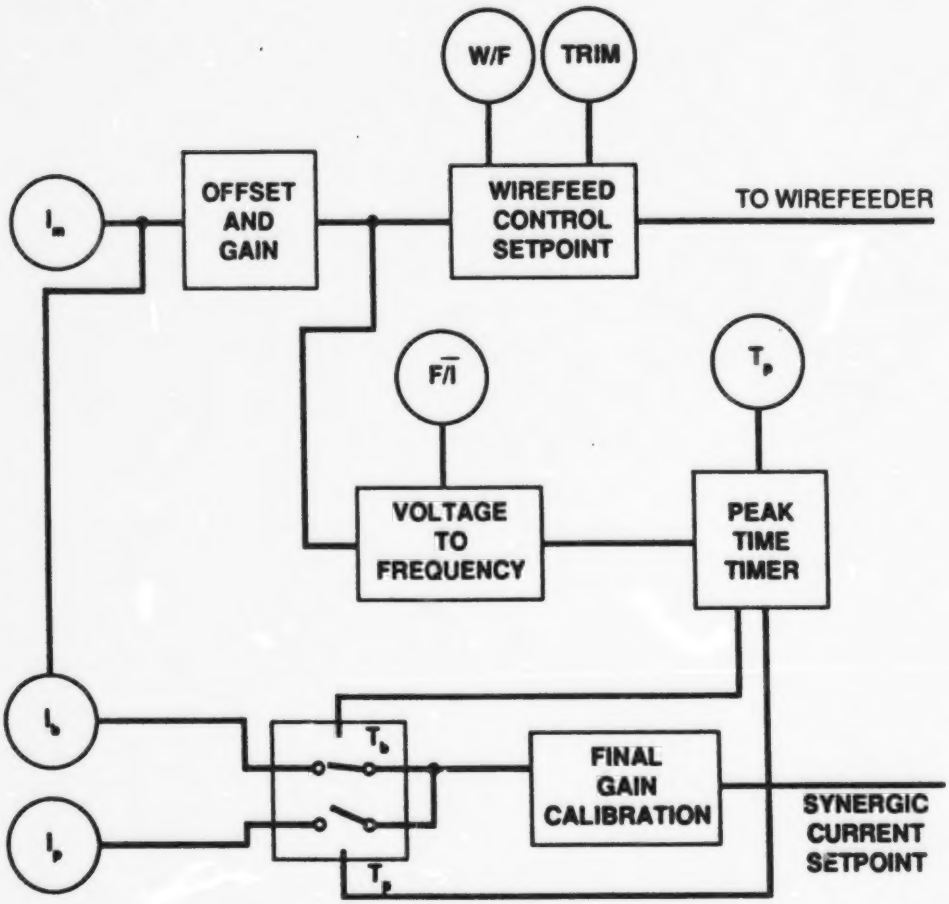

Figure 2: M450PS Modified Synergic Pulse Logic Circuit.

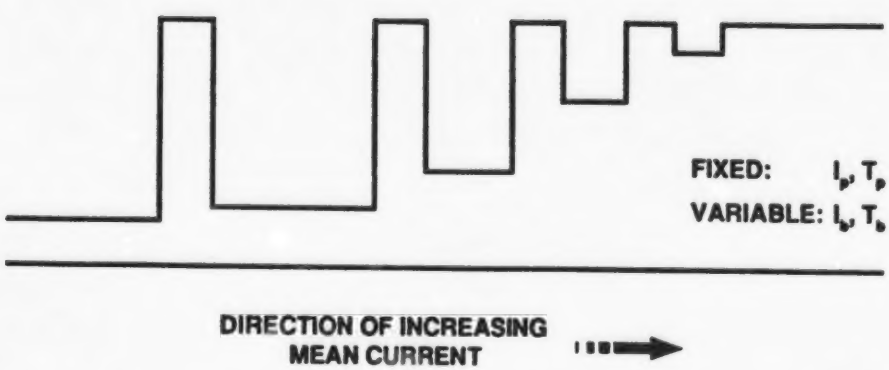

Figure 3: M450PS Synergic Waveform as Modified to Maintain One Drop Per Pulse.

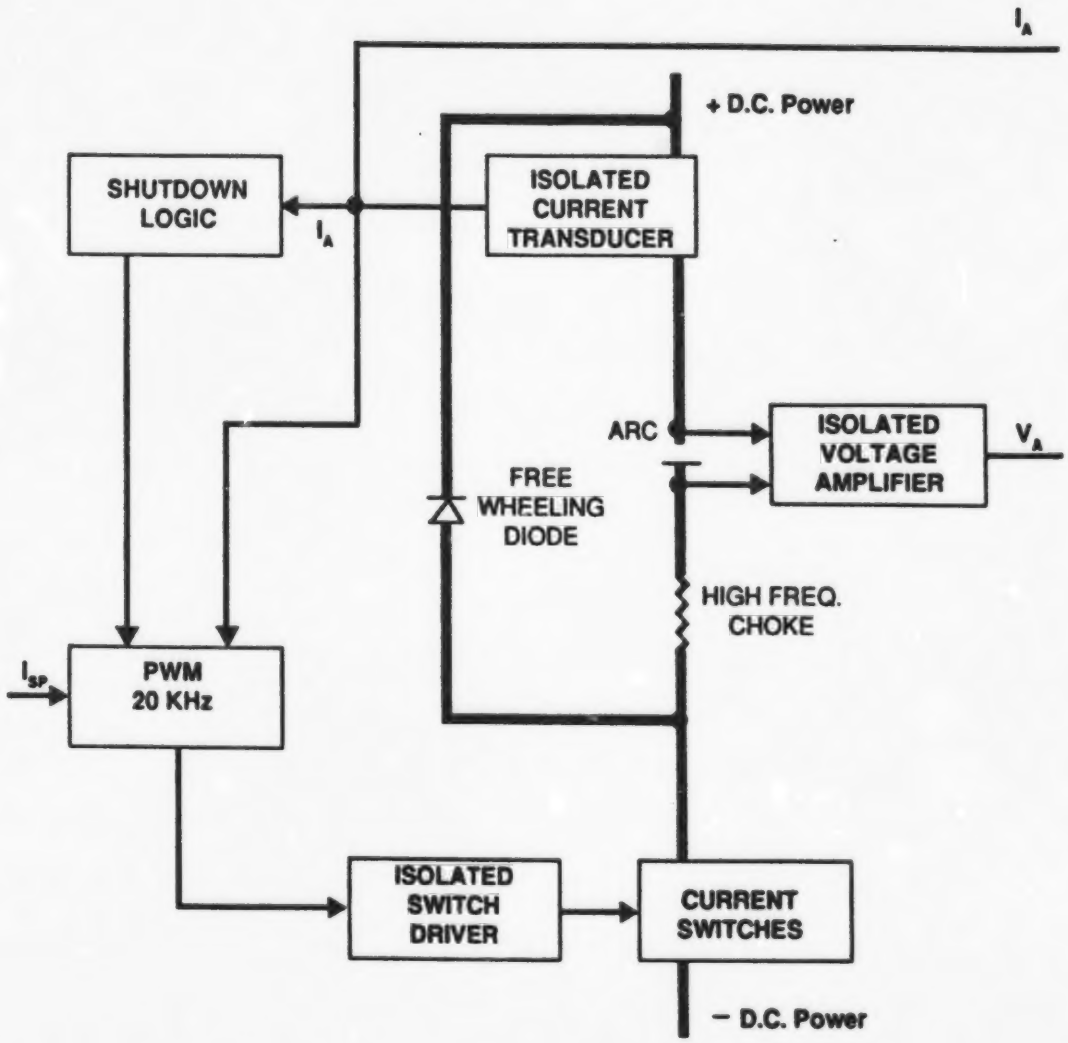

Figure 4: Instantaneous Arc Current Control.

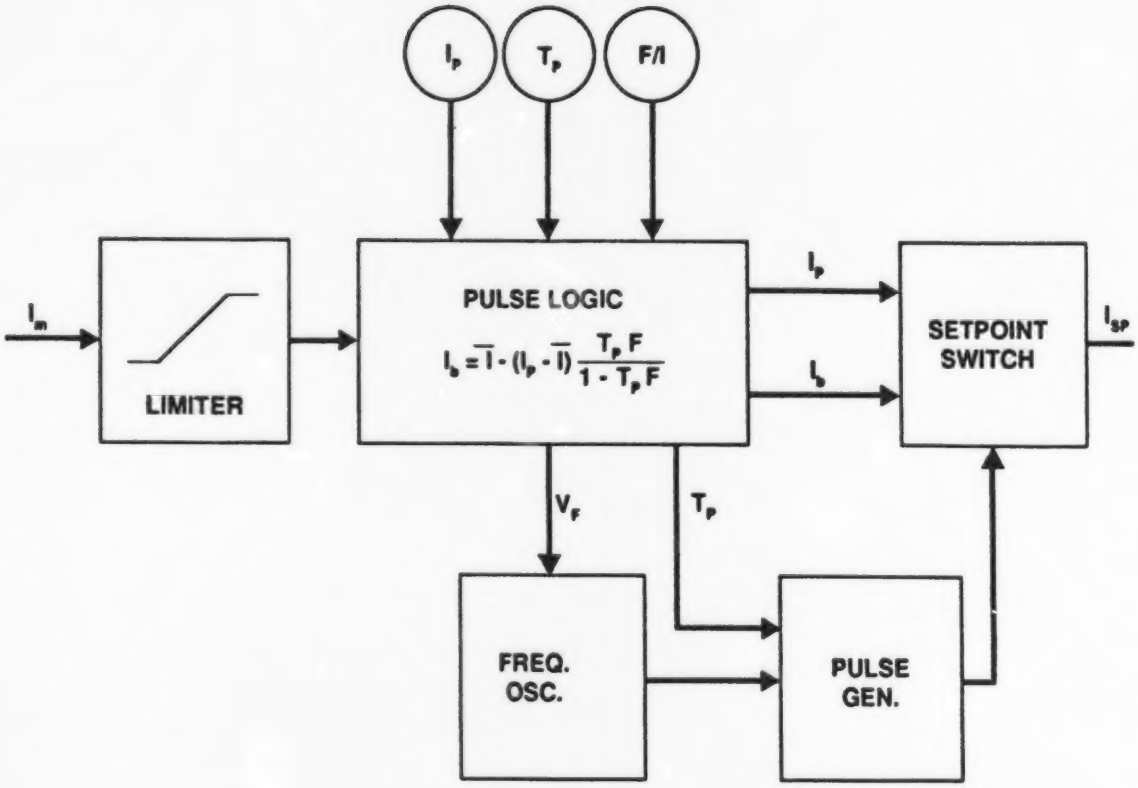

Figure 5: Synergic Pulse Logic Control.

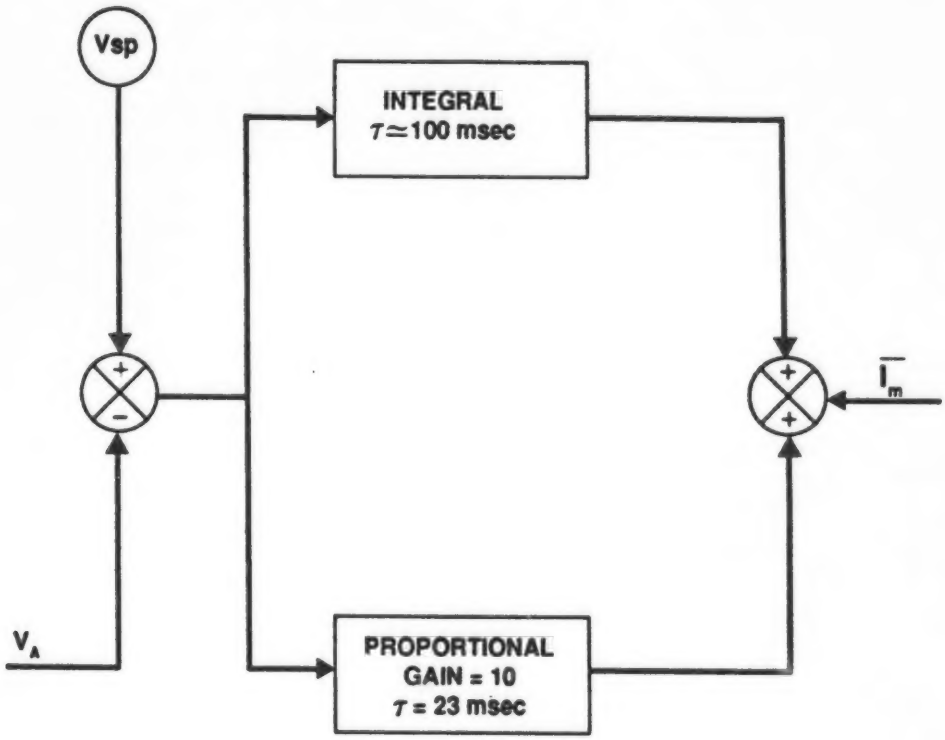

Figure 6: Average Arc Voltage Control.

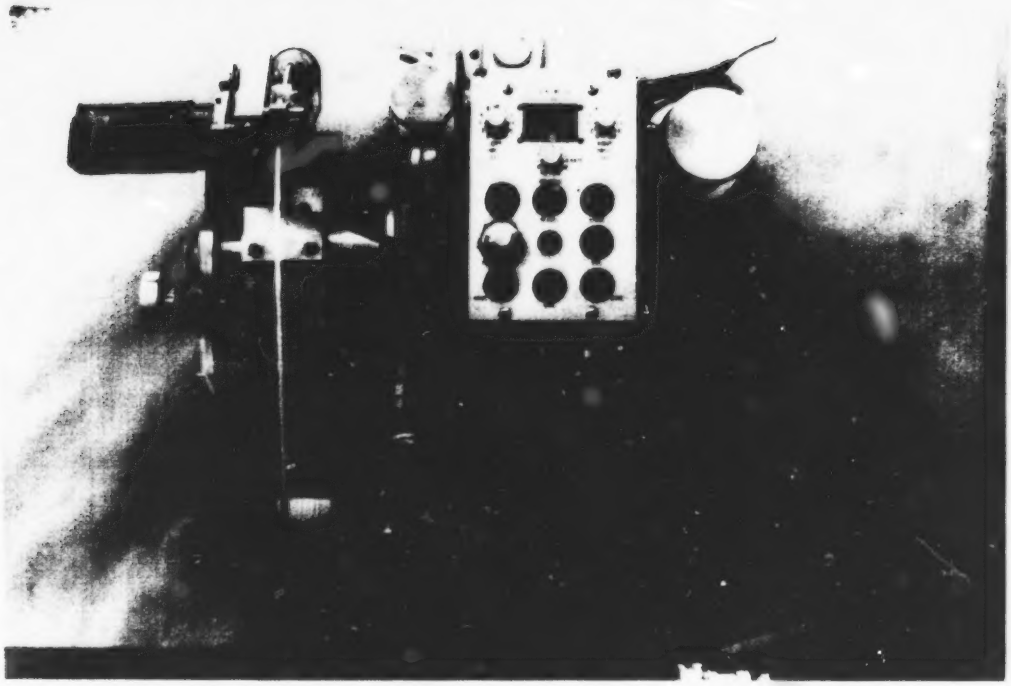

a) CRC-Evans Model M-200

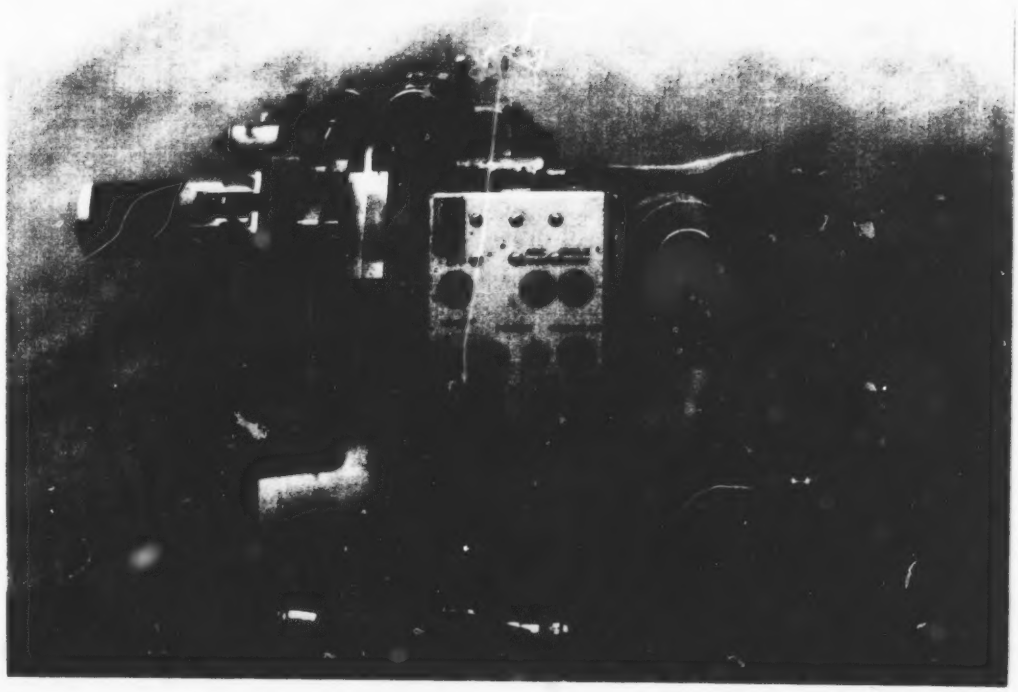

b) CRC-Evans Model P-100

Figure 7: Mechanized Welding Systems

a)

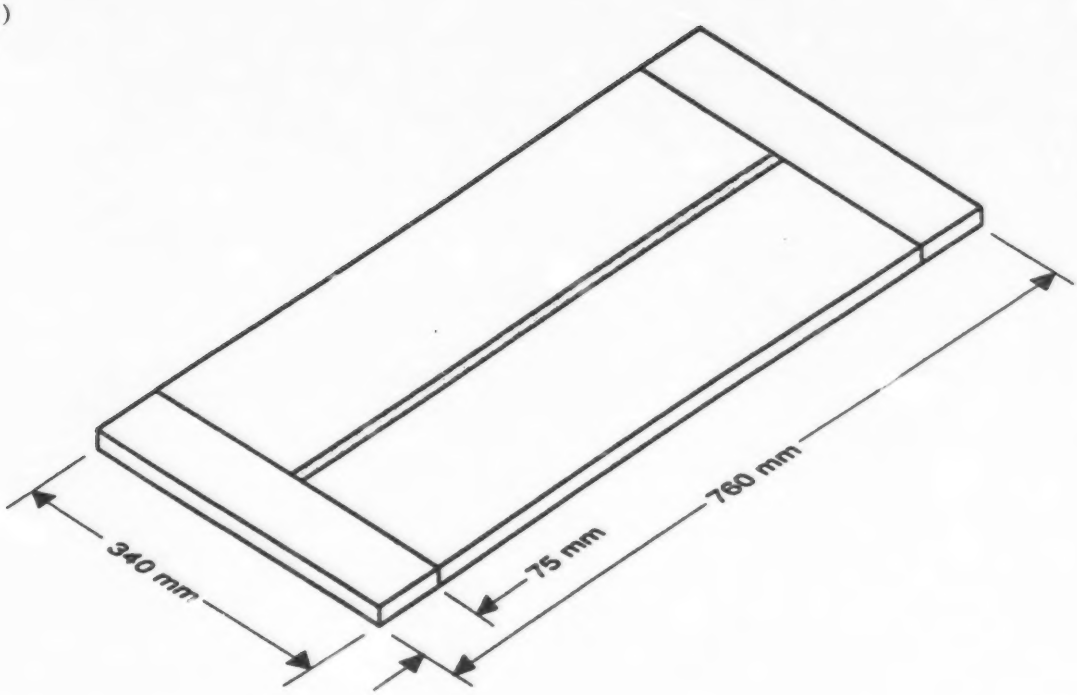

b)

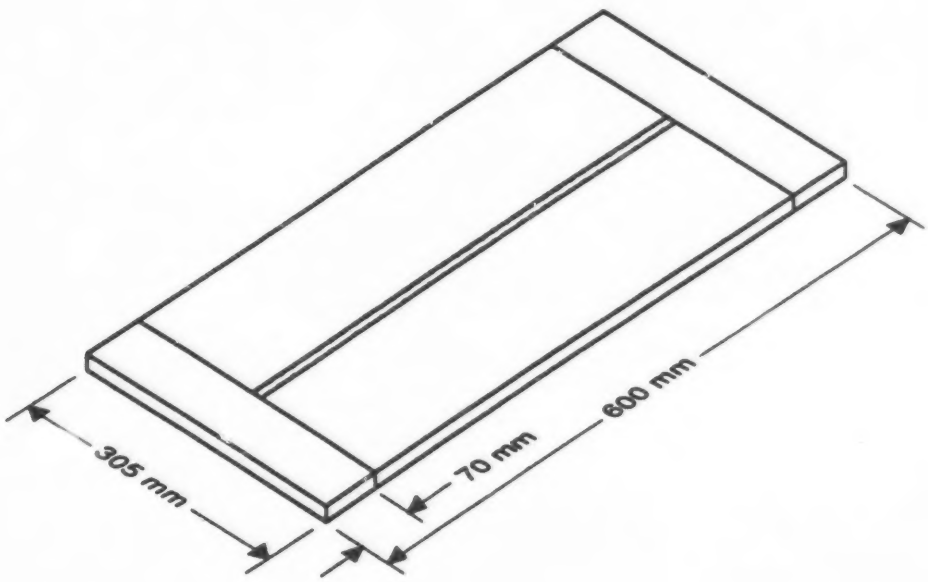

Figure 8: Test Panel Assembly.

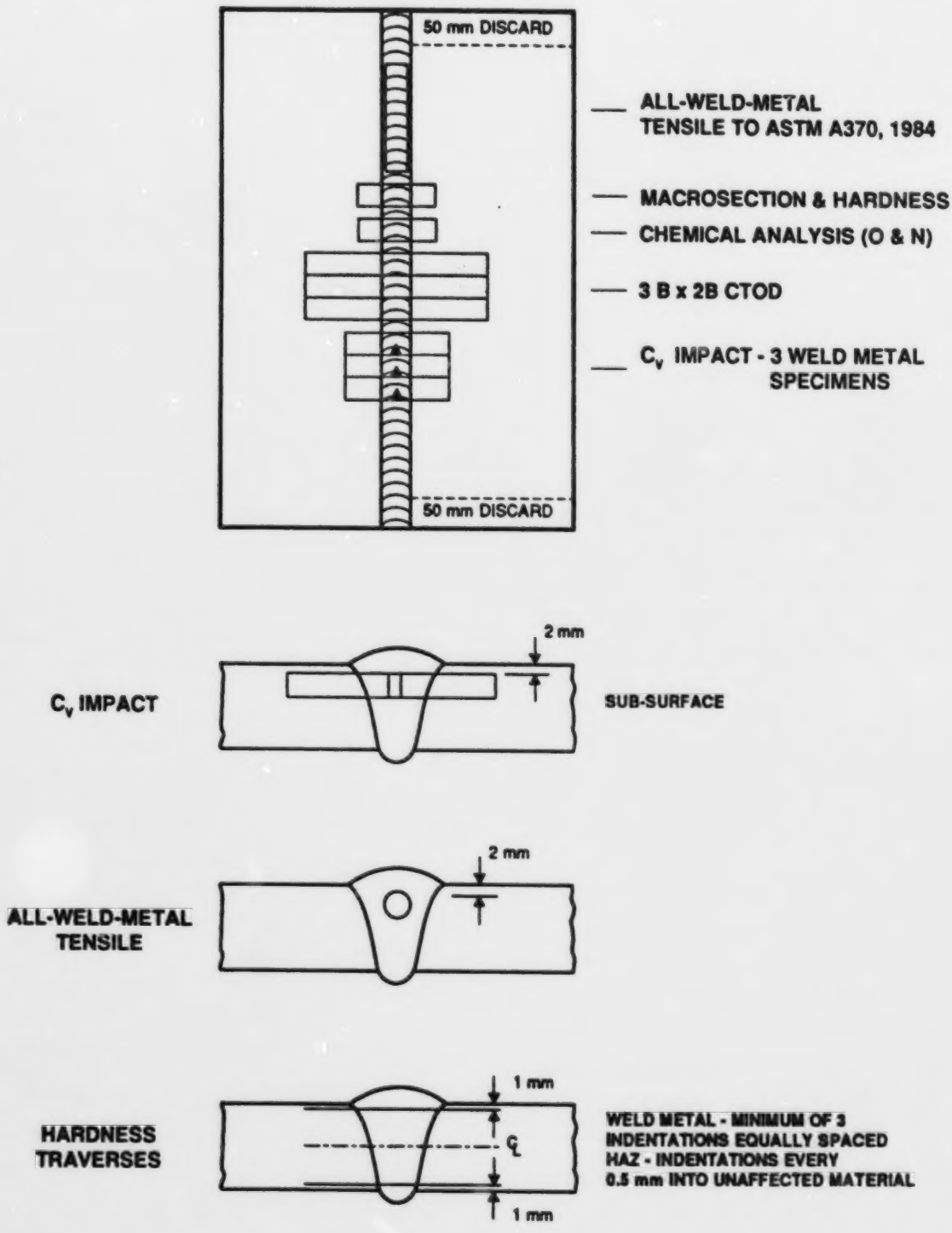

Figure 9: Mechanical Test Specimen Location.

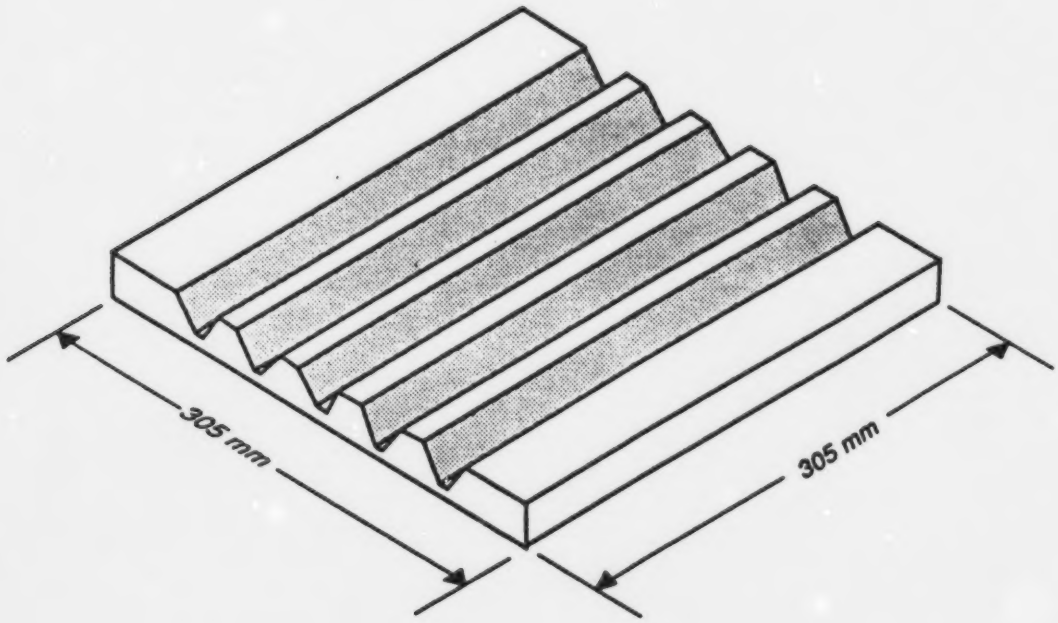

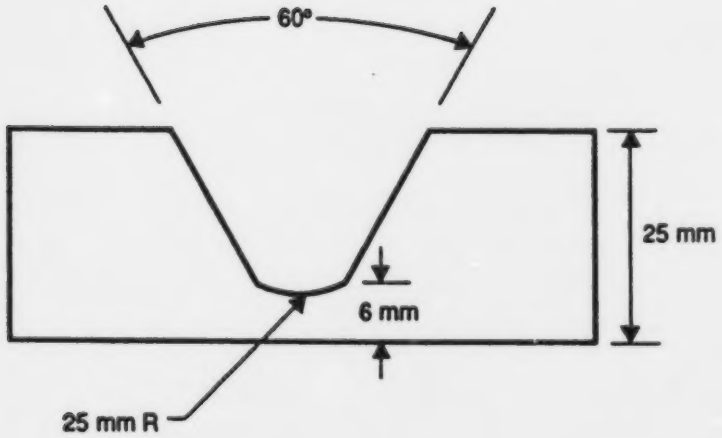

Figure 10: Profile for Bead-In-Groove Weld Deposits with Vertical Up Welding Parameters.

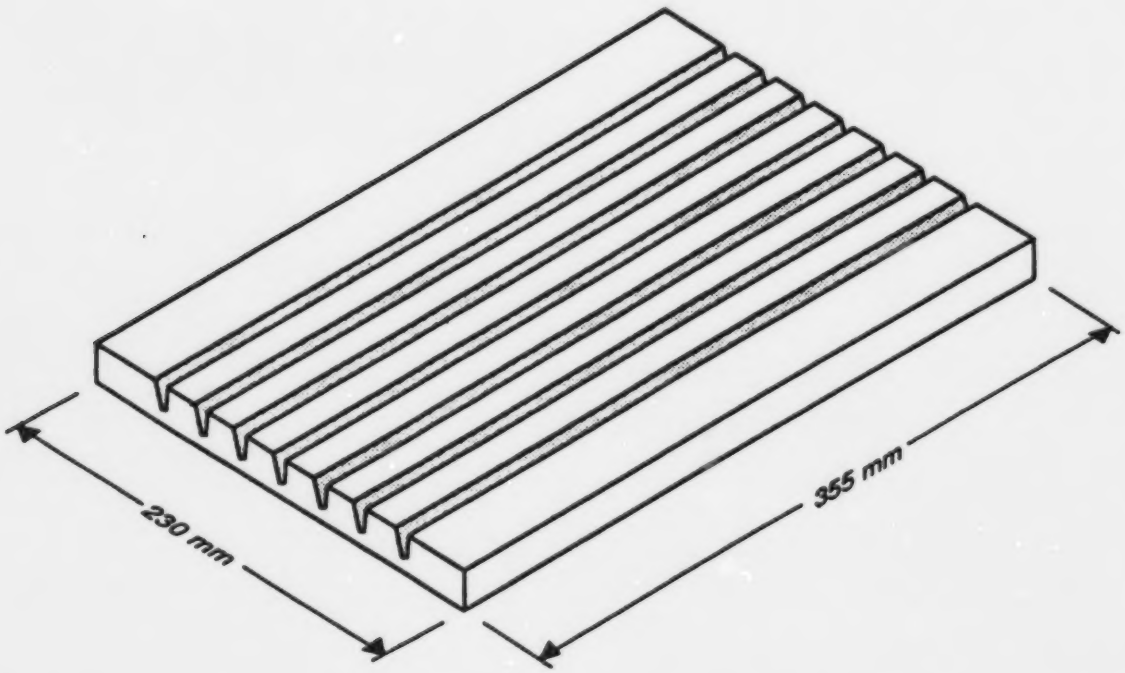

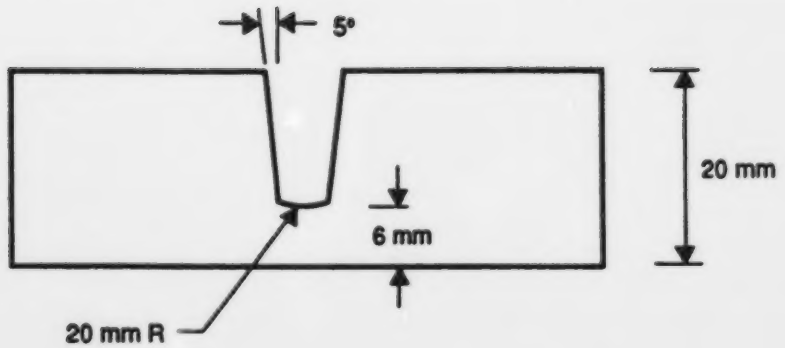

Figure 11: Profile for Bead-In-Groove Weld Deposits with Vertical Down Welding Parameters.

a) Vertical-Up

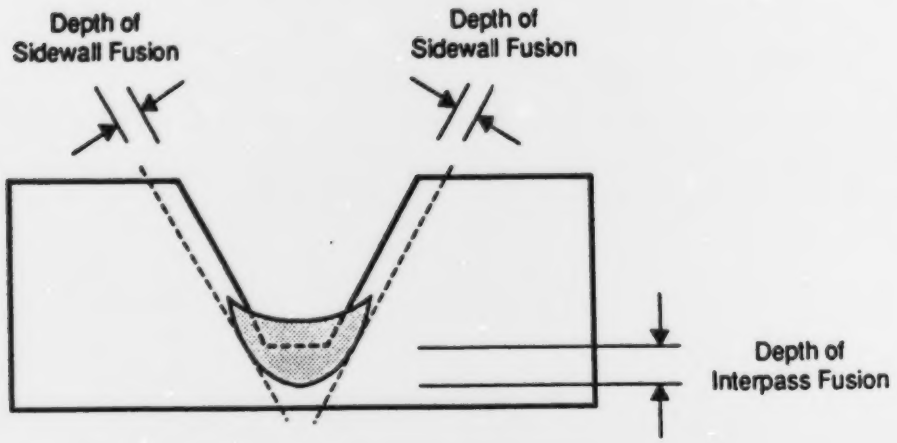

b) Vertical-Down

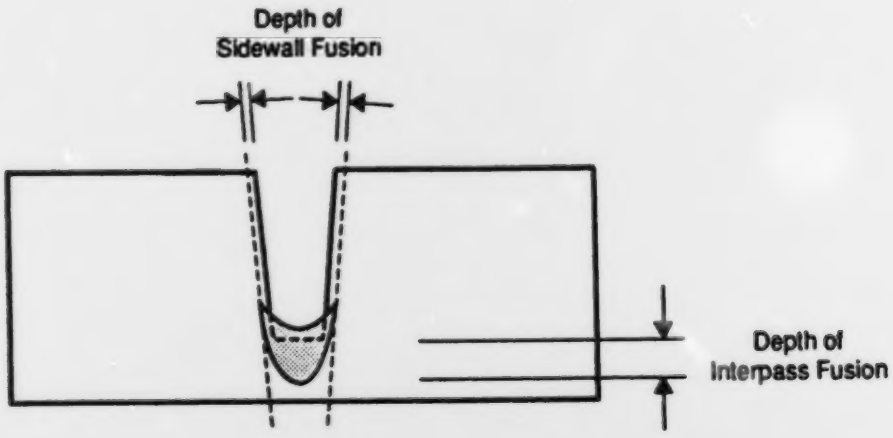

DEFINITION - Depth of Fusion is the distance that fusion extends into the base metal or into adjacent beads from the surface melted during welding

Figure 12: Measurement of Sidewall and Interpass Fusion.

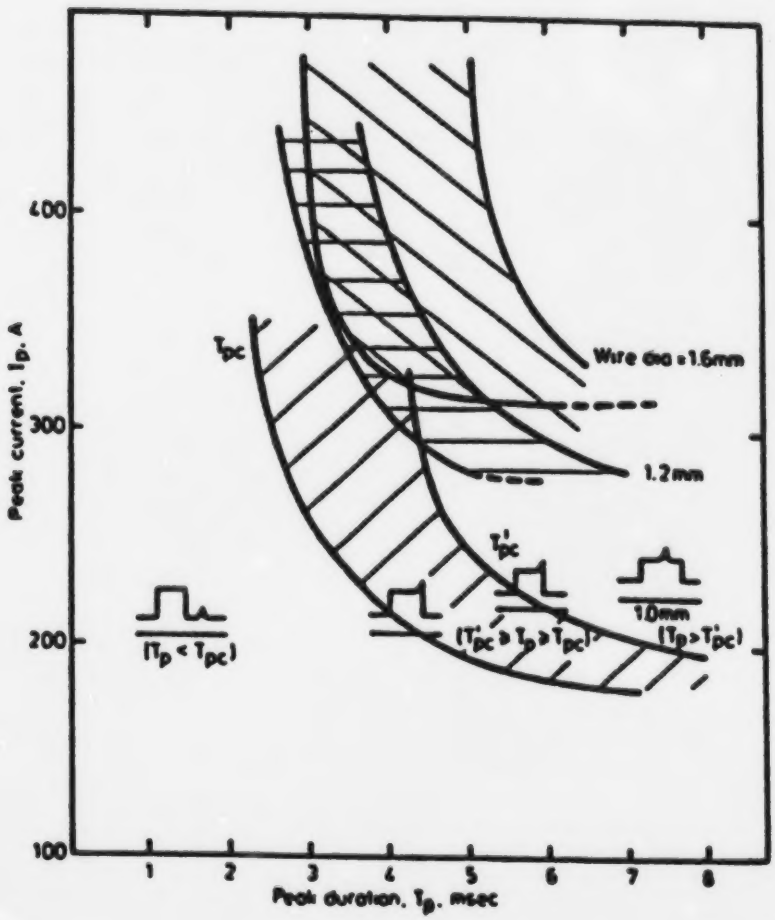

Figure 13: Influence of Peak Parameters on Droplet Detachment for Mild Steel Wire in Argon/5%CO_2 [After Allum (4)]

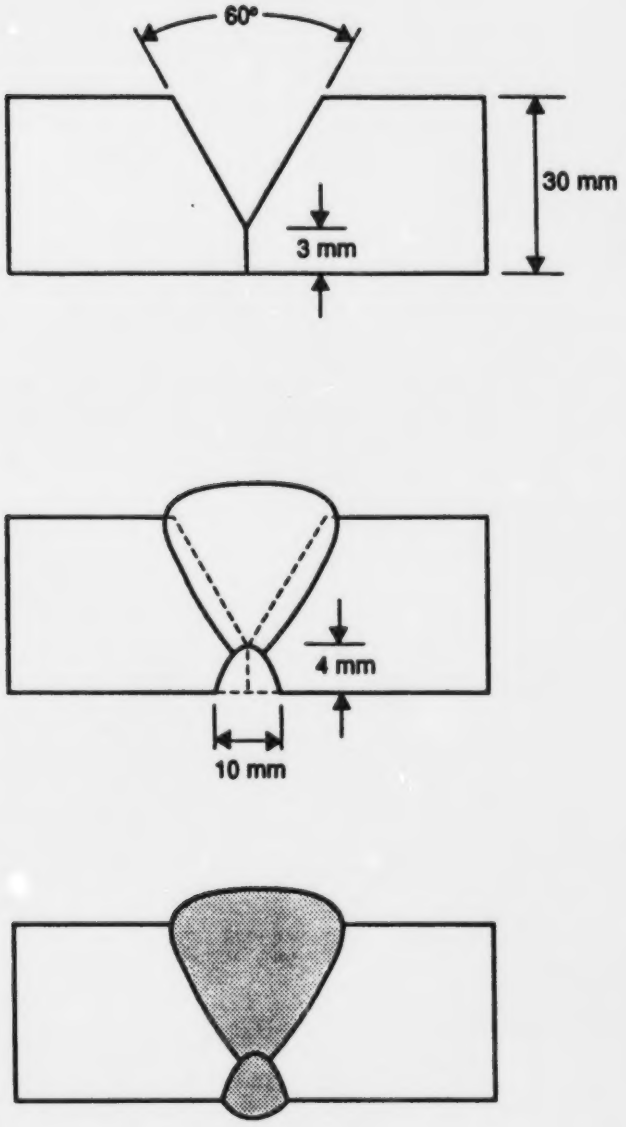

Figure 14: Edge Preparation and Backgouge Profile for LT60 Procedure Weld.

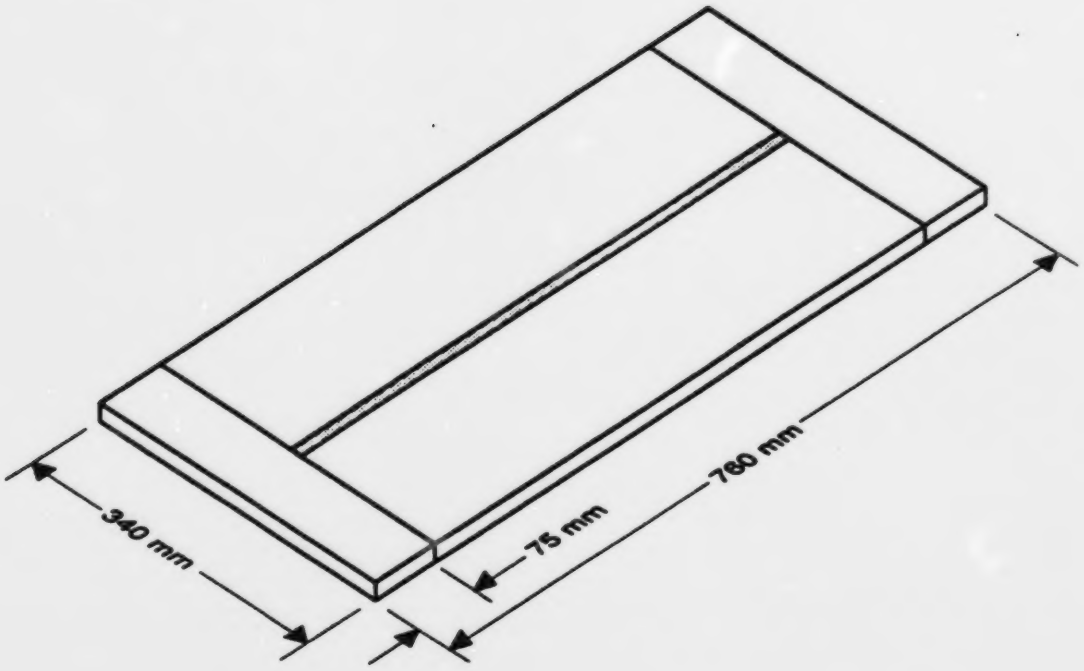

Figure 15: Welding Procedure Test Panel Assembly.

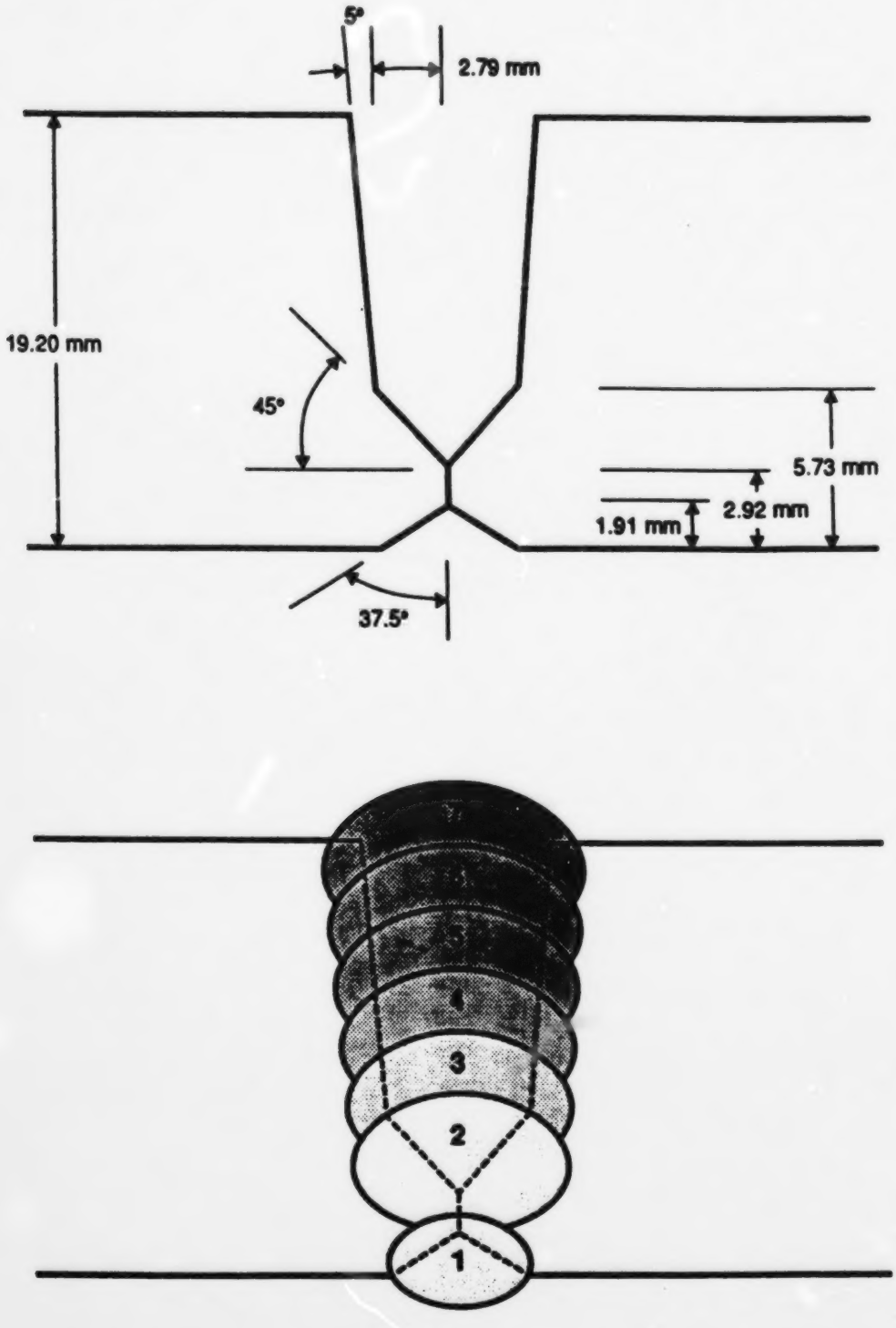

Figure 16: Joint Design and Bead Deposition Detail for the Gr 483 Steel Line Pipe Weld Procedure.

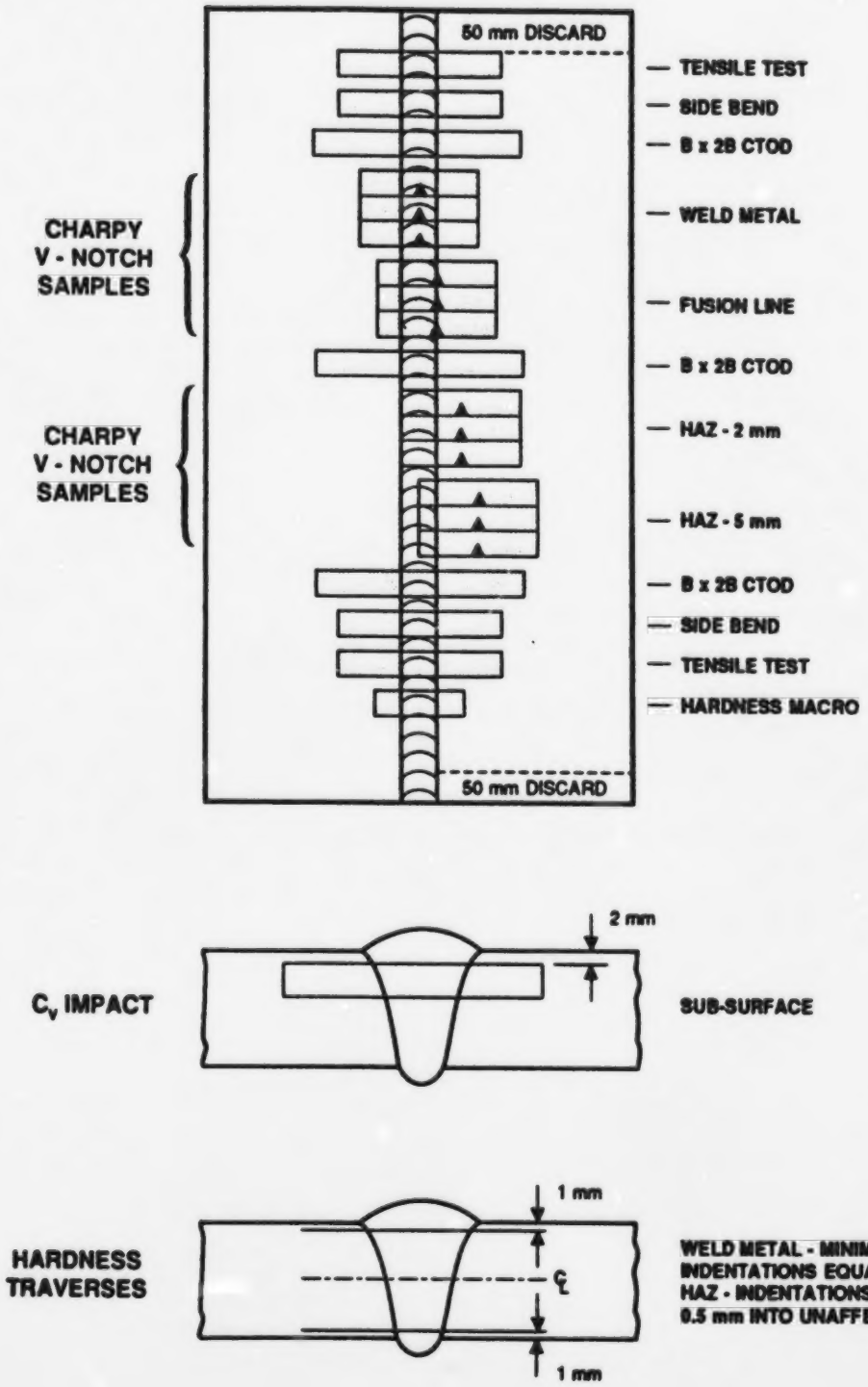

Figure 17: Mechanical Test Specimen Location for LT60 Weld Procedure Qualification.

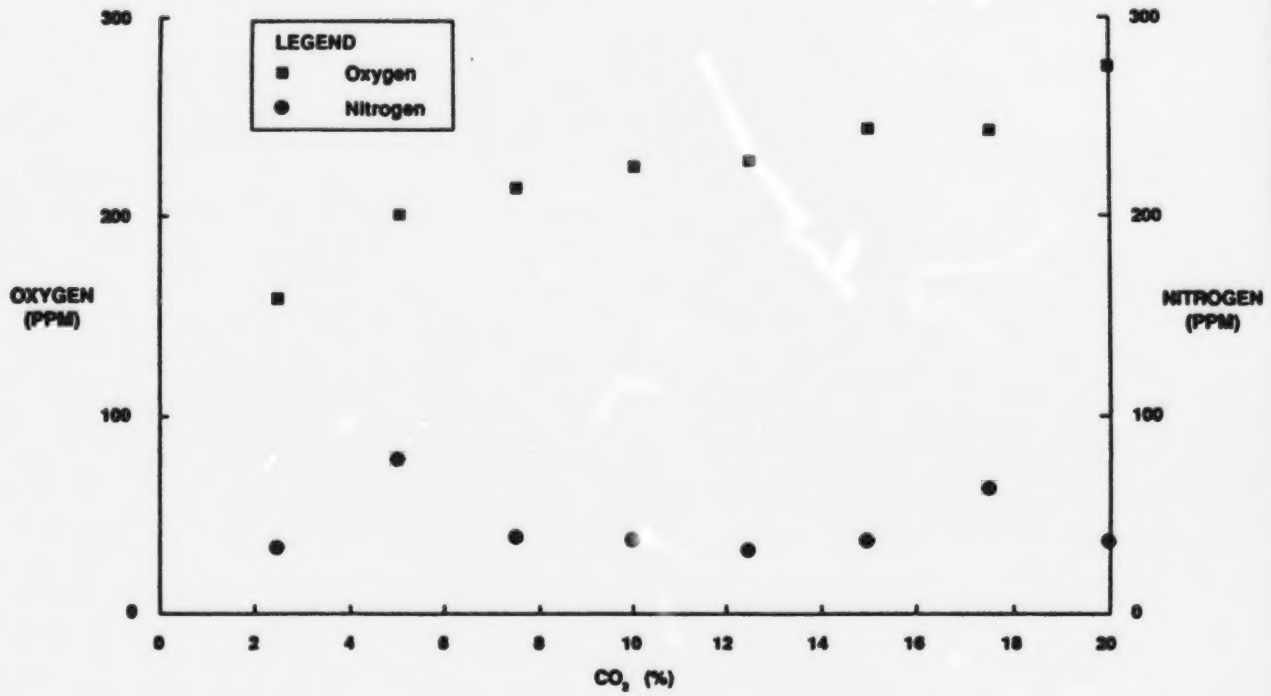

Figure 18: Effect of Increasing Oxidation Potential on C-Mn-Ti-B Weld Metal.

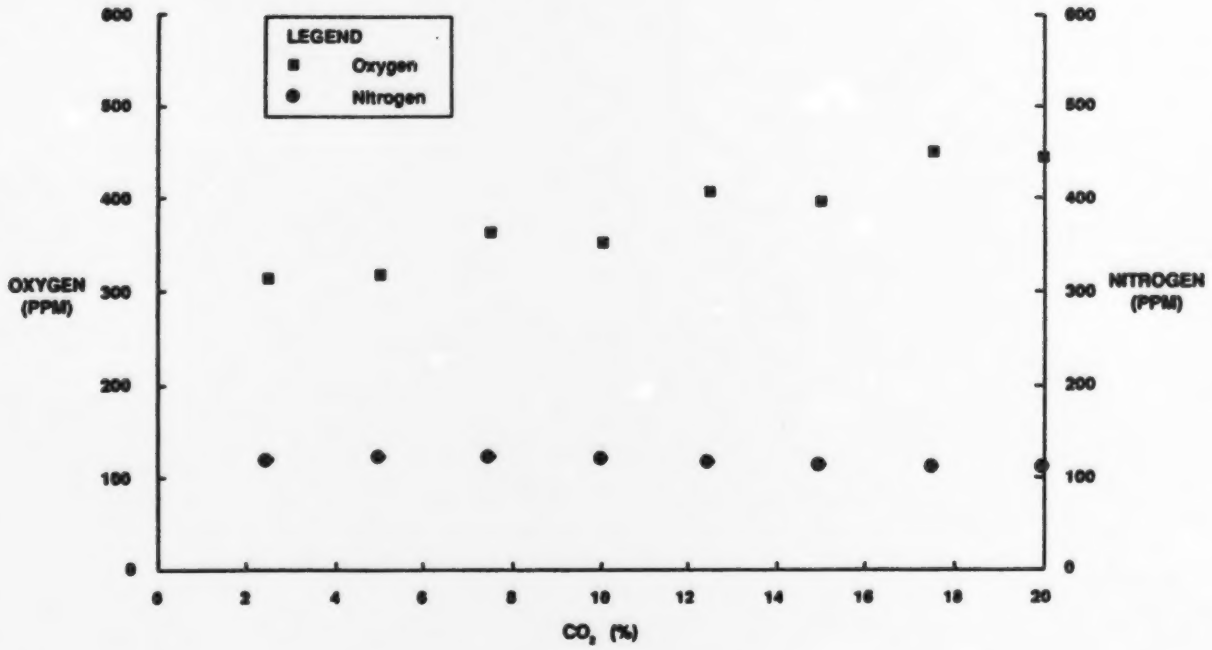

Figure 19: Effect of Increasing Oxidation Potential of C-Mn-Si-Ti Weld Metal.

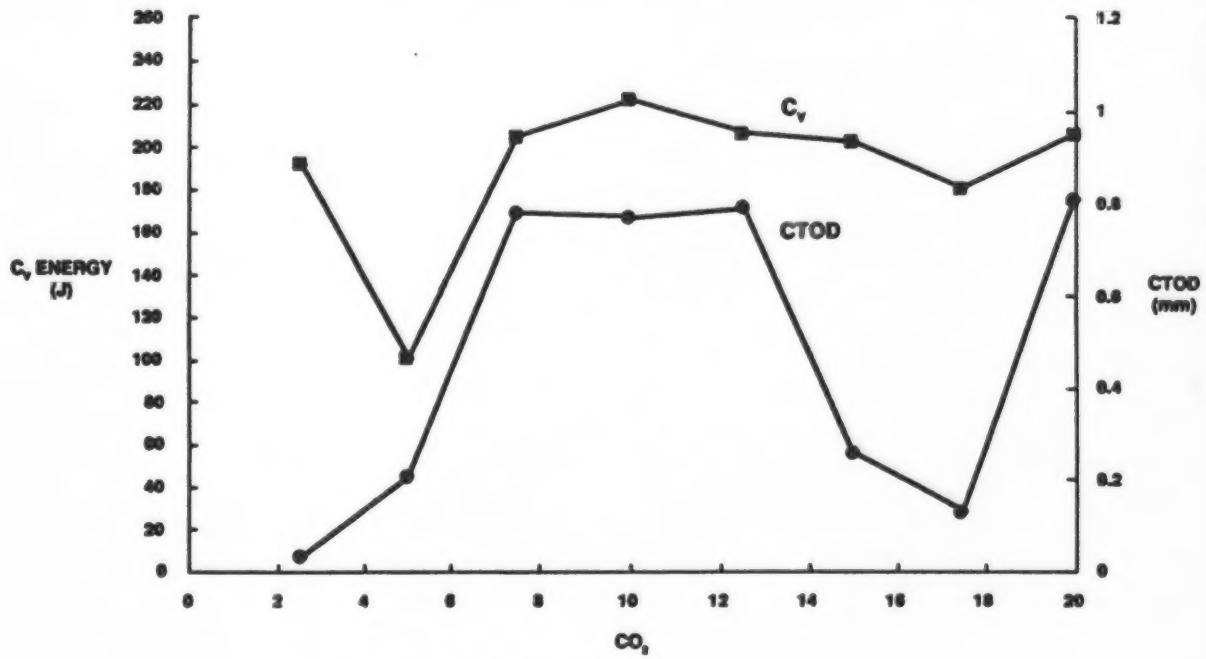

Figure 20: Effect of Increasing Oxidation Potential on C-Mn-Ti-B Weld Metal Toughness Properties.

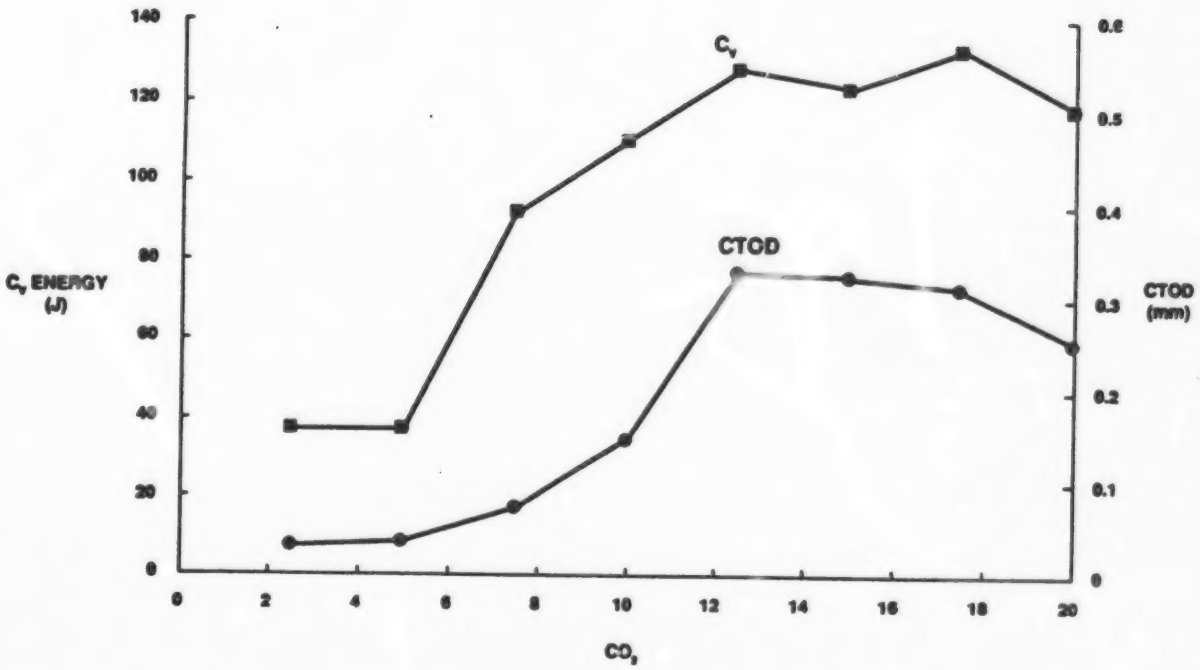

Figure 21: Effect of Increasing Oxidation Potential on C-Mn-Si-Ti Weld Metal Toughness Properties.

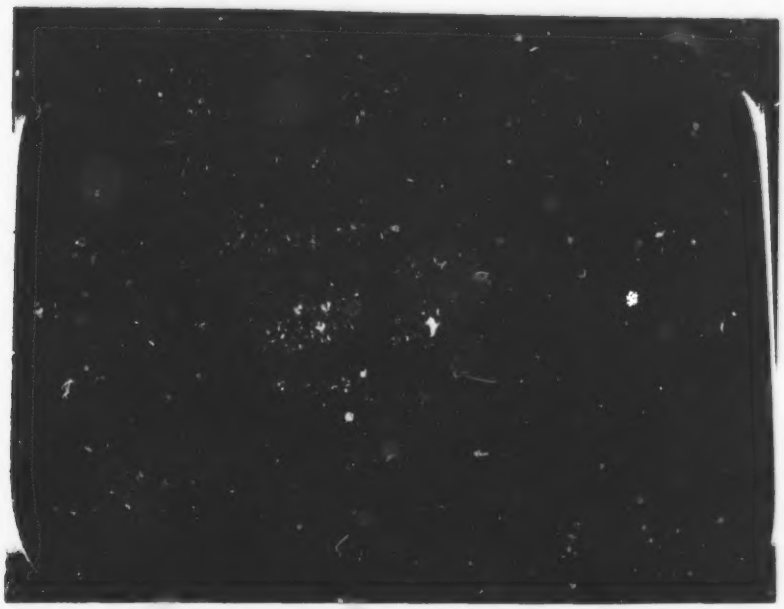

a) C-Mn-Ti-B/Ar-5CO_2

b) C-Mn-Ti-B/Ar-20CO_2

Figure 22: Macrosections of Welds made in Lloyds LT60 Test Panels. Mag X2.2

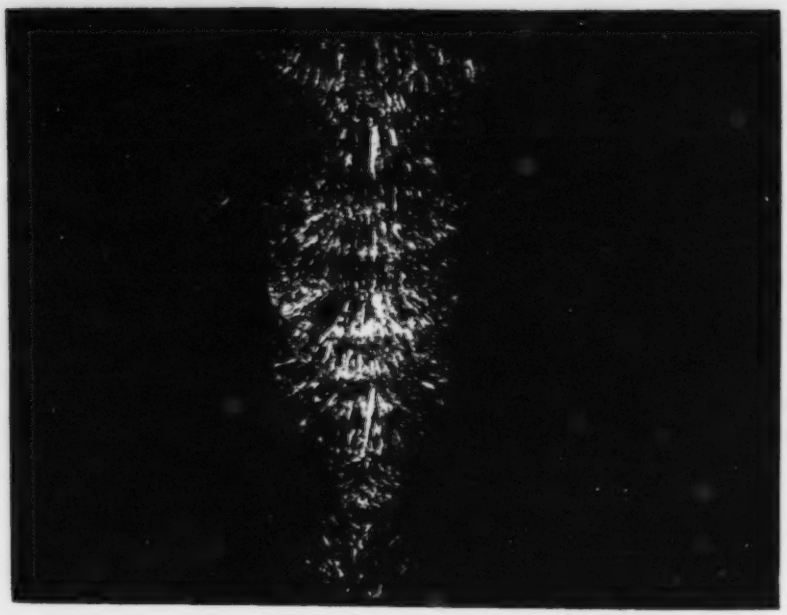

a) C-Mn-Si-Ti/Ar-5CO_2

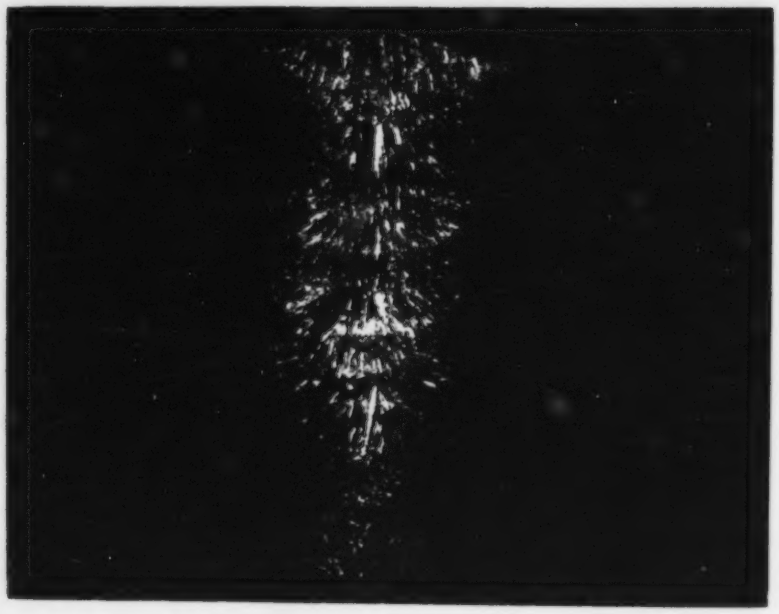

b) C-Mn-Si-Ti/Ar-20CO_2

Figure 23: Macrosections of Welds made in Gr 483 MPa Steel Line Pipe. Mag X3.8

a) Ar-5CO_2

b) Ar-10CO_2

Figure 24: Typical Microstructural Features in the C-Mn-Ti-B Deposits. Mag X500

c) Ar-17.5CO_2

Figure 24 (cont)

a) Ar-5CO_2

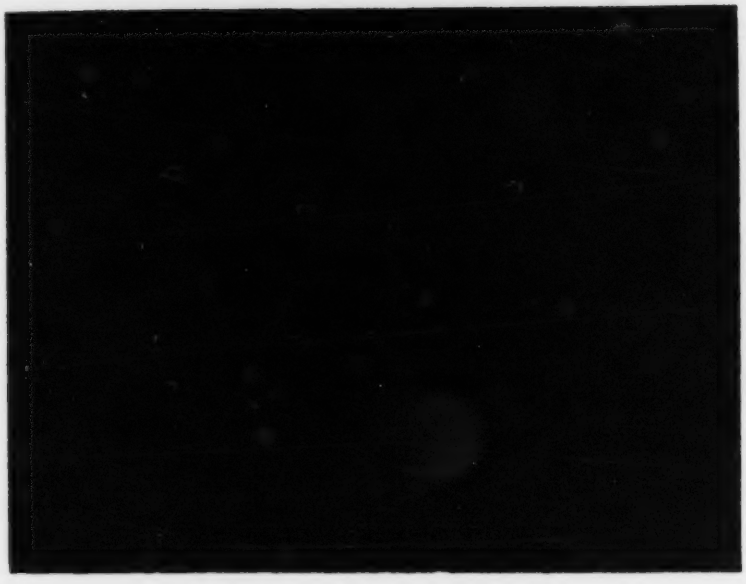

b) Ar-12.5CO_2

Figure 25: Typical Microstructural Features in the C-Mn-Si-Ti Deposits. MAG X500

c) Ar-20CO_2

Figure 25 (cont)

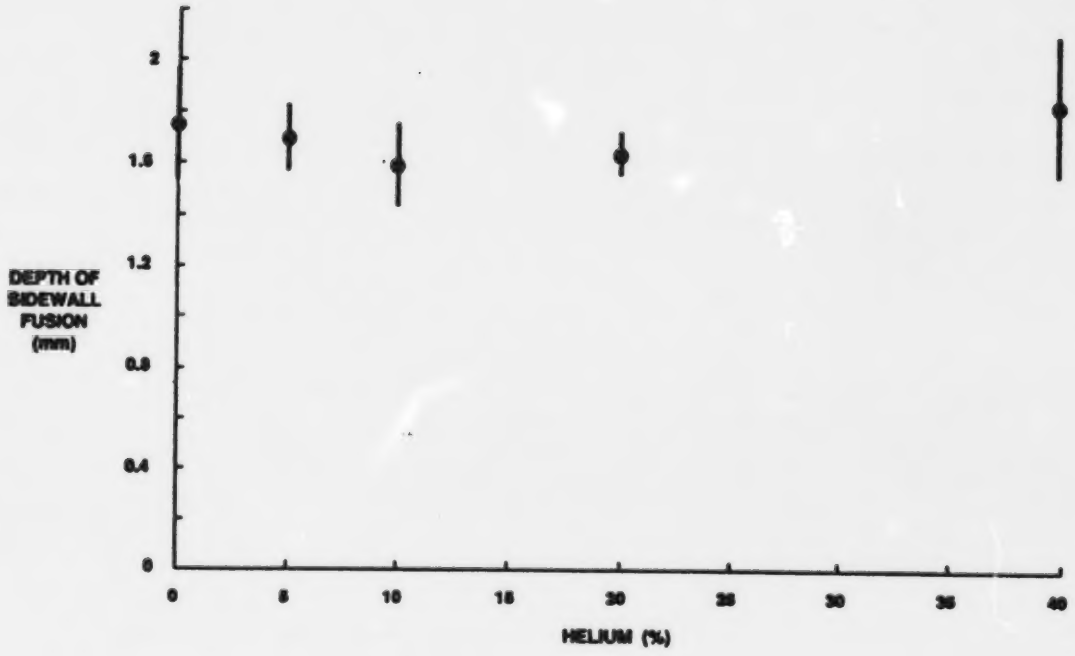

Figure 26: Effect of Helium on V-Groove Sidewall Fusion.

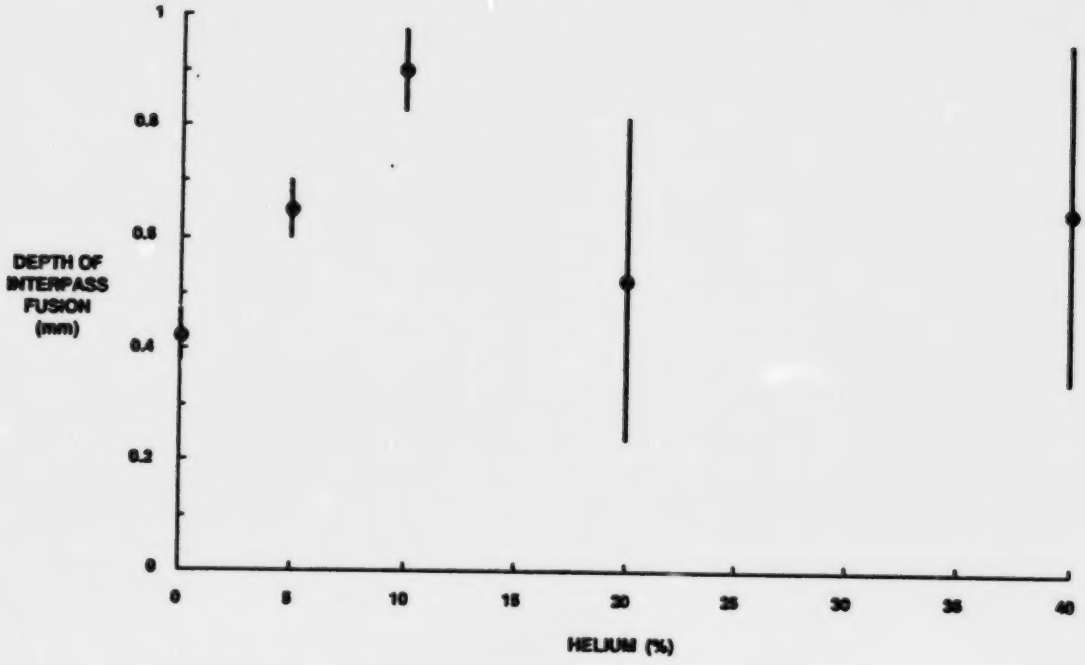

Figure 27: Effect of Helium on V-Groove Interpass Fusion.

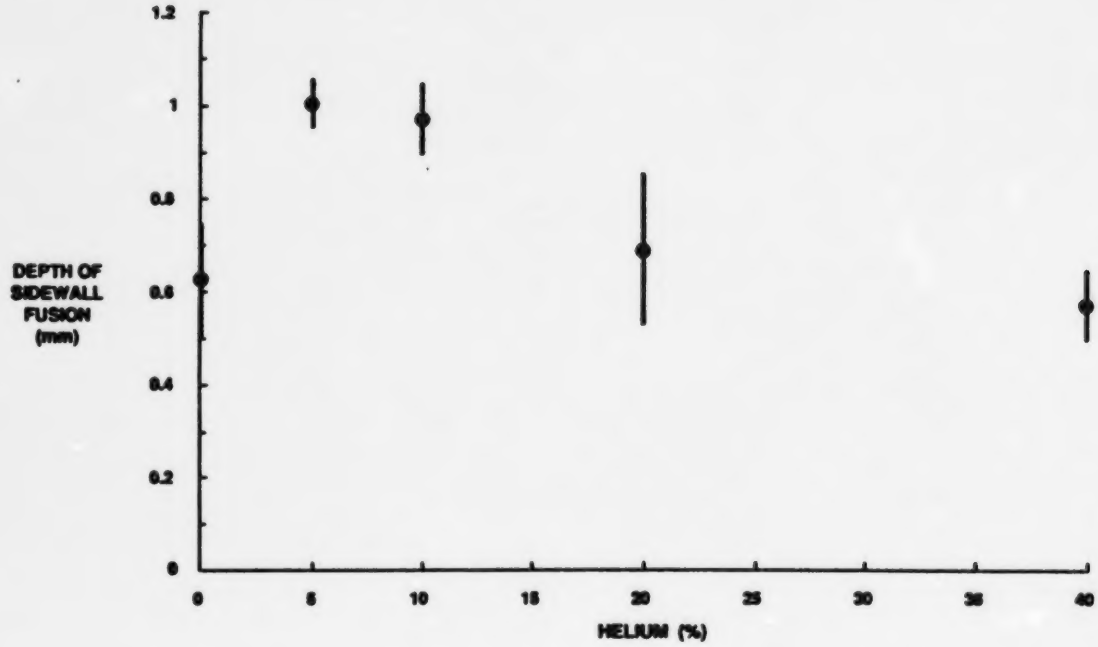

Figure 28: Effect of Helium on Narrow Gap Sidewall Fusion.

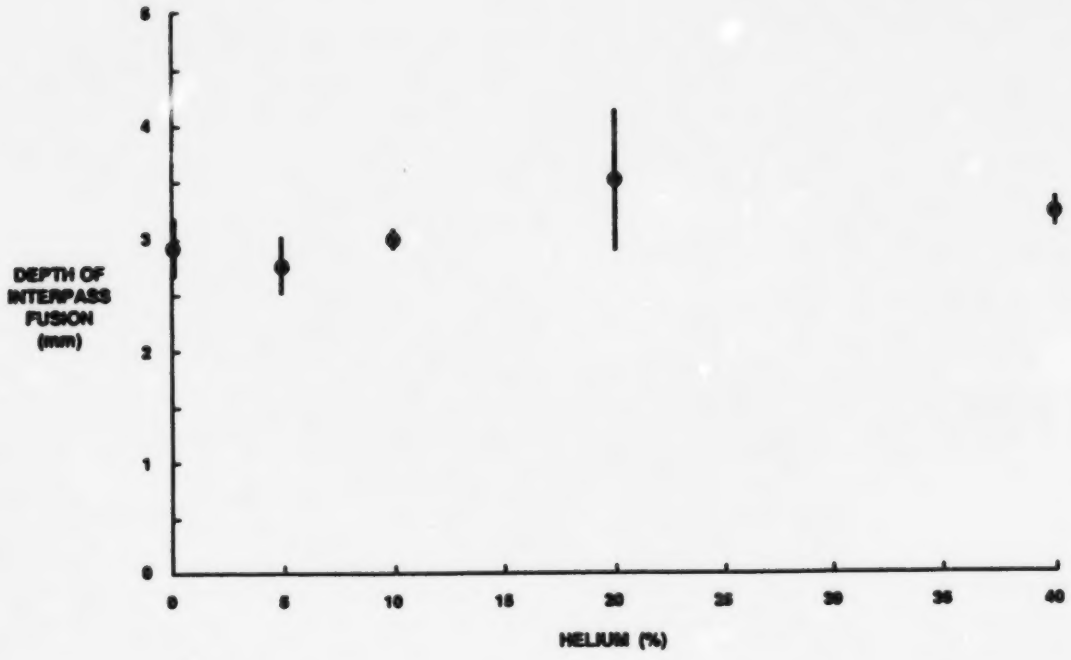

Figure 29: Effect of Helium on Narrow Gap Interpass Fusion.

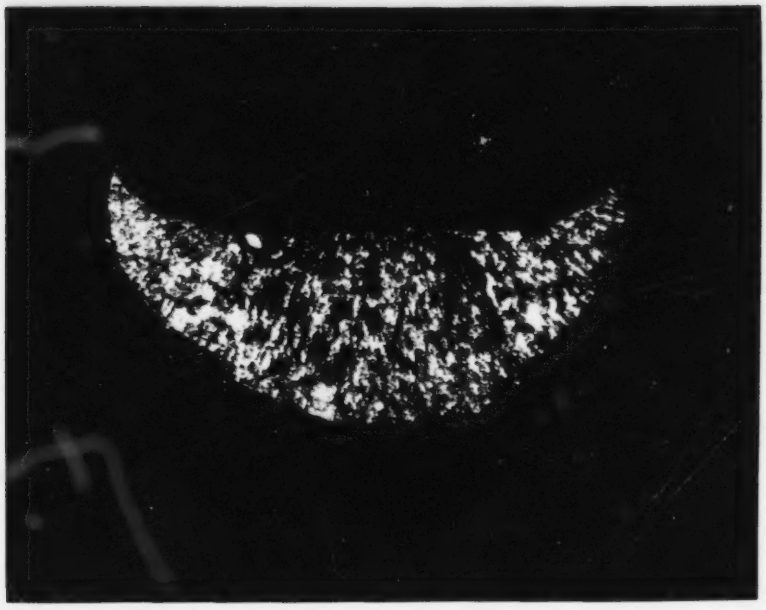

a) Base Composition: Ar-10CO_2

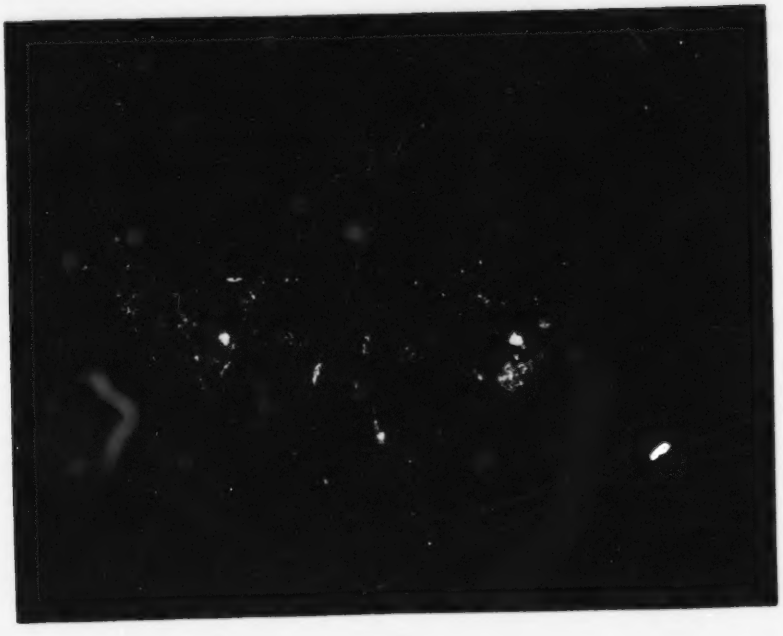

b) Ar-5He-10CO_2

Figure 30: Effect of Helium Content on Bead Shape in V-Groove Preparation; C-Mn-Ti-B/10CO_2 Mag X4.3

c) Ar-10He-10CO_2

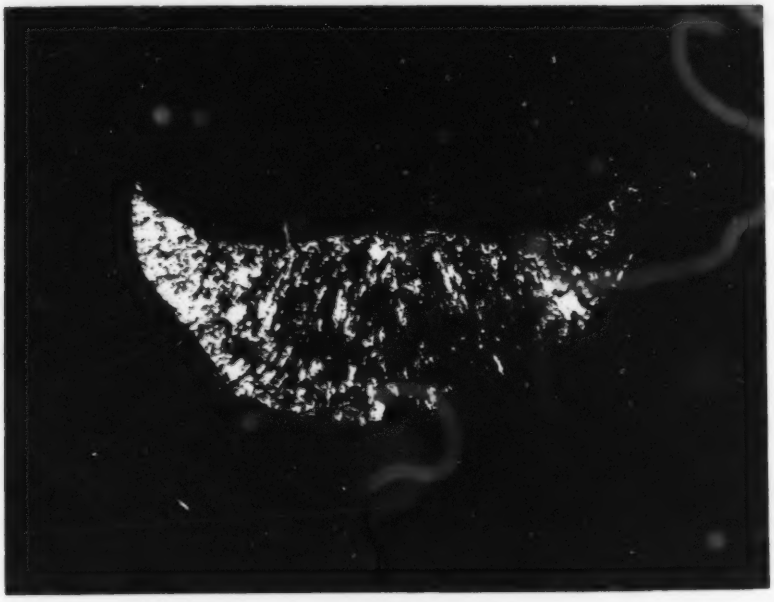

d) Ar-20He-10CO_2

Figure 30: (cont)

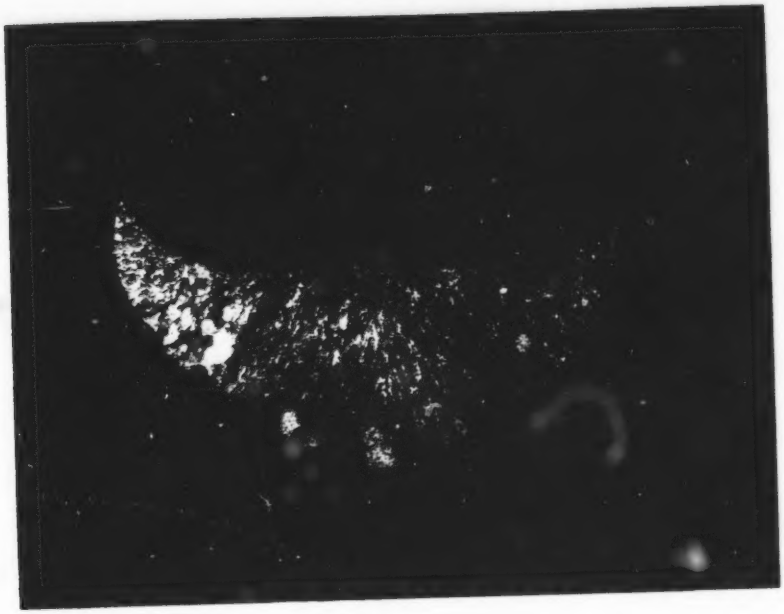

e) Ar-40He-10CO_2

Figure 30 (cont)

a) Ar-12.5CO_2

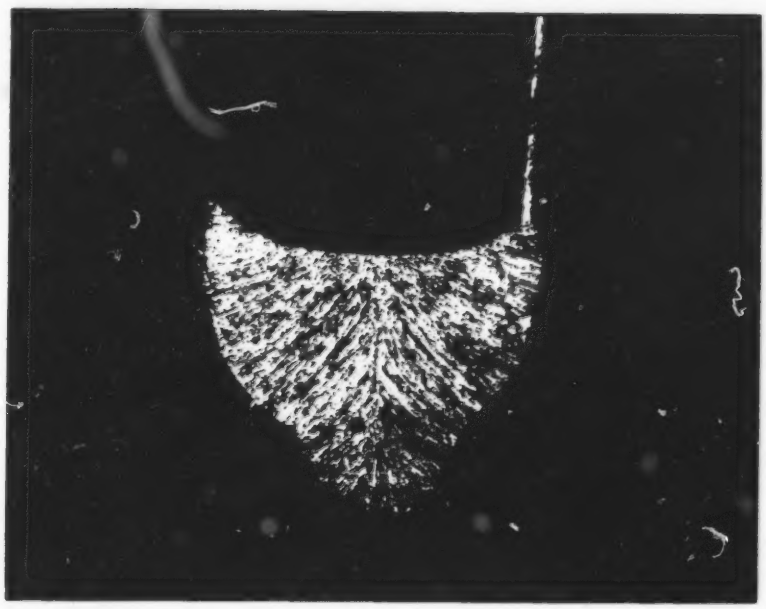

b) Ar-5He-12.5CO_2

Figure 31: Effect of Helium Additions on Bead Shape in Narrow Gap Preparation; C-Mn-Si-Ti/12.5CO_2 Mag X5.5

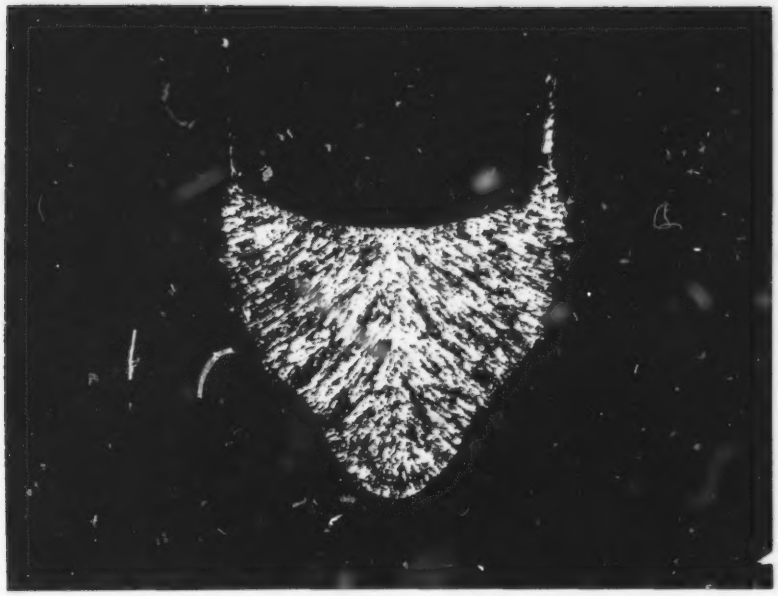

c) Ar-10He-12.5CO_2

d) Ar-20He-12.5CO_2

Figure 31 (cont)

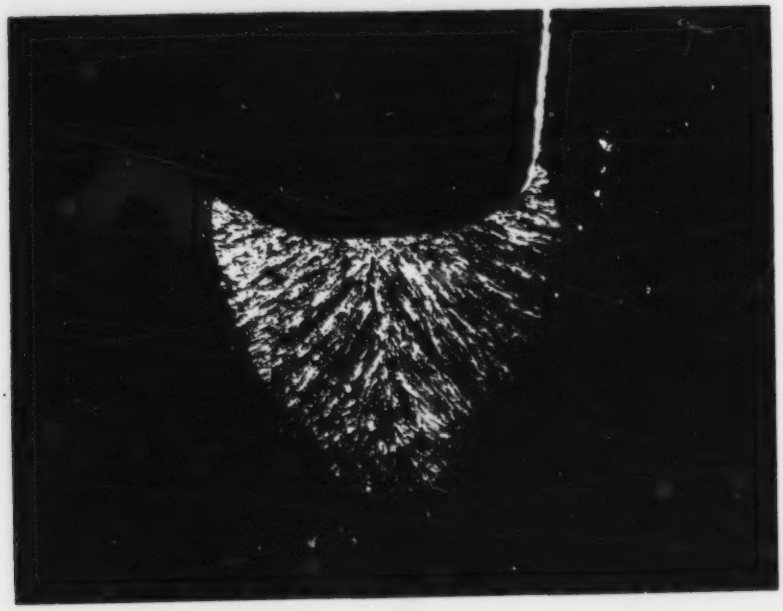

e) Ar-40He-12.5CO_2

Figure 31 (cont)

a) Ar-10He-10CO_2

b) Ar-10He-10CO_2-0.5H_2

Figure 32: Effect of O_2 and H_2 Additions on Bead Shape; C-Mn-Ti-B/Ar-10He-10CO_2 Mag X4.8

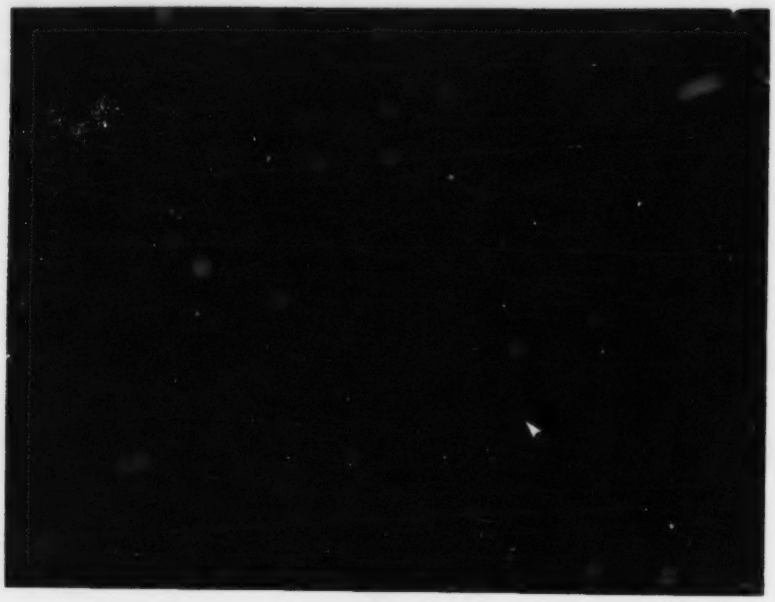

c) Ar-10He-5O_2

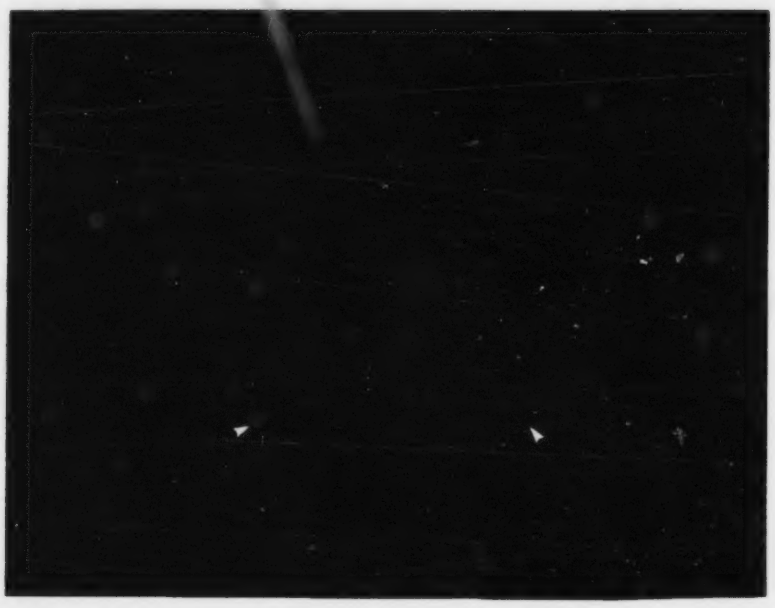

d) Ar-10He-5O_2-0.5H_2

Figure 32 (cont)

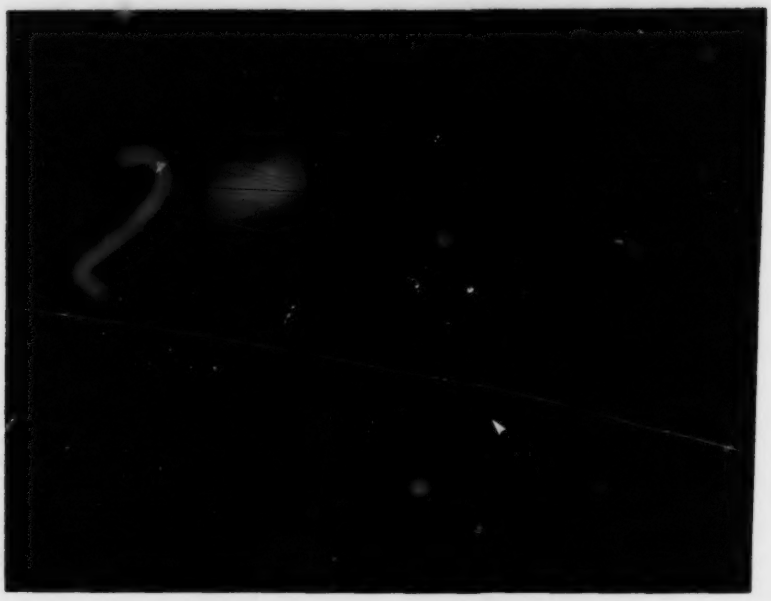

e) Ar-10He-4CO_2-3O_2

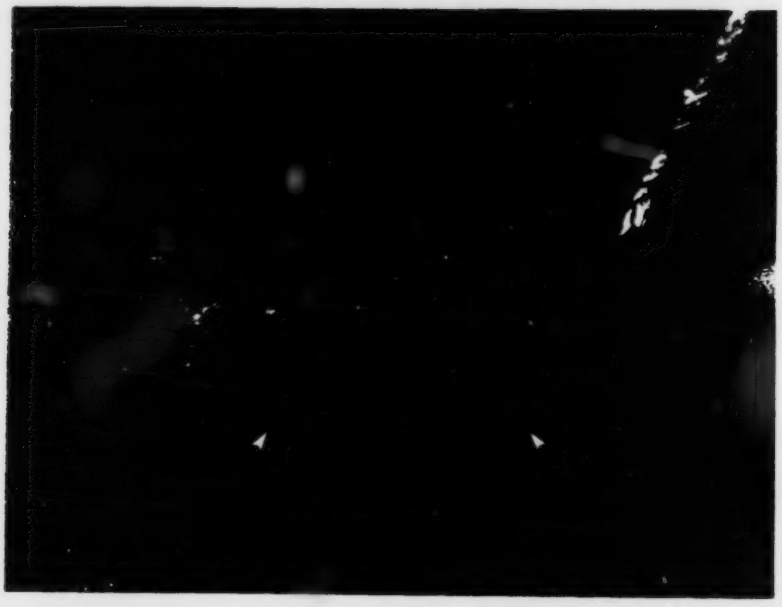

f) Ar-10He-4CO_2-3O_2-0.5H_2

Figure 32 (cont)

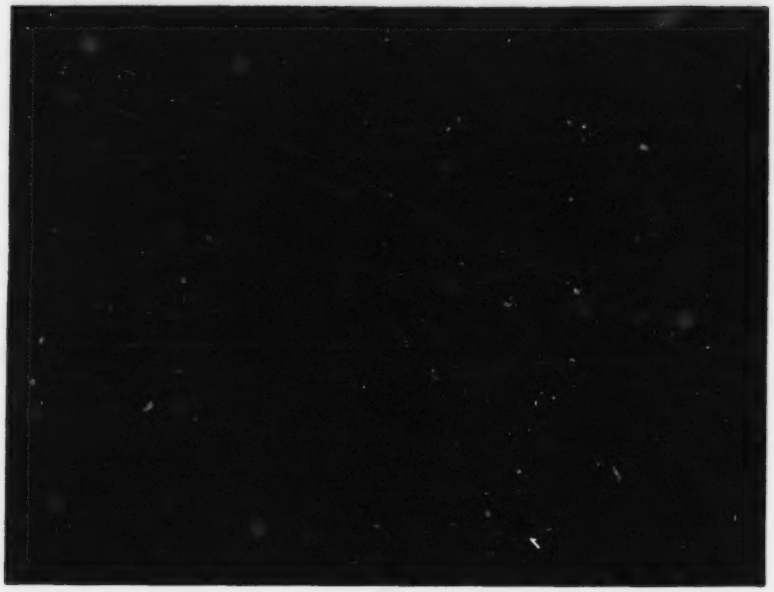

g) Ar-10He-6CO_2-2O_2

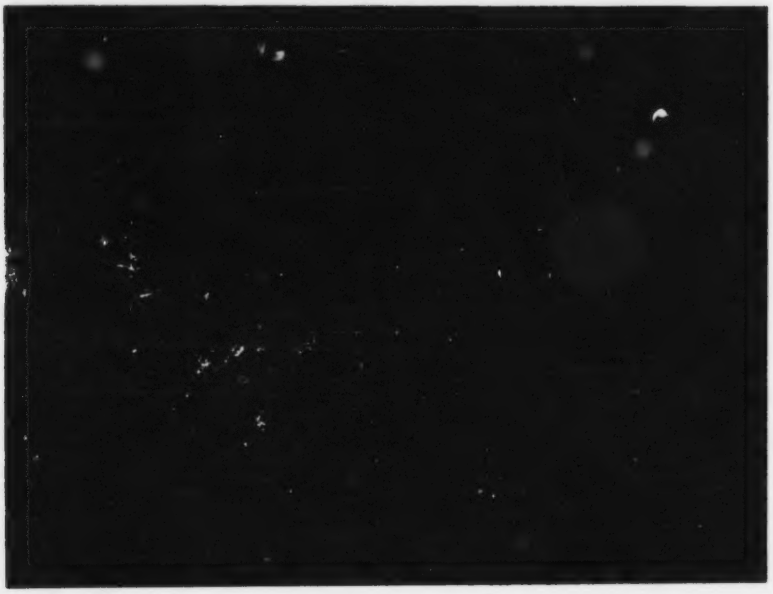

h) Ar-10He-6CO_2-2O_2-0.5H_2

Figure 32 (cont)

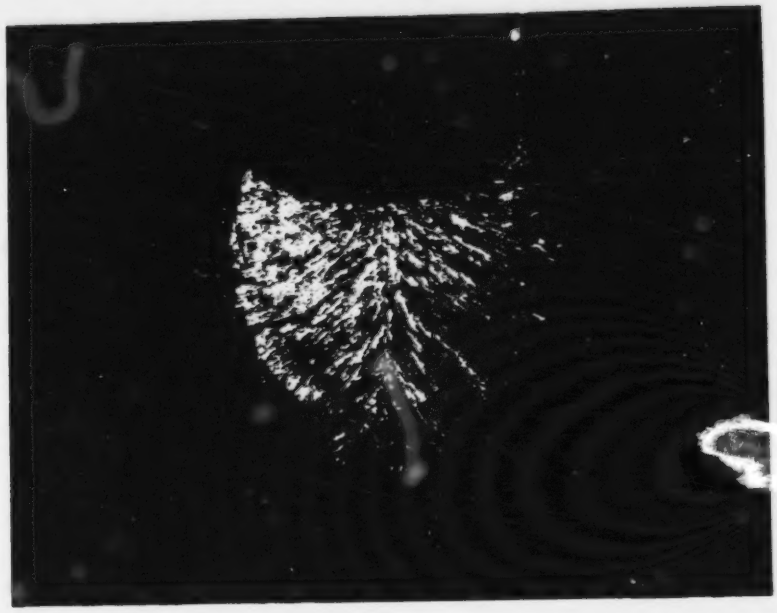

a) Ar-5He-12.5CO_2

b) Ar-5He-12.5CO_2-0.5H_2

Figure 33: Effect of O_2 and H_2 Additions on Bead Shape C-Mn-Si-Ti/Ar-5He-12.5CO_2 Mag X6

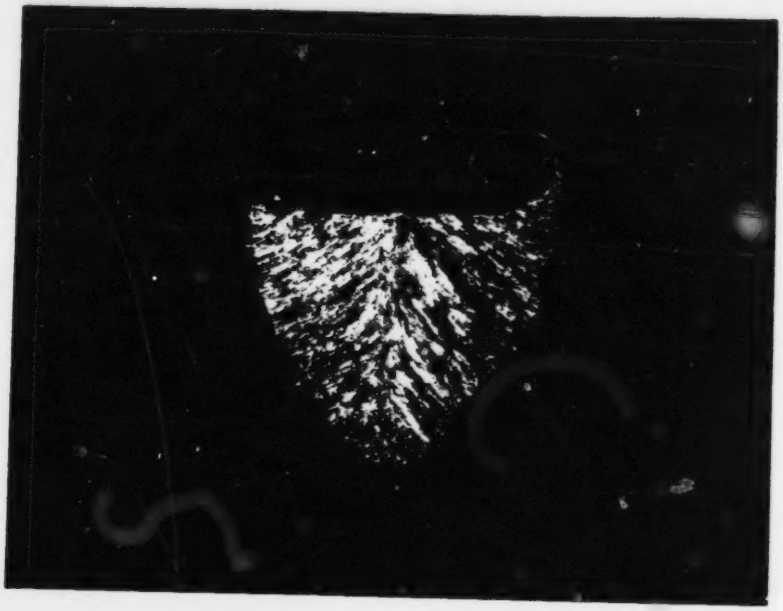

c) Ar-5He-60_2

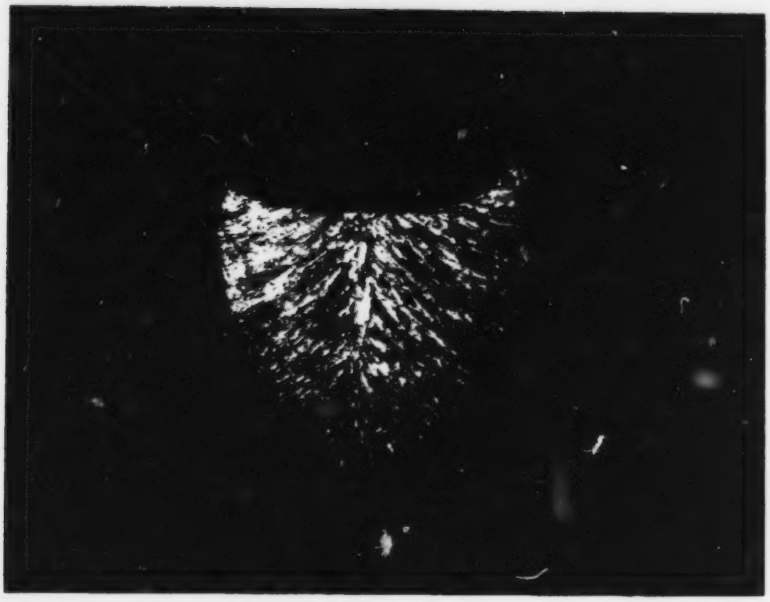

d) Ar-5He-60_2-$0.5H_2$

Figure 33 (cont)

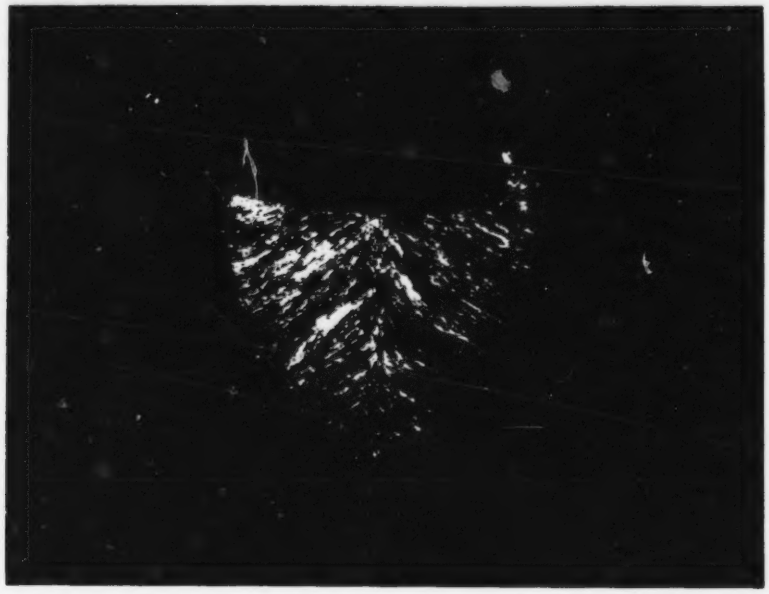

e) Ar-5He-6.5CO_2-3O_2

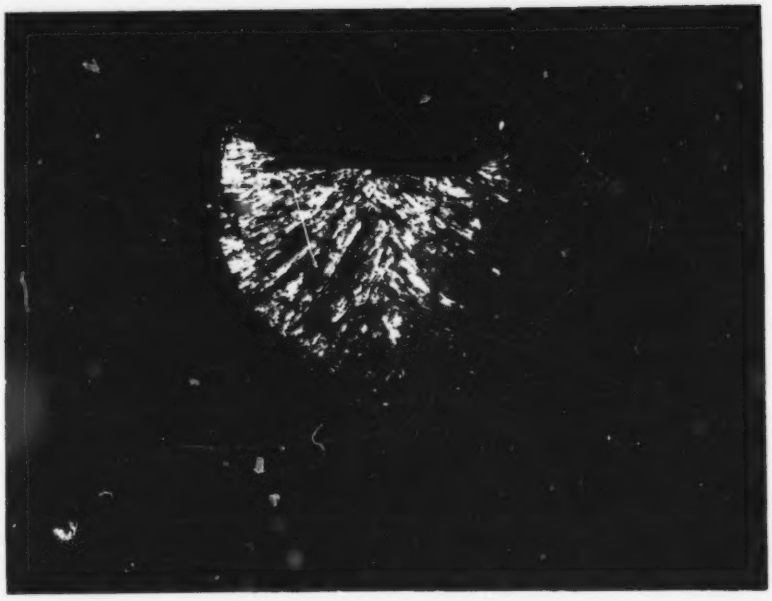

f) Ar-5He-6.5CO_2-3O_2-0.5H_2

Figure 33 (cont)

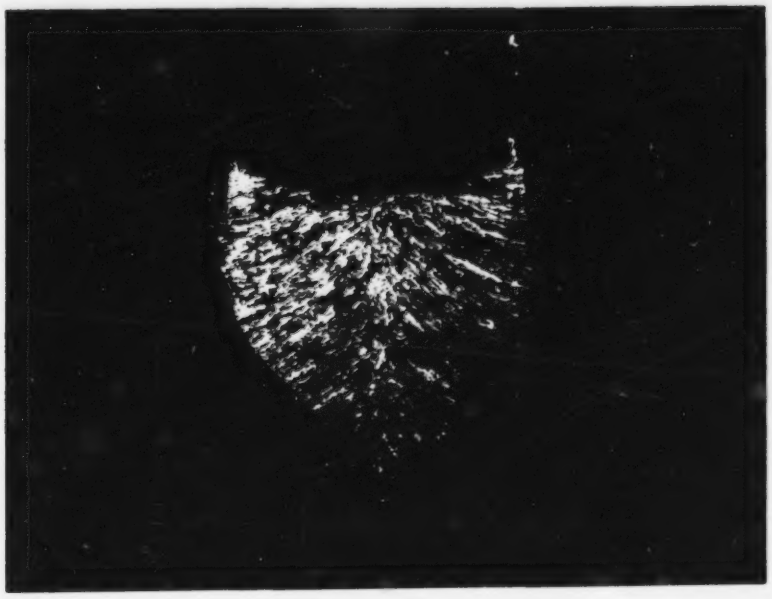

g) Ar-5He-10.5CO_2-10$_2$

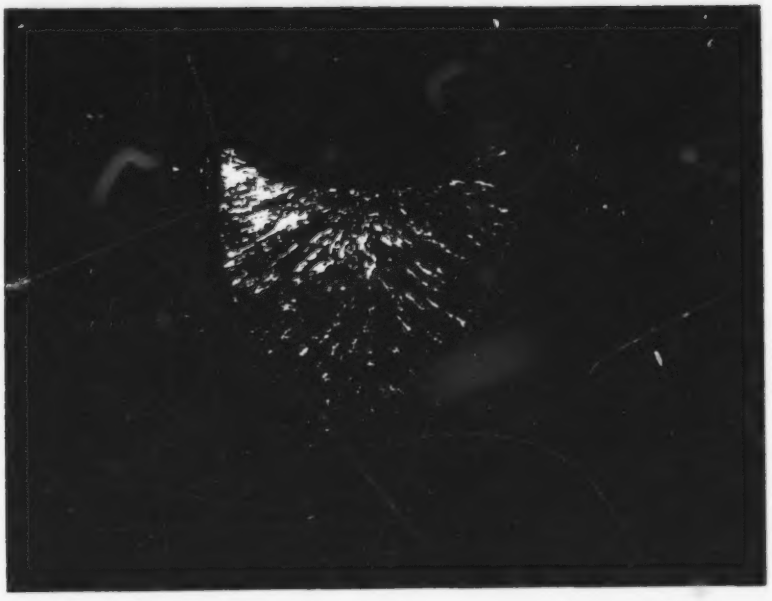

h) Ar-5He-10.5CO_2-10$_2$-0.5H_2

Figure 33 (cont)

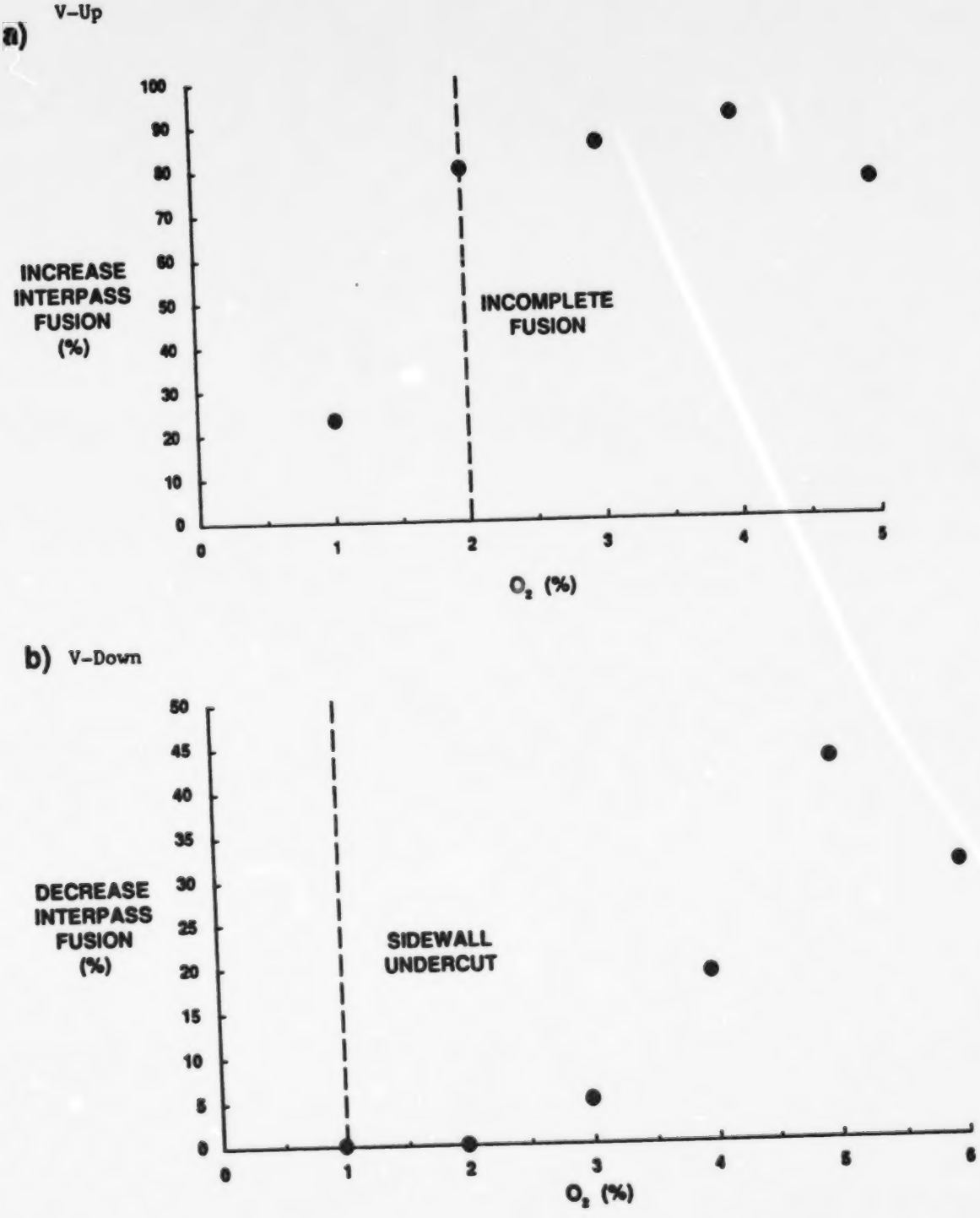

Figure 34: Effect of Oxygen on Interpass Fusion.

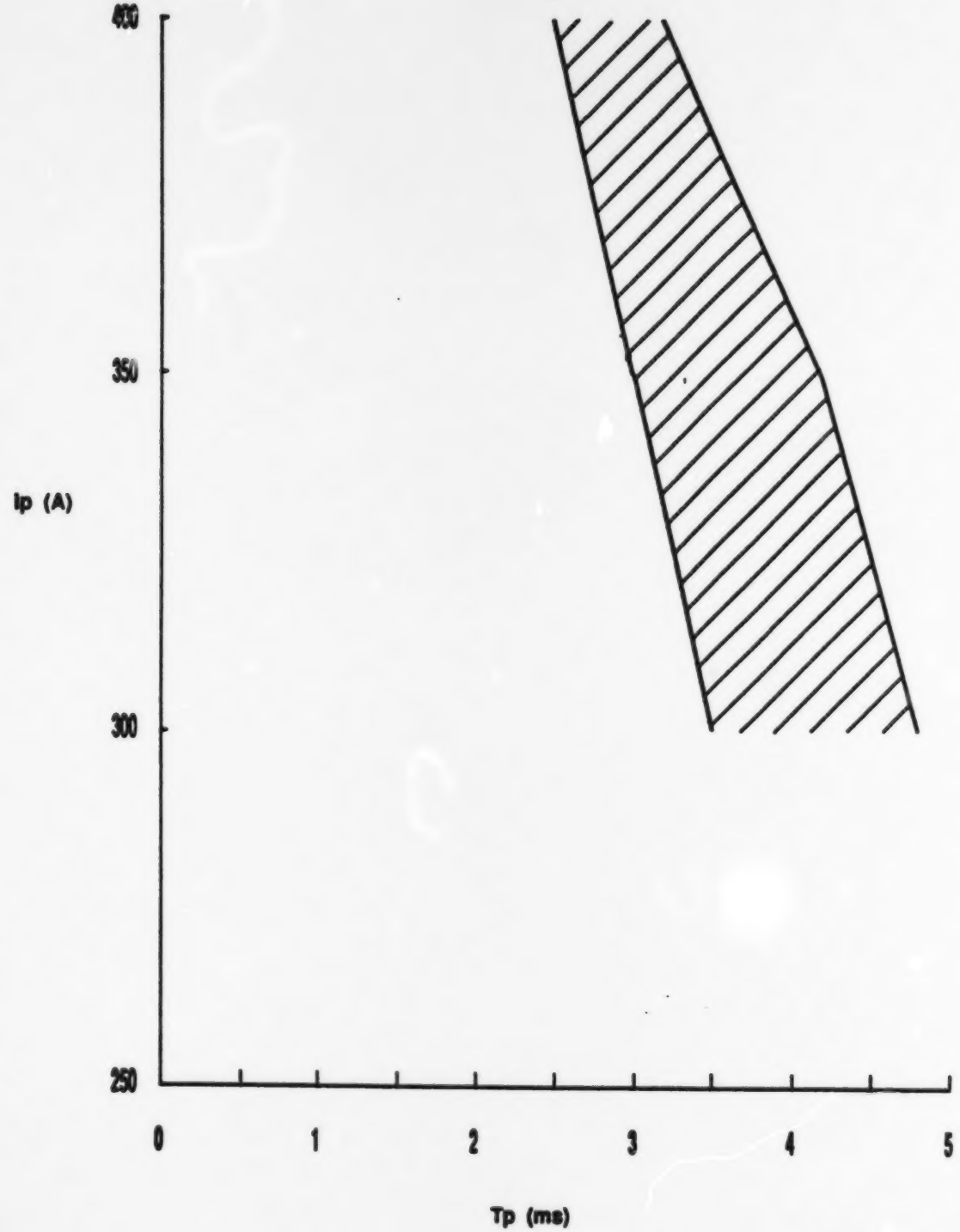

Figure 35: Zone for Satisfactory Metal Transfer and Arc Stability in Ar-10He-6CO_2-2O_2

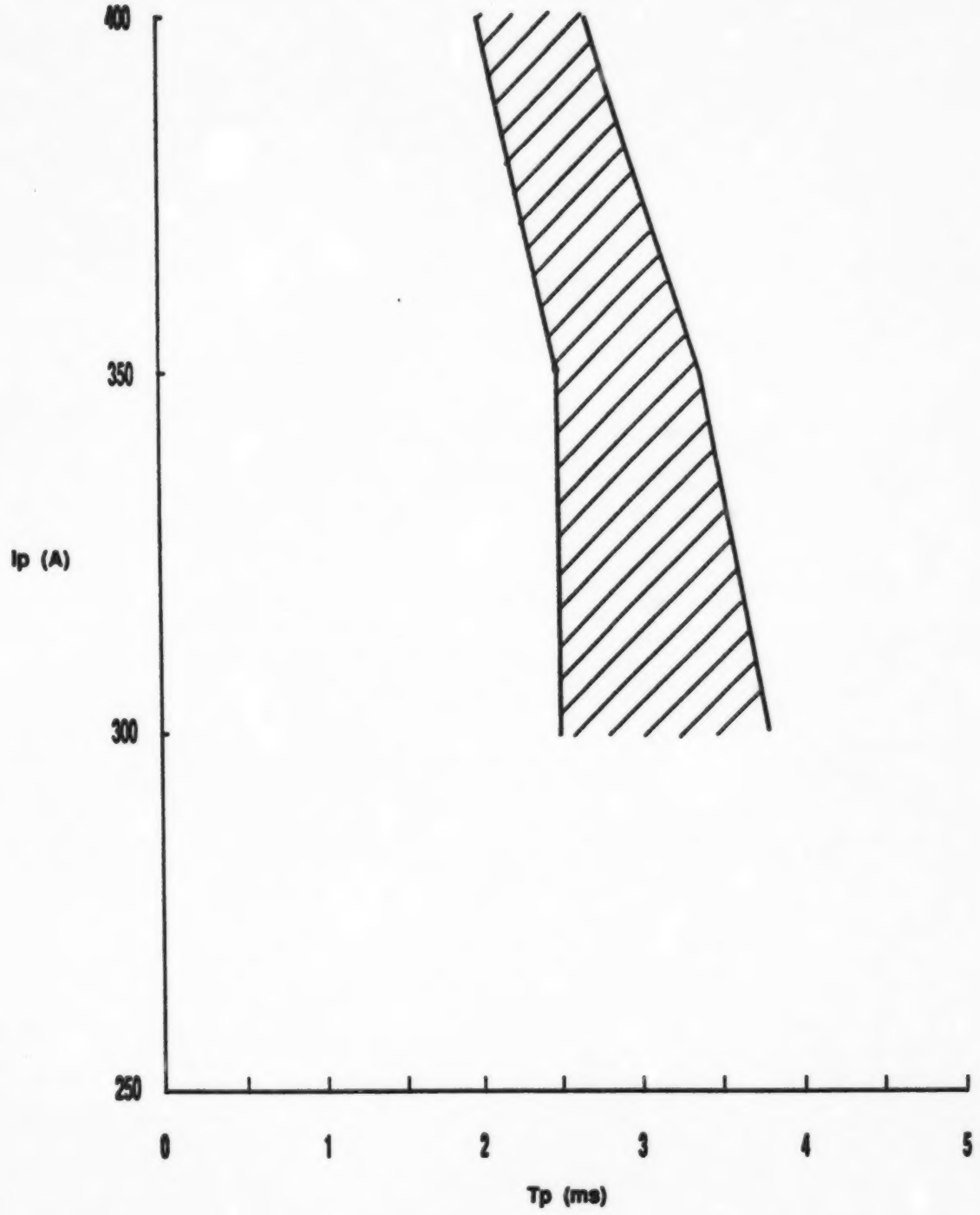

Figure 36: Zone for Satisfactory Metal Transfer and Arc Stability in Ar-5He-12.5CO

a) Vertical Up Weld in Lloyds LT60 Plate. Mag X2.25

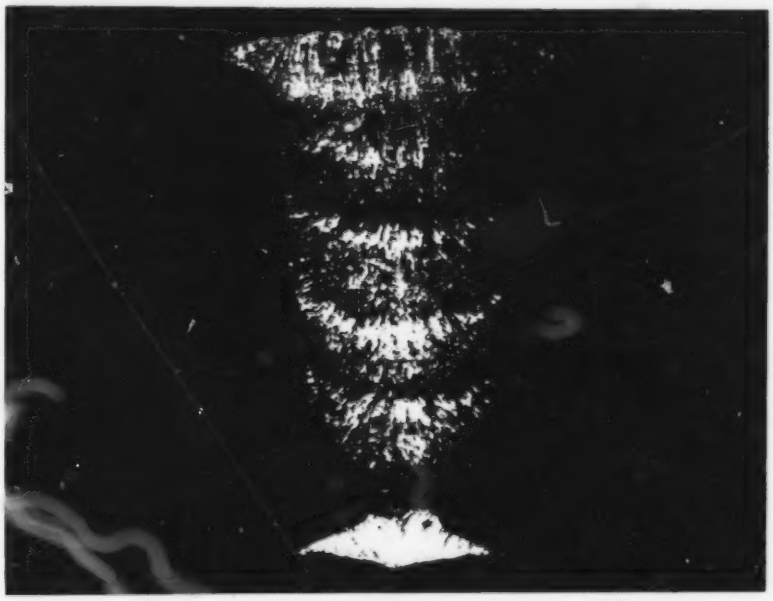

b) Vertical Down Weld in GR 483 MPa Steel Line Pipe. Mag X3.75

Figure 37: Macrosections of Procedure Welds.

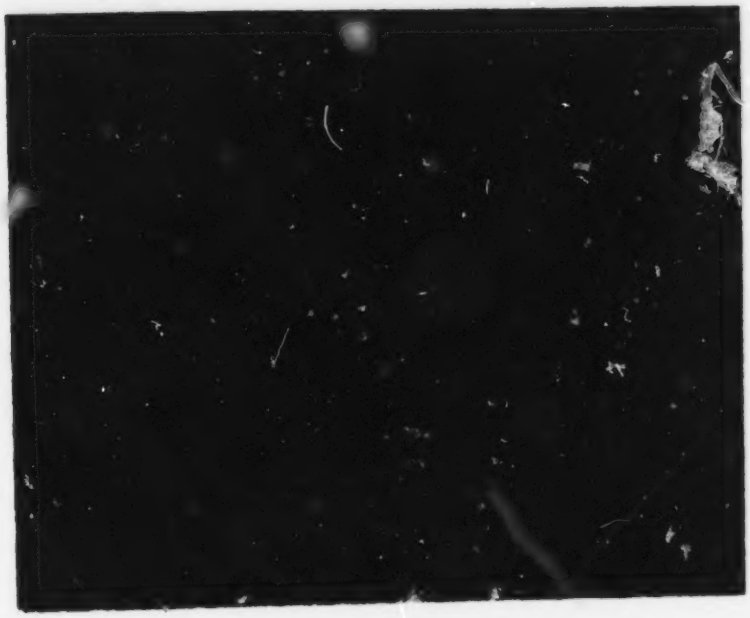

a) As-Depositied C-Mn-Ti-B/Ar-10He-6CO_2-2O_2

b) As-Deposited C-Mn-Si-Ti/Ar-5He-12.5CO_2

Figure 38: Typical Microstructural Features of Procedure Qualification Welds. MAG X500